Reports of the Department of Mathematical Information Technology
Series B. Scientific Computing
No. B 4/2014

On displacement-velocity coupling and the origin of in-plane stresses in orthotropic moving continua

Matti Kurki Juha Jeronen
Tytti Saksa Tero Tuovinen

University of Jyväskylä
Department of Mathematical Information Technology
P.O. Box 35 (Agora)
FI–40014 University of Jyväskylä
FINLAND
fax +358 14 260 2731
http://www.mit.jyu.fi/

ISBN 978-951-39-5742-1 (nid.)
ISBN 978-951-39-6937-0 (PDF)
ISSN 1456-436X

On displacement-velocity coupling and the origin of in-plane stresses in orthotropic moving continua*

Matti Kurki Juha Jeronen Tytti Saksa Tero Tuovinen

May 22, 2014

Abstract

In this paper, we address the problem of the origin of in-plane stresses in continuous, two-dimensional high-speed webs. In the case of thin, slender webs, a typical modeling approach is the application of a stationary in-plane model, without considering the effects of in-plane velocity field. However, for high-speed webs this approach is insufficient, because it neglects the coupling between the total material velocity and the deformation experienced by the material. By using a mixed Lagrange–Euler approach in model derivation, the solid continuum problem can be transformed to solid a continuum flow problem. Mass conservation in the flow problem, and the behaviour of free edges in the two-dimensional case, are both seen to influence the velocity field. We concentrate on the steady-state solutions of the model, and study briefly the coupled nature of material viscoelasticity and transport velocity in one dimension. Analytical solutions of the one-dimensional equation are presented with both elastic and viscoelastic material assumptions. Numerical solution of the two-dimensional elastic problem is also presented. Due to the nature of the velocity-dependent contraction, a nonlinear FEM solution procedure is used. The results indicate that inertial effects produce an additional contribution to elastic contraction in unsupported, free webs.

Keywords: axially moving, orthotropic, viscoelastic, elastic, one-dimensional, two-dimensional, free edges

1 Introduction

In the handling of continuous, high-speed webs the origin of in-plane stresses creates a scientific problem, which is not yet completely understood. Especially, the

*This research was supported by the Finnish Cultural Foundation.

type of the web material has a significant effect on both qualitative and quantitative characteristics of the in-plane stresses. Web tension in the moving continuous web systems can usually be controlled in the direction of the transport velocity, the tension being generated by a velocity difference between the starting and ending lines of the span. At high transport velocities, both web stress and web stability are of concern, not only in this longitudinal direction, but also in the direction perpendicular to the main transport velocity in the plane of the web.

Axially moving materials have many applications in industry, e.g. in paper production, and their mechanics have been studied widely. In the processing of different kinds of thin, laterally moving solid webs, challenges are met, such as the efficiency of production and effects caused by the high processing speed. The first studies of the vibrations of travelling elastic materials date back to the end of the 19th century (Skutch, 1897 [62]) and to the middle of the 20th century (Sack, 1954 [56]; Archibald and Emslie, 1958 [1]). A string model for the moving material was used in all of these studies. Later on, in the 1960s and 1970s, many researchers continued studies on moving strings and beams, concentrating mainly on various aspects of free and forced transverse vibrations (e.g. Miranker [45], Swope and Ames [65], Mote et. al. [47, 48, 49] and Simpson [60]).

The stability of small transverse vibrations of travelling two-dimensional rectangular membranes and plates have been studied by Ulsoy and Mote [70], and Lin [39]. When the web is advancing through a process without external support, the inertial forces depending on the web speed are coupled with web tension. Also the transverse behaviour of the web and the response of the fluid (air) surrounding the web are coupled (see e.g. [9, 53]). Studies modelling the moving web coupled with the surrounding air have been made by Pramila et al. [50, 54, 32]. In their studies, it was found that the surrounding air significantly reduces the eigenfrequencies and critical velocities of the web, when compared to the vacuum case. Chang and Moretti [9] studied membranes using potential flow theory, and Banichuk et al. [5, 6] used the flat panel model coupled with potential flow. This research was extended by Jeronen [30], where the eigenfrequency spectra were investigated for this model and for the moving string with damping. In Watanabe et al. [71], two different methods of analysis were developed for the phenomenon of paper flutter. One of these was a flutter simulation using a Navier–Stokes code, and the other method was based on a potential flow analysis of an oscillating thin airfoil.

Lin and Mote studied an axially moving membrane in a 2D formulation, predicting the equilibria of the displacement and the stress distribution under transverse loading [40]. Later, they continued studying the wrinkling of axially moving rectangular webs with a small flexural stiffness [41]. They predicted the critical value of the non-linear component of the edge loading after which the web wrinkles, and the corresponding wrinkled shape of the web. It is also known that the lack of web tension will result in a loss of stability of the moving web, which from the application viewpoint, disturbs the required smooth advancing of the web (see e.g. [4, 3]). On the other hand, high tension may cause web breaks, which deteriorates production efficiency (see e.g. [2, 55, 57, 61]).

Paper has often been modelled as an orthotropic elastic solid. Elastic constants have been measured for some paper-like materials by Mann, Baum and Habeger [42]; and Baum, Brennan and Habeger [7]. Recently, for anisotropic solids, Erkkilä et al. [17] have studied competent parameters based on modeled stress-strain curves for further construction of a material model. Out-of-plane Poisson ratios, specifically, have been recently studied by Stenberg and Fellers [64], who reported that paper is an auxetic material: stretching in the machine direction will cause the paper web to thicken in the out-of-plane direction. The relevant Poisson ratio, ν_{13}, is negative, and $|\nu_{13}|$ may be as large as 3.0. Incompressible and slightly compressible orthotropic and transversely isotropic materials have been investigated by Itskov and Aksel [29], who discovered nontrivial conditions that the elastic constants must satisfy in order to obtain incompressible or slightly compressible behaviour.

Considering wet paper material, the viscoelastic properties play an important role in the behaviour of the web, and thus, need to be included in the model. The first study on transverse vibration of travelling viscoelastic material was carried out by Fung et. al. using a string model [19]. Extending their work, they studied the viscous damping effect in their later research [20]. Viscoelastic strings and beams have recently been studied extensively, see e.g. [44, 73]. Oh et al. studied critical speeds, eigenvalues and natural modes of the transverse displacement of axially moving viscoelastic beams using the spectral element method [38, 51]. Chen and Zhao [14] presented a modified finite difference method to simplify a non-linear model of an axially moving string. They studied numerically the free transverse vibrations of both elastic and viscoelastic strings. Chen and Yang studied free vibrations of viscoelastic beams travelling between simple supports with torsion strings [13]. They studied the viscoelastic effect by perturbing the similar elastic problem and using the method of multiple scales. Very recently, Yang et al. studied vibrations, bifurcation, and chaos of axially moving viscoelastic plates using finite differences and a non-linear model for transverse displacements [72].

Marynowski and Kapitaniak studied differences between the Kelvin-Voigt and Burgers models in the modelling of the internal damping of axially moving viscoelastic beams. They found out that both models gave accurate results with small damping coefficients, but with a large damping coefficient, the Burgers model was more accurate [43]. In 2007, they compared the models with the Zener model studying the dynamic behaviour of an axially moving viscoelastic beam [44]. They found out that the Burgers and Zener models gave similar results for the critical transport speed whereas, the Kelvin-Voigt model gave a greater critical speed compared to the other two models.

The origin and structure of the in-plane stress and strain distribution in a moving solid web seems to be an exceptionally unknown area. The models used with web materials are often based on assumptions of isotropic or orthotropic material properties (see e.g. [7, 67]). The material is considered as viscoelastic or viscoplastic, but in the models, there is usually no coupling between the in-plane strain and the web velocity effects (see e.g. [23, 52, 69]).

Time-dependent, in-plane vibrations of a moving continuous membrane were

studied by Shin et al. [58]. In their work, in-plane vibration modes of an isotropic web were studied between the traction lines. Also Guan et. al. have studied viscoelastic web behaviour in both steady state and unsteady state cases [21, 22].

Traditionally, the partial time derivative has been used instead of the material derivative in the viscoelastic constitutive relations, but Mockensturm and Guo suggested that the material derivative should be used [46]. They studied non-linear vibrations and the dynamic response of axially moving viscoelastic strings. Kurki and Lehtinen also independently suggested that the material derivative should be used in the constitutive relations, in their study concerning the in-plane displacement field of a travelling viscoelastic plate [36, 34].

In a study by Chen et al., the material derivative was used in the viscoelastic constitutive relations [10]. They studied parametric vibration of axially accelerating viscoelastic strings. Chen and Ding studied the stability of axially accelerating viscoelastic beams using the method of multiple scales, and the material derivative was used in the viscoelastic constitutive relations [15]. Chen and Wang studied the stability of axially accelerating viscoelastic beams using asymptotic perturbation analysis and the material derivative in the viscoelastic relations [12]. The material derivative was also used in a recent paper by Chen and Ding, where the dynamic vibration response of axially moving viscoelastic beams was studied [11]. A non-linear model was used, taking into account the coupling of the transverse displacement with the longitudinal (in-plane) displacement. However, the transverse behaviour of the beam was their main focus.

In this paper, we propose to modify the classical two-dimensional model of a moving viscoelastic web by accounting for the coupling between the velocity field and the in-plane strain. A two-dimensional, thin open loop (non-conservative system) made of orthotropic membrane is stretched using a relative speed difference between the traction lines. The orthotropic viscoelastic material assumption is applied, using a viscoelastic model of the Kelvin–Voigt type. An originally Lagrange-based ”material” deformation formulation is used as the control volume, to which the mixed Lagrange-Euler-based ”spatial” formulation is then applied (see e.g. [66, 33]). With this method it is possible to handle solid, moving web behaviour using a control volume approach similar to the treatment of fluid flows. Preliminary one-dimensional studies have been reported in the paper [35]. In the present paper, the steady state of the two-dimensional moving continuum, in the pure elastic case, is solved using the nonlinear finite element method.

2 Strain generated by velocity difference of subsequent rollers

A continuous, moving web creates a flow continuum which is possible to consider as a solid medium experiencing flow. Due to its solid nature, the web continuum is always under a stress state, which is caused by a strain state, which further can be expressed in terms of the velocity difference between subsequent supporting rollers,

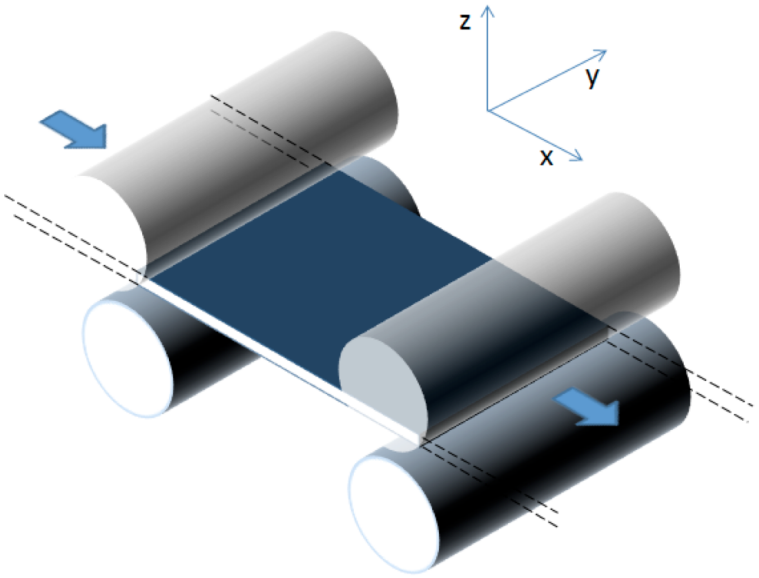

Figure 1: Schematic representation of the setup for modelling a moving viscoelastic web, stressed at the traction lines represented by the rollers. The arrows depict axial motion.

by the means of a mass conservation argument.

Consider an orthotropic material having initially (i.e. in the undeformed state) constant density ρ_0, undergoing steady-state longitudinal transport at velocity $\mathbf{U} = (U_x, 0, 0)$, depicted in Figure 1. Let us assume that the material axes 1, 2 and 3 are aligned with the global coordinate axes x, y and z, respectively. The continuity equation, as expressed in the Eulerian frame, is

$$\frac{\partial \rho}{\partial t} + \nabla \cdot (\rho \mathbf{U}) = 0 \,, \tag{1}$$

where ρ is density of the material, and $\partial/\partial t$ is the partial time derivative in the Eulerian frame. In a steady state, the equation reduces to

$$\nabla \cdot (\rho \mathbf{U}) = 0 \,. \tag{2}$$

Mass conservation requires that the flow rates at the incoming and outgoing flow control areas match; this requirement is readily obtained from equation (2). Let us consider a stationary control volume

$$\Omega = \{\, (x, y, z) : \, 0 < x < \ell \,, \; 0 < y < b \,, \; 0 < z < h \,\} \,,$$

where ℓ is the length of the span between the rollers, b is the width of the span, and h is the thickness of the sheet of material. Integrating equation (2) over the control volume Ω, applying the divergence theorem, and noting that ρ is a scalar, we have

$$\int_\Omega \nabla \cdot (\rho \mathbf{U}) \, \mathrm{d}\Omega = \int_{\partial\Omega} \rho \, (\mathbf{n} \cdot \mathbf{U}) \, \mathrm{d}\Gamma \,, \tag{3}$$

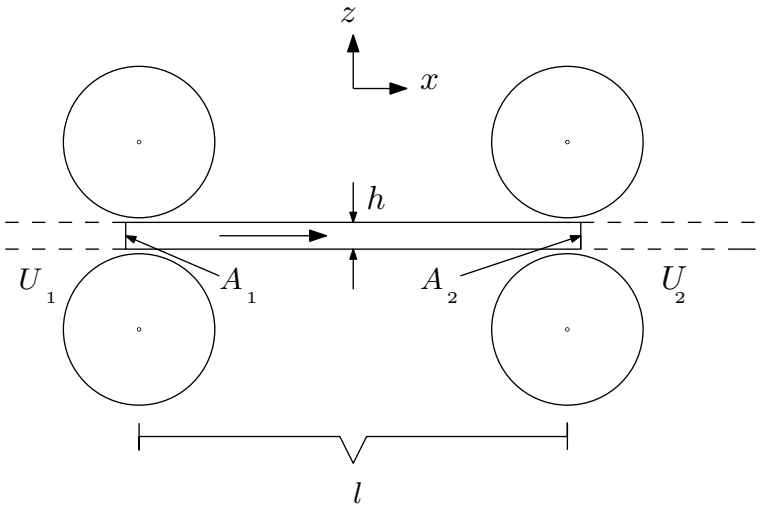

Figure 2: Solid web continuum flowing between the incoming and outgoing flow control areas (two-dimensional surfaces) A_1 and A_2, at longitudinal speeds U_1 and U_2 at the beginning and ending traction lines (respectively).

where $\partial\Omega$ is the closed surface delimiting the control volume Ω, and $\mathbf{n}$ represents outer unit normal vector. The differential $\mathrm{d}\Gamma$ refers to integration over a surface.

As is shown in Figure 2, flows in and out of the control volume occur only at the surfaces A_1 and A_2. Let us assume that ρ and $\mathbf{U}$ are constant across these in- and outflow surfaces, but that their values may change between these surfaces. In practice, there may exist small variations in the velocity at the outlet due to material straining, but for small strains and high velocity, constant velocity along these surfaces is a reasonable approximation.

Under these assumptions, the mass balance in the equation (3) becomes

$$-\rho_1 A_1 U_1 + \rho_2 A_2 U_2 = 0 \; . \tag{4}$$

The subscripts 1 and 2 for ρ and U refer to the (constant) values on the surfaces A_1 and A_2, respectively. Note the form of the velocity field, $\mathbf{U} = (U_x, 0, 0)$. Finally, it is convenient to rewrite (4) as

$$U_1 \frac{\rho_1 A_1}{\rho_2 A_2} - U_2 = 0 \; . \tag{5}$$

In order to manipulate equation (5) further, we must consider the ratios of the densities and the cross-sectional areas. When subjected to a small-displacement deformation $\mathbf{u} = (u, v, w)$, the volume V of a differential element initially (in the undeformed state) having volume V_0 becomes

$$V = V_0\big[1 + \nabla \cdot \mathbf{u}\big] \equiv V_0\big[1 + \varepsilon_x + \varepsilon_y + \varepsilon_z\big] \; , \tag{6}$$

as is known from the theory of elasticity. Here ε_x, ε_y and ε_z are the axial strains with respect to x, y and z -directions. Because the total mass M of the differential element

is conserved in the small deformation, it follows for the density ρ that

$$\rho \equiv \frac{M}{V} = \frac{1}{V_0}\,\frac{M}{V/V_0} = \frac{M}{V_0}\,\frac{1}{V/V_0} = \rho_0\big[1 + \varepsilon_x + \varepsilon_y + \varepsilon_z\big]^{-1} \,, \tag{7}$$

by (6) and the definition $\rho_0 \equiv M/V_0$.

Let us assume that the material is subjected to pure axial stress. This induces an axial strain ε_x, and via the Poisson effect, also the strains ε_y and ε_z in the two orthogonal directions:

$$\varepsilon_y = -\nu_{12}\varepsilon_x \,, \quad \varepsilon_z = -\nu_{13}\varepsilon_x \,, \tag{8}$$

where ν_{12} and ν_{13} are the (orthotropic) Poisson ratios for stretching in the direction of the material axis 1, describing the resulting contraction on material axes 2 and 3, respectively. This purely elastic approximation neglects all viscous effects, but since a steady state is being considered, this is reasonable. The cross-sectional area of the web is

$$A \;=\; (1 + \varepsilon_z)h(1 + \varepsilon_y)b \;\approx\; bh\,(\,1 + \varepsilon_y + \varepsilon_z\,) \,, \tag{9}$$

where second-order small terms have been neglected. Combining equations (8) and (9), we have

$$A = bh\,(\,1 - (\nu_{12} + \nu_{13})\varepsilon_x\,) \equiv bh\,(\,1 - \nu_{1A}\varepsilon_x\,) \,, \tag{10}$$

where the effective Poisson ratio for the change in cross-sectional area, when stretched along material axis 1, is defined as

$$\nu_{1A} \equiv \nu_{12} + \nu_{13} \,. \tag{11}$$

As was noted in the introduction, for paper materials, it is known (see e.g. the study by Stenberg and Fellers [64]) that $\nu_{13} < 0$, and that $|\nu_{13}|$ may be as large as 3.0. Typically, we will thus have $\nu_{1A} < 0$: the cross-sectional area may actually increase under tension, because the thickness increases. Even though the thickness itself is typically small, it may undergo a large relative change, and therefore must be considered when calculating the area of the cross-section.

It also follows from equations (6), (8) and (11) that

$$V = V_0\big[1 + (1 - \nu_{1A})\varepsilon_x\big] \,. \tag{12}$$

It should be pointed out that if for some particular material $\nu_{1A} = 1$, then $V = V_0$, and such a material behaves incompressibly when stretched along material axis 1. The effective Poisson ratio contains the directional Poisson ratios ν_{12} and ν_{13}. The only requirement for incompressibility under uniaxial stretching is that the sum of ν_{12} and ν_{13} is unity; unlike the isotropic case, neither of them needs to be 0.5.

Furthermore, the values of ν_{23}, ν_{21}, ν_{31} and ν_{32} still remain free. Elastic compatibility is required, but this brings in additional free parameters, because elastic compatibility involves not only the Poisson ratios, but also the Young moduli; e.g. $E_1\nu_{21} = E_2\nu_{12}$. Depending on the set of parameter values chosen, it is possible that an orthotropic material behaves incompressibly in axial stretching only when the deformation is applied along some particular axis.

It is thus evident that the conditions of incompressibility for anisotropic materials are more complicated than for isotropic materials, where the only requirement is $\nu = 0.5$. For a more thorough consideration of incompressibility in orthotropic and transversely isotropic materials, see the study by Itskov and Aksel [29].

By combining equations (7), (8) and (11), we obtain

$$\rho = \frac{\rho_0}{1 + (1 - \nu_{1A})\varepsilon_x} \, . \tag{13}$$

In the following, we shall assume that the material, subjected to constant axial tension at the rollers (traction lines), has zero strain at A_1, and experiences some nonzero axial strain ε_x at A_2, due to the applied axial stress. Preliminary one-dimensional results [35] indicate that such a strain state occurs at least for an axially travelling Kelvin–Voigt viscoelastic material; see also the treatment of the one-dimensional case further below, where we will show this briefly. By equation (10), the cross-sectional areas at the inflow and outflow surfaces A_1 and A_2 become

$$A_1 = bh \, , \qquad A_2 = bh(1 - \nu_{1A}\varepsilon_x) \, , \tag{14}$$

and by equation (13), the material densities on these surfaces are

$$\rho_1 = \rho_0 \, , \qquad \rho_2 = \frac{\rho_0}{1 + (1 - \nu_{1A})\varepsilon_x} \, . \tag{15}$$

By inserting equations (14) and (15) into the mass balance equation (5), simplifying, and solving for ε_x, we obtain the result

$$\varepsilon_x = \frac{\dfrac{U_2}{U_1} - 1}{1 + \left[\dfrac{U_2}{U_1} - 1\right] \nu_{1A}} \, . \tag{16}$$

Equation (16) gives the axial strain, at the traction line at $x = \ell$, for the problem of in-plane (visco-)elastic deformation, corresponding to given roller speeds U_1 and U_2. Obviously, in order for the model to remain valid, the given velocities must be such that the strain according to (16) remains in the small-deformation range.

The transport velocity of the flowing solid continuum in the above case is assumed to be controlled only in the x (longitudinal) direction; all in-plane deformations in the y (widthwise) direction are determined by the (visco-)elastic response. It should also be kept in mind that equation (16) only applies in a steady-state flow, i.e. when the web flows smoothly without time-dependent disturbances.

The traction lines at the cross-sectional areas A_1 and A_2 affect only the surfaces of the web, which implies that stress and strain waves advancing inside the web thickness can cross the traction lines. Therefore in the boundary conditions of moving continuous webs, in reality, one should consider rather complicated friction-based force transmission phenomena at web-roll contact areas [34].

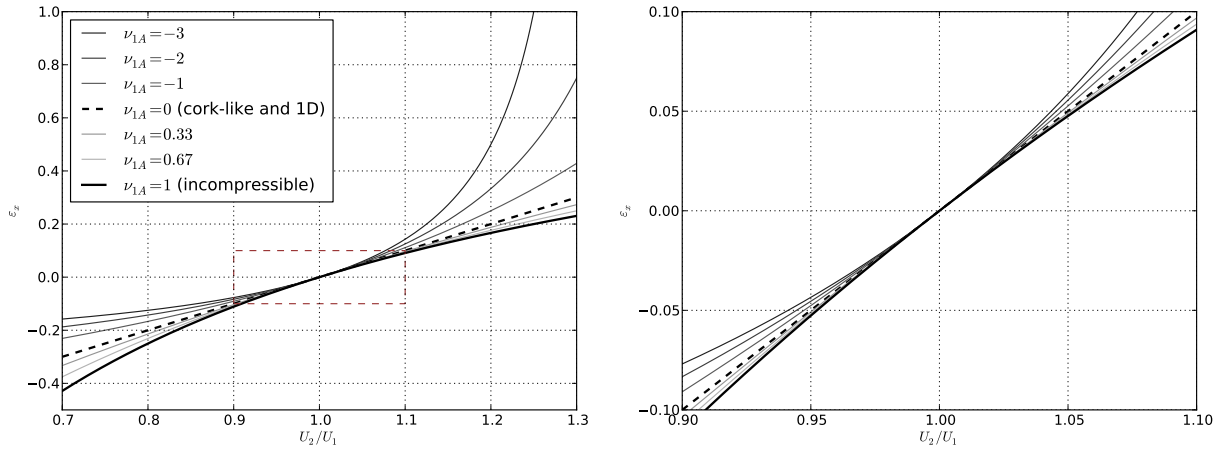

Figure 3: Roller-induced axial strain ε_x as a function of velocity ratio U_2/U_1, based on equations (16)–(18). *Left*: Overall behaviour of the functions, showing their curvature (only the line for $\nu_{1A} = 0$ is straight). *Right*: Zoomed-in view. Location of the zoomed area is shown by the dashed box in the left subfigure.

In the special case of a material which behaves incompressibly when stretched along axis 1, we have $\nu_{1A} = 1$. By inserting this into (16) and simplifying, we obtain

$$\varepsilon_x = 1 - \frac{U_1}{U_2} \,, \tag{17}$$

which holds only when $\nu_{1A} = 1$.

In the limit $\nu_{1A} \to 0$, equation (16) simplifies to

$$\varepsilon_x = \frac{U_2}{U_1} - 1 \,. \tag{18}$$

This corresponds to cork-like materials, which do not exhibit the Poisson effect. Note, however, that if the material is an auxetic orthotropic one, it is possible that $\nu_{13} = -\nu_{12}$, also leading to $\nu_{1A} = 0$.

The result (18) also arises in the case of a one-dimensional string model. Consider a compressible travelling string, undergoing steady-state flow through the span $0 < x < \ell$. Mass conservation now requires

$$R_1 U_1 - R_2 U_2 = 0 \,, \tag{19}$$

with similar definitions for the subscripts as above. Here R is the linear density, $[R] = \mathrm{kg/m}$, and the cross-sectional area of the string is assumed constant. As the string becomes stretched or compressed, the linear density changes as

$$R = \frac{R_0}{1 + \varepsilon_x} \,, \tag{20}$$

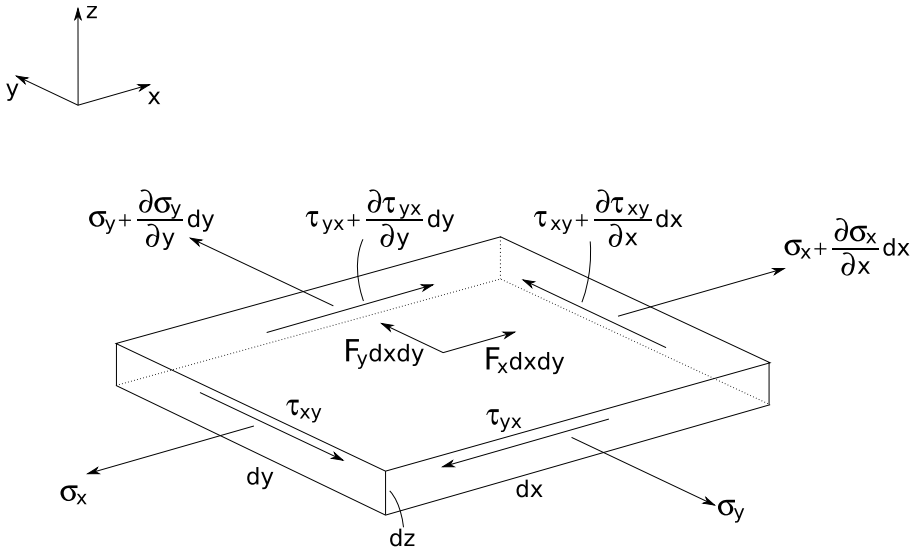

Figure 4: Differential parallelepiped and forces acting in the in-plane directions x and y.

where R_0 is the (constant) linear density in the initial (unstretched) state. Equation (20) follows directly from equation (7) and the assumption that the cross-sectional area is constant (whence $\varepsilon_y = \varepsilon_z = 0$).

As before, let as assume that at $x = 0$ the strain in the string is zero, and at $x = \ell$, the string experiences some nonzero strain ε_x due to axial tension applied at the ends of the span. As was noted above, this is consistent for a travelling Kelvin–Voigt viscoelastic string. Hence $R_1 = R_0$, and R_2 is given by equation (20). By combining equations (19) and (20), and solving for ε_x, the equation (18) is obtained.

The behaviour of equations (16)–(18) is illustrated in Figure 3.

3 The governing equations

In this section we will define the stresses and strains, deformations, material assumptions and velocity-dependent in-plane inertial forces for the moving web. This leads to both one- and two-dimensional models, and equations for the viscoelastic moving web continuum application.

The standard approach for describing structural deformations is the Lagrangean description. However, longitudinal in-plane deformations in axially moving materials are more challenging. One possibility is to actually move the medium at the desired speed, and update the boundary conditions at each timestep [63]. Another possibility is to use an 'Eulerian' flow description, and by this the actual deformation of the moving continuum can be handled using a mixed Lagrange–Euler description [33]. The Eulerian description is a standard approach in fluid dynamics where the observer is 'watching' a control volume, where possible deformations will appear [63, 37].

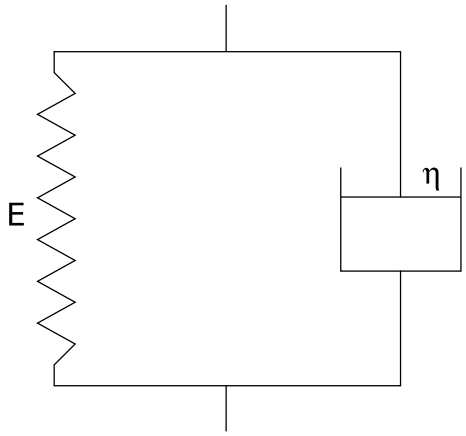

Figure 5: Schematic representation of the classical Kelvin-Voigt rheological model in one dimension. E is Young's modulus, η is the material viscosity.

In this paper, we consider two-dimensional in-plane membrane behaviour. Based on Figure 4, one can derive the following well-known force balance [68]:

$$\frac{\partial \sigma_x}{\partial x} + \frac{\partial \tau_{yx}}{\partial y} + F_x = 0 \,, \tag{21}$$

$$\frac{\partial \tau_{xy}}{\partial x} + \frac{\partial \sigma_y}{\partial y} + F_y = 0 \,, \tag{22}$$

where τ_{yx} and τ_{xy} are shear stresses and F_x and F_y are (external) body forces. The linear Cauchy strains are

$$\varepsilon_{xx} = \frac{\partial u}{\partial x} \,, \;\; \varepsilon_{yy} = \frac{\partial v}{\partial y} \,, \;\; \varepsilon_{xy} = \frac{\partial u}{\partial y} \,, \;\; \varepsilon_{yx} = \frac{\partial v}{\partial x} \,, \;\; \gamma_{xy} = \left(\frac{\partial u}{\partial y} + \frac{\partial v}{\partial x} \right) \,. \tag{23}$$

We will use the material assumption of orthotropic viscoelasticity. In the mixed Lagrange–Euler description, the strains

$$\varepsilon_{ij} = \varepsilon_{ij} \left(x, y, t \right) \tag{24}$$

lead to the time derivatives

$$\frac{\mathrm{d}\varepsilon_{ij}}{\mathrm{d}t} = \frac{\partial \varepsilon_{ij}}{\partial t} + \frac{\partial \varepsilon_{ij}}{\partial x} \frac{\mathrm{d}x}{\mathrm{d}t} + \frac{\partial \varepsilon_{ij}}{\partial y} \frac{\mathrm{d}y}{\mathrm{d}t} = \frac{\partial \varepsilon_{ij}}{\partial t} + \frac{\partial \varepsilon_{ij}}{\partial x} U_x + \frac{\partial \varepsilon_{ij}}{\partial y} U_y \,, \tag{25}$$

where (U_x, U_y) is the velocity field and $\mathrm{d}/\mathrm{d}t$ is the material derivative.

With fibrous, composite-type materials, the mechanical deformation response properties are the result of complicated material preprocessing, which results in orthotropic anisotropy and material time-dependence (see e.g. [69], [31], [52] and

[8]). It is possible to derive a vast number of different rheological models for time-dependent material behaviour, but the fundamental behaviour of continuous flow of a solid viscoelastic web can be analyzed using the simple Kelvin–Voigt model shown in Figure 5. The singular stress response to a step strain does not matter, because we are considering a steady state where no rapidly changing strains occur; hence the Kelvin–Voigt model is sufficient for the present application.

The stress-strain behaviour of one-dimensional Kelvin-Voigt material (see e.g. [18]) is simply

$$\sigma = \mathrm{E}\varepsilon + \eta \frac{\mathrm{d}\varepsilon}{\mathrm{dt}} \,, \tag{26}$$

where E is Young's modulus and η is the material viscosity. We will apply a two-dimensional, orthotropic plane stress extension of the above model, based on practical observations of fibrous web materials [67, 69]:

$$\sigma_x = \frac{E_x}{1-\nu_{12}\nu_{21}} \left(\varepsilon_{xx} + \nu_{21}\varepsilon_{yy}\right) + \frac{\eta_x}{1-\varphi_{12}\varphi_{21}} \left(\frac{\mathrm{d}\varepsilon_{xx}}{\mathrm{dt}} + \varphi_y \frac{\mathrm{d}\varepsilon_{yy}}{\mathrm{dt}}\right) \tag{27}$$

$$\sigma_y = \frac{E_y}{1-\nu_{12}\nu_{21}} \left(\varepsilon_{yy} + \nu_{12}\varepsilon_{xx}\right) + \frac{\eta_y}{1-\varphi_{12}\varphi_{21}} \left(\frac{\mathrm{d}\varepsilon_{yy}}{\mathrm{dt}} + \varphi_x \frac{\mathrm{d}\varepsilon_{xx}}{\mathrm{dt}}\right) \tag{28}$$

$$\tau_{yx} = \tau_{xy} = \mathrm{G}\gamma_{xy} + \Pi \frac{\mathrm{d}\gamma_{xy}}{\mathrm{dt}} \tag{29}$$

Here φ_{12} and φ_{21} are the viscous analogues of the orthotropic in-plane Poisson ratios ν_{12} and ν_{21}, G is a shear modulus, γ is a shear strain and Π is the viscous shear modulus.

Often, problems considering the in-plane behaviour of a continuous material are written using only an elastic model, involving the moduli of elasticity E_x and E_y, and the strain variables ε_{xx} and ε_{yy}. However, in practice all the elastic-related material properties are measured with some definite speed, and therefore apparent elasticity includes both elastic and viscous material properties [18]. Fundamentally, all materials exhibit some form of viscoelasticity, typically measured by normal and complex moduli E and E', respectively. It should also be pointed out that the viscoelastic Poisson ratios φ_{12} and φ_{21} cannot be calculated using compliances from the theory of elasticity [24].

The force balance equations (21) and (22) include also the body forces F_x and F_y, which are important especially with fibrous cellulose-based materials. Moisture-dependent dimension changes can be significant, which generates stresses in addition to those related to the strains based on external velocity differences (equation (16)).

Next, let us consider the dynamic equilibrium. According to Newton's second law, time-dependent dynamical behaviour always includes inertial forces. Two-dimensional inertial forces in in-plane membrane behaviour can be accounted for

using the following dynamic equilibrium equations (see e.g. [59]):

$$\frac{\partial \sigma_x}{\partial x} + \frac{\partial \tau_{xy}}{\partial y} + F_x = \rho \frac{\mathrm{d}^2 u}{\mathrm{d}t^2} \tag{30}$$

$$\frac{\partial \sigma_y}{\partial y} + \frac{\partial \tau_{yx}}{\partial x} + F_y = \rho \frac{\mathrm{d}^2 v}{\mathrm{d}t^2} \tag{31}$$

Note that the operator $\mathrm{d}^2/\mathrm{d}t^2$ describes the inertial behaviour in the Lagrangean reference frame. Thus the inertial terms depending on the displacements u and v, in the Eulerian frame, must be presented using the material derivative:

$$\frac{\mathrm{d}u}{\mathrm{d}t} = \frac{\partial u}{\partial t} + \sum_{i=1,2} \frac{\partial u}{\partial x_i} \frac{\mathrm{d}x_i}{\mathrm{d}t} \tag{32}$$

$$\frac{\mathrm{d}v}{\mathrm{d}t} = \frac{\partial v}{\partial t} + \sum_{i=1,2} \frac{\partial v}{\partial x_i} \frac{\mathrm{d}x_i}{\mathrm{d}t} \tag{33}$$

The second material derivatives of the displacements u and v are

$$\begin{aligned} \frac{\mathrm{d}^2 u}{\mathrm{d}t^2} = {} & \frac{\partial^2 u}{\partial t^2} + 2U_x \frac{\partial^2 u}{\partial x \partial t} + 2U_y \frac{\partial^2 u}{\partial y \partial t} + U_x^2 \frac{\partial^2 u}{\partial x^2} + 2U_x U_y \frac{\partial^2 u}{\partial x \partial y} + U_y^2 \frac{\partial^2 u}{\partial y^2} \\ & + \frac{\partial u}{\partial x} \left(\frac{\partial U_x}{\partial x} U_x + \frac{\partial U_x}{\partial y} U_y + \frac{\partial U_x}{\partial t} \right) + \frac{\partial u}{\partial y} \left(\frac{\partial U_y}{\partial x} U_x + \frac{\partial U_y}{\partial y} U_y + \frac{\partial U_y}{\partial t} \right) \end{aligned} \tag{34}$$

$$\begin{aligned} \frac{\mathrm{d}^2 v}{\mathrm{d}t^2} = {} & \frac{\partial^2 v}{\partial t^2} + 2U_x \frac{\partial^2 v}{\partial x \partial t} + 2U_y \frac{\partial^2 v}{\partial y \partial t} + U_x^2 \frac{\partial^2 v}{\partial x^2} + 2U_x U_y \frac{\partial^2 v}{\partial x \partial y} + U_y^2 \frac{\partial^2 v}{\partial y^2} \\ & + \frac{\partial v}{\partial x} \left(\frac{\partial U_x}{\partial x} U_x + \frac{\partial U_x}{\partial y} U_y + \frac{\partial U_x}{\partial t} \right) + \frac{\partial v}{\partial y} \left(\frac{\partial U_y}{\partial x} U_x + \frac{\partial U_y}{\partial y} U_y + \frac{\partial U_y}{\partial t} \right) \end{aligned} \tag{35}$$

By substituting the equations (34) – (35) and (27) – (29) into the equations (30) and (31), we obtain the following time-dependent two-dimensional equations for the in-plane, plane stress membrane behaviour of the moving viscoelastic web:

$$\begin{aligned} & \left(C_{11} - \rho U_x^2\right) \frac{\partial^2 u}{\partial x^2} + \left(C_{66} - \rho U_y^2\right) \frac{\partial^2 u}{\partial y^2} + C_{12} \frac{\partial^2 v}{\partial x \partial y} + C_{66} \frac{\partial^2 v}{\partial x \partial y} + K_{11} U_x \frac{\partial^3 u}{\partial x^3} \\ & + K_{11} U_y \frac{\partial^3 u}{\partial x^2 \partial y} + K_{11} \frac{\partial^3 u}{\partial x^2 \partial t} + \left(K_{12} + K_{66}\right) U_y \frac{\partial^3 v}{\partial x \partial y^2} + K_{66} U_y \frac{\partial^3 u}{\partial y^3} \\ & + \left(K_{12} + K_{66}\right) U_x \frac{\partial^3 v}{\partial x^2 \partial y} + \left(K_{12} + K_{66}\right) \frac{\partial^3 v}{\partial x \partial y \partial t} + K_{66} U_x \frac{\partial^3 u}{\partial x \partial y^2} + K_{66} \frac{\partial^3 u}{\partial y^2 \partial t} + F_x \\ = {} & \rho \frac{\partial^2 u}{\partial t^2} + 2\rho U_x U_y \frac{\partial^2 u}{\partial x \partial y} + 2\rho U_x \frac{\partial^2 u}{\partial x \partial t} + 2\rho U_y \frac{\partial^2 u}{\partial y \partial t} \\ & + \rho \frac{\partial u}{\partial y} \left(\frac{\partial U_x}{\partial x} U_x + \frac{\partial U_x}{\partial y} U_y + \frac{\partial U_x}{\partial t} \right) + \rho \frac{\partial u}{\partial y} \left(\frac{\partial U_y}{\partial x} U_x + \frac{\partial U_y}{\partial y} U_y + \frac{\partial U_y}{\partial t} \right) \end{aligned} \tag{36}$$

and

$$\begin{aligned}
&\left(C_{22}-\rho U_y^2\right)\frac{\partial^2 v}{\partial y^2}+\left(C_{66}-\rho U_x^2\right)\frac{\partial^2 v}{\partial x^2}+C_{21}\frac{\partial^2 u}{\partial x\partial y}+C_{66}\frac{\partial^2 v}{\partial x\partial y}+K_{22}U_y\frac{\partial^3 v}{\partial y^3}\\
&+K_{22}U_x\frac{\partial^3 v}{\partial x\partial y}^{\,2}+K_{22}\frac{\partial^3 v}{\partial x^2\partial t}+\left(K_{21}+K_{66}\right)U_x\frac{\partial^3 u}{\partial x^2\partial y}+K_{66}U_x\frac{\partial^3 v}{\partial x^3}\\
&+\left(K_{21}+K_{66}\right)U_y\frac{\partial^3 u}{\partial x\partial y^2}+\left(K_{21}+K_{66}\right)\frac{\partial^3 u}{\partial x\partial y\partial t}+K_{66}U_y\frac{\partial^3 v}{\partial x^2\partial y}+K_{66}\frac{\partial^3 v}{\partial y^2\partial t}+F_y\\
&= \quad \rho\frac{\partial^2 v}{\partial t^2}+2\rho U_xU_y\frac{\partial^2 v}{\partial x\partial y}+2\rho U_x\frac{\partial^2 v}{\partial x\partial t}+2\rho U_y\frac{\partial^2 v}{\partial y\partial t}\\
&+\rho\frac{\partial v}{\partial x}\left(\frac{\partial U_x}{\partial x}U_x+\frac{\partial U_x}{\partial y}U_y+\frac{\partial U_x}{\partial t}\right)+\rho\frac{\partial v}{\partial y}\left(\frac{\partial U_y}{\partial x}U_x+\frac{\partial U_y}{\partial y}U_y+\frac{\partial U_y}{\partial t}\right)\,,
\end{aligned}\tag{37}$$

where the coefficients are

$$C_{11}=\frac{E_x}{1-\nu_{12}\nu_{21}}\,,\qquad C_{22}=\frac{E_y}{1-\nu_{12}\nu_{21}}\,,\tag{38}$$

$$C_{12}=C_{11}\nu_{21}=C_{22}\nu_{12}=C_{21}\,,\qquad C_{66}=G\,,\tag{39}$$

$$K_{11}=\frac{\eta_x}{1-\varphi_{12}\varphi_{21}}\,,\qquad K_{22}=\frac{\eta_y}{1-\varphi_{12}\varphi_{21}}\,,\tag{40}$$

$$K_{12}=K_{11}\varphi_{21}=K_{22}\varphi_{12}=K_{21}\,,\qquad K_{66}=\Pi\,.\tag{41}$$

The equations (36) and (37) are nonlinear. Nonlinearity appears in the velocities U_x and U_y, which are dependent on the deformation. There are also nonlinear Navier–Stokes type convection terms, the significance of which is small if the strains defined in the equation (23) can be considered small.

4 Steady state of one-dimensional viscoelastic moving continuum

One-dimensional application of the equations (36) and (37) will lead to the following time-dependent solid continuum flow equation [35]:

$$\begin{aligned}
&\rho\frac{\partial^2 u}{\partial t^2}+2\rho U_x\frac{\partial^2 u}{\partial x\partial t}+\rho U_x^2\frac{\partial^2 u}{\partial x^2}+\rho\frac{\partial u}{\partial x}\left(\frac{\partial U_x}{\partial x}U_x+\frac{\partial U_x}{\partial t}\right)\\
&=E_x\frac{\partial^2 u}{\partial x^2}+\eta_x\left(\frac{\partial^3 u}{\partial x^2\partial t}+U_x\frac{\partial^3 u}{\partial x^3}\right)
\end{aligned}\tag{42}$$

In a steady state, where there is no time-dependent fluctuation in the displacement, we can write the following equation for ideal, undisturbed axial narrow web flow:

$$\eta_x U_x \frac{\partial^3 u}{\partial x^3} + \left(E_x - \rho U_x^2\right) \frac{\partial^2 u}{\partial x^2} - \rho \frac{\partial u}{\partial x} \left(\frac{\partial U_x}{\partial x} U_x \right) = 0 \ . \tag{43}$$

In general, equation (43) is nonlinear due to the dependence of U_x on $\partial u/\partial x$. To see how this arises in the one-dimensional case, recall equation (16) and its one-dimensional specialization (18), which were obtained via a mass conservation argument. There are now two possibilities. The strain $\varepsilon_{xx} = \partial u/\partial x$ (equation (23)) either depends on x, or is constant along the span.

Let us first investigate the case where the strain depends on x. This was a starting assumption in the derivation of (18); if it holds, then also (18) holds. Let the velocity U_1 at the beginning of the span be fixed. By rearranging, (18) becomes

$$U_2 = U_1[1 + \varepsilon_{xx}] \ , \tag{44}$$

where we now use the notation ε_{xx} for the strain.

Because mass conservation must hold for any value of x, equation (44) is valid along the whole span, and we have $U_x(x) = U_2(x)$. However, because $\varepsilon_{xx} = \varepsilon_{xx}(x) = (\partial u/\partial x)(x)$ appears on the right-hand side of (44), actually $U_2 = U_2(\varepsilon_{xx})$. Thus, if the strain varies along the span, mass conservation implies that a linear relationship exists between the strain and velocity fields.

Because U_x is now a linear function of ε_{xx}, all terms of (43) involving factors of U_x and its derivatives become nonlinear with respect to the unknown u and its derivatives. Using U_2 from (44) as U_x in (43), we see that the nonlinearity is of a polynomial form; up to cubic terms are present. Numerical FEM solution of the nonlinear equation has been presented in [35].

The other possibility is that the strain is a constant along the whole span, in which case the starting assumption leading to (18) does not hold. On the other hand, a constant value for $\varepsilon_{xx} = \partial u/\partial x$ implies $\partial^2 u/\partial x^2 = \partial^3 u/\partial x^3 \equiv 0$. Let us investigate the nontrivial case where $\varepsilon_{xx} \neq 0$. The first and second terms in equation (43) vanish. Dividing by the nonzero constant strain $\partial u/\partial x$ and the material density $\rho \neq 0$, all that remains is

$$\frac{\partial U_x}{\partial x} U_x = 0 \ . \tag{45}$$

Equation (45) must hold pointwise at any x. Thus for each fixed x, either $\partial U_x/\partial x = 0$ or $U_x = 0$. More interesting of the two is $\partial U_x/\partial x = 0$, which leads to $U_x =$ constant.

We conclude that if a constant strain is observed, this implies that the velocity must also be constant. However, the reverse is not true, as we will see below. The value of the constant strain is determined by the boundary conditions, which were not analyzed here.

For the rest of this section, we again let ε_{xx} vary along the span, concentrating on the special case where U_x is approximately constant:

$$U_x(x) = U_0 + \phi(x) \ . \tag{46}$$

Here U_0 is a constant, and the arbitrary function $\phi(x)$ and its derivatives are considered small. If the strain variable and its derivatives are small, and the velocity field is of the form (44), this representation is applicable. Inserting (46) into (43) and dropping second-order small terms leads to a linear equation, namely

$$\eta_x U_0 \frac{\partial^2 \varepsilon_{xx}}{\partial x^2} + \left(E_x - \rho U_0^2\right) \frac{\partial \varepsilon_{xx}}{\partial x} = 0 \ . \tag{47}$$

To obtain this form, it is not sufficient that ϕ itself is small; also $\partial\phi/\partial x$ must be small to avoid an additional term $-\rho\varepsilon_{xx}[\partial\phi/\partial x]U_0$ on the left-hand side. Observe that equation (47) is exact in the case where U_x is (an exact) constant. Thus any conclusions will apply to cases with exactly constant as well as approximately constant transport velocities.

By comparing the equation (47) and the heat equation in presence of convection (see e.g. [66]):

$$k_T \frac{\partial^2 T}{\partial x^2} - \rho c_p U \frac{\partial T}{\partial x} = 0 \ , \tag{48}$$

where T is the temperature and U is the velocity of the medium, c_p is the specific heat of the object and k_T the heat diffusion coefficient, one can observe great similarity between the two.

The equation (47) can be solved using analytical methods. First, as a special case, if only pure elasticity is present ($\eta_x = 0$), the solution is of the form [35]

$$\left(E_x - \rho U_0^2\right) \varepsilon_{xx} = C \ . \tag{49}$$

In this case the solution describes Hookean behaviour, i.e., the strain ε_{xx} is constant along the whole span regardless of the magnitude of the constant transport velocity U_0. The corresponding stress field, from equation (26) with $\eta_x = 0$ and (49), is also constant:

$$\sigma_x = E_x \varepsilon_{xx} = \frac{E_x C}{(E_x - \rho U_0^2)} \equiv C' \ . \tag{50}$$

The values of the constants C and C' are determined by the boundary conditions. Because (49) is a first-order ordinary differential equation with respect to ε_{xx}, for this variable we may set only one boundary condition. Choosing this boundary condition as $\varepsilon_{xx}(\ell) = \varepsilon_T$, from (49) we have $C = (E_x - \rho U_0^2)\,\varepsilon_T$, which leads to $\varepsilon_{xx}(x) = \varepsilon_T$ (for all x), and for the stress $\sigma_x = E_x \varepsilon_T$. This may seem trivial, but it provides an important point of comparison for the following case.

Consider a material with viscosity $\eta_x \neq 0$. Equation (47) becomes, after division by $\eta_x U_0$,

$$\frac{\partial^2 \varepsilon_{xx}}{\partial x^2} + \left(\frac{E_x - \rho U_0^2}{\eta_x U_0}\right) \frac{\partial \varepsilon_{xx}}{\partial x} = 0 \ . \tag{51}$$

The differential equation is of the second order in ε_{xx}, hence two boundary conditions are required. With the choices $\varepsilon_{xx}(0) = 0$ and $\varepsilon_{xx}(\ell) = \varepsilon_T$, the analytical solution of the equation (51) is [34, 36]:

$$\varepsilon_{xx}(x) = \varepsilon_T \frac{1 - e^{-kx}}{1 - e^{-k\ell}} \ , \qquad \text{where} \quad k = \frac{E_x - \rho U_0^2}{\eta_x U_0} \ . \tag{52}$$

We have thus obtained the following result: for a Kelvin–Voigt viscoelastic material moving at a constant or an approximately constant transport velocity, loaded only by a prescribed strain at the ends of the span, the strain grows logarithmically along the span. This is unlike the case of purely elastic material, where the strain along the span is constant.

As $x \to \ell$, the strain approaches the same value it had in the elastic case, ε_T. Additionally, if ℓ is large, the exponential terms approximately vanish in most of the domain, and the strain approximately obtains its elastic value everywhere except in a short boundary layer at the start of the span. The larger k is, the shorter is the boundary layer. Especially, the boundary layer vanishes in the limits $\eta_x \to 0$ and $U_0 \to 0$, where $k \to \infty$ (see definition of k in equation (52)). This agrees with the elastic solution.

The physical conclusion is that the strain ε_{xx} depends on x only if both the viscosity η_x and the transport velocity U_0 are nonzero. In other words, in the context of this analysis, the effect appears only if the material is both viscoelastic and subjected to axial motion.

Finally, let us find the corresponding stress field. The stress, which is based on the strain in the equation (52), is a superposition of elastic and viscous stress components ([35]; see also equation (26)):

$$\sigma_x = E_x \varepsilon_{xx} + \eta_x \frac{\mathrm{d}\varepsilon_{xx}}{\mathrm{d}t} \ . \tag{53}$$

Straightforward analytical solution of the stress is easy to obtain only in the linearized, one-dimensional, steady-state case having constant transport velocity [35]. Using equations (24) and (25), the time derivative of the strain, in mixed Lagrange–Euler form, can be written for the steady-state solution as follows:

$$\frac{\mathrm{d}\varepsilon_{xx}}{\mathrm{d}t} = \frac{\partial \varepsilon_{xx}}{\partial x} U_x \ . \tag{54}$$

Inserting (54) into (53), using (46) for U_x, noting that both $\partial \varepsilon_{xx}/\partial x$ and $\phi(x)$ are small, and then using the analytical solution (52), we obtain the stress field as

$$\sigma_x = E_x \varepsilon_T \frac{1 - e^{-kx}}{1 - e^{-k\ell}} + \eta_x U_0 \varepsilon_T \frac{k e^{-kx}}{1 - e^{-k\ell}} \ . \tag{55}$$

where the elastic and viscous contributions are apparent. Both contributions follow a logarithmic curve. By expanding the multiplicative factor k in the second term of the equation (55) (using again (52)), the result simplifies to

$$\sigma_x = \frac{\varepsilon_T}{1 - e^{-k\ell}} \left(E_x - \rho U_0^2 e^{-kx} \right) , \tag{56}$$

which shows the total stress more clearly. Equation (56) is valid for $\eta_x \neq 0$, $U_0 \neq 0$. We observe that also the total stress follows a logarithmic curve.

Unlike the strain, the stress remains always slightly smaller than its elastic value $E_x \varepsilon_T$, even near the end of the span as $x \to \ell$. Physically, this observation can be interpreted as a viscous relaxation effect.

For large ℓ, the exponentials again approximately vanish in most of the domain, and the stress approximately obtains its elastic value, except in a short boundary layer at the start of the span. The previous observations regarding k apply also here.

We have thus seen that for a narrow strip of Kelvin–Voigt material moving at a constant or an approximately constant transport velocity, both the strain and stress fields follow a logarithmic shape along the span. This effect appears only if the material is both viscoelastic and subjected to axial motion.

5 The weak form and the natural boundary conditions

In the following, we will concentrate on the two-dimensional, steady-state, purely elastic case. This is obtained from the equations (36) – (37) by omitting time-dependent terms and setting the viscous coefficients to zero.

The aim in the rest of this paper is to numerically study the two-dimensional, orthotropic, elastic moving continuum plane stress problem using the finite element method (FEM). The above approach was extremely useful for the one-dimensional analysis that was performed, but it is difficult to correctly derive the weak form by starting from the equations (36) – (37).

The difficulty arises because the equations contain terms with mixed derivatives, $\partial^2 u/\partial x \partial y$ and $\partial^2 v/\partial x \partial y$. It is not immediately clear how these terms should be considered when applying integration by parts in the component-form equations. Each such mixed term can be integrated by parts in either the x or the y direction, and each such choice will produce different contributions to the natural boundary conditions of the weak problem. Most combinations of choices lead to boundary conditions which make no physical sense, and the correct combination of choices is not obvious.

Hence, we will derive the weak form in cartesian tensor notation. Although in the present study only a rectangular sheet will be studied, this approach provides the additional advantage of arbitrary domain shape. We start with the general dynamic equilibrium equations (30) – (31), rewritten in tensor notation, and then expand the second material derivative. The dynamic equilibrium reads

$$\rho \frac{\mathrm{d}^2 \mathbf{u}}{\mathrm{d}t^2} - \nabla \cdot \boldsymbol{\sigma}^{\mathrm{T}} = \mathbf{F} \ , \tag{57}$$

where $(\dots)^{\mathrm{T}}$ denotes the transpose of a rank-2 tensor. In the case where $\mathbf{U}$ is not time-dependent, the second material derivative expands as

$$\frac{\mathrm{d}^2 \mathbf{u}}{\mathrm{d}t^2} = \frac{\mathrm{d}}{\mathrm{d}t}\left(\frac{\partial \mathbf{u}}{\partial t} + \mathbf{U} \cdot \nabla \mathbf{u}\right) = \frac{\partial^2 \mathbf{u}}{\partial t^2} + 2\mathbf{U} \cdot \nabla \left(\frac{\partial \mathbf{u}}{\partial t}\right) + (\mathbf{U} \cdot \nabla)(\mathbf{U} \cdot \nabla \mathbf{u}) \ . \tag{58}$$

Applying (58), the steady-state form of equation (57) becomes

$$\rho \, (\mathbf{U} \cdot \nabla)(\mathbf{U} \cdot \nabla \mathbf{u}) - \nabla \cdot \boldsymbol{\sigma}^{\mathrm{T}} = \mathbf{F} \ . \tag{59}$$

Next, we will use the principle of virtual work. Let us take the dot product of the equation (59) with a vector-valued test function (virtual displacement) $\boldsymbol{\phi}$, and integrate the equation over the two-dimensional domain

$$\Omega \equiv \{\, (x, y) :\ 0 < x < \ell\,,\ 0 < y < b \,\}\ . \tag{60}$$

We assume that the material density ρ can be approximated as a constant and obtain

$$\rho \int_\Omega \boldsymbol{\phi} \cdot (\mathbf{U} \cdot \nabla)(\mathbf{U} \cdot \nabla \mathbf{u})\ \mathrm{d}\Omega - \int_\Omega \boldsymbol{\phi} \cdot [\nabla \cdot \boldsymbol{\sigma}^{\mathrm{T}}]\ \mathrm{d}\Omega = \int_\Omega \boldsymbol{\phi} \cdot \mathbf{F}\ \mathrm{d}\Omega\ . \tag{61}$$

In order to integrate by parts in the equation (61), we make use of the following two identities:

$$\int_\Omega \boldsymbol{\phi} \cdot [\nabla \cdot \boldsymbol{\sigma}^{\mathrm{T}}]\ \mathrm{d}\Omega = \int_{\partial\Omega} \boldsymbol{\phi} \cdot (\mathbf{n} \cdot \boldsymbol{\sigma}^{\mathrm{T}})\ \mathrm{d}\Gamma - \int_\Omega \nabla\boldsymbol{\phi} : \boldsymbol{\sigma}\ \mathrm{d}\Omega\ , \tag{62}$$

$$\begin{aligned} \int_\Omega \boldsymbol{\phi} \cdot (\mathbf{U} \cdot \nabla)(\mathbf{U} \cdot \nabla \mathbf{u}) &= \int_{\partial\Omega} \mathbf{n} \cdot [(\mathbf{U} \cdot \nabla \mathbf{u}) \cdot (\boldsymbol{\phi} \otimes \mathbf{U})]\ \mathrm{d}\Gamma \\ &\quad - \int_\Omega (\mathbf{U} \cdot \nabla \mathbf{u}) \cdot [\nabla \cdot (\mathbf{U} \otimes \boldsymbol{\phi})]\ \mathrm{d}\Omega\ . \end{aligned} \tag{63}$$

where $\mathbf{n}$ is the outer unit normal, and the notational conventions are

$$(\nabla \mathbf{a})_{ij} \equiv \partial_i a_j\ , \quad (\nabla \cdot \mathbf{A})_j \equiv \partial_i A_{ij} \quad (\mathbf{a} \otimes \mathbf{b})_{ij} = a_i b_j\ , \quad \mathbf{A} : \mathbf{B} \equiv A_{ij} B_{ji}\ . \tag{64}$$

Here $\mathbf{a}$ and $\mathbf{b}$ are vectors, and $\mathbf{A}$ and $\mathbf{B}$ are rank-2 tensors. The summation convention for repeated indices applies. Note the ordering of indices in the gradient.

The integration-by-parts formula (62) is standard in the theory of elasticity; only the formula (63) requires explanation. Observe that for any differentiable vector fields $\mathbf{a}$, $\mathbf{b}$ and $\mathbf{c}$,

$$\nabla \cdot (\mathbf{a} \cdot (\mathbf{b} \otimes \mathbf{c})) = \mathbf{b} \cdot (\mathbf{c} \cdot \nabla \mathbf{a}) + \mathbf{a} \cdot (\nabla \cdot (\mathbf{c} \otimes \mathbf{b}))\ . \tag{65}$$

By integrating the equation (65) over the domain Ω, applying the divergence theorem to the left-hand side, and choosing $\mathbf{a} = (\mathbf{U} \cdot \nabla \mathbf{u})$, $\mathbf{b} = \boldsymbol{\phi}$, and $\mathbf{c} = \mathbf{U}$, relation (63) follows.

Using equations (62) and (63) in (61), we obtain

$$\begin{aligned} &- \rho \int_\Omega (\mathbf{U} \cdot \nabla \mathbf{u}) \cdot [\nabla \cdot (\mathbf{U} \otimes \boldsymbol{\phi})]\ \mathrm{d}\Omega + \int_\Omega \nabla\boldsymbol{\phi} : \boldsymbol{\sigma}\ \mathrm{d}\Omega \\ &+ \rho \int_{\partial\Omega} \mathbf{n} \cdot [(\mathbf{U} \cdot \nabla \mathbf{u}) \cdot (\boldsymbol{\phi} \otimes \mathbf{U})]\ \mathrm{d}\Gamma - \int_{\partial\Omega} \boldsymbol{\phi} \cdot (\mathbf{n} \cdot \boldsymbol{\sigma}^{\mathrm{T}})\ \mathrm{d}\Gamma = \int_\Omega \boldsymbol{\phi} \cdot \mathbf{F}\ \mathrm{d}\Omega\ . \end{aligned} \tag{66}$$

By using the identity

$$\nabla \cdot (\mathbf{U} \otimes \boldsymbol{\phi}) = (\nabla \cdot \mathbf{U})\boldsymbol{\phi} + \mathbf{U} \cdot \nabla\boldsymbol{\phi} \tag{67}$$

and rearranging

$$\boldsymbol{\phi} \cdot (\mathbf{n} \cdot \boldsymbol{\sigma}^{\mathrm{T}}) = (\mathbf{n} \cdot \boldsymbol{\sigma}^{\mathrm{T}}) \cdot \boldsymbol{\phi} = \mathbf{n} \cdot (\boldsymbol{\sigma}^{\mathrm{T}} \cdot \boldsymbol{\phi})\ , \tag{68}$$

we have

$$-\rho\int_\Omega(\mathbf{U}\cdot\nabla\mathbf{u})\cdot[(\nabla\cdot\mathbf{U})\boldsymbol{\phi}+\mathbf{U}\cdot\nabla\boldsymbol{\phi}]\,\mathrm{d}\Omega+\int_\Omega\nabla\boldsymbol{\phi}:\boldsymbol{\sigma}\,\mathrm{d}\Omega$$
$$+\int_{\partial\Omega}\mathbf{n}\cdot\left[\rho\,(\mathbf{U}\cdot\nabla\mathbf{u})\cdot(\boldsymbol{\phi}\otimes\mathbf{U})-\boldsymbol{\sigma}^{\mathrm{T}}\cdot\boldsymbol{\phi}\right]\mathrm{d}\Gamma=\int_\Omega\boldsymbol{\phi}\cdot\mathbf{F}\,\mathrm{d}\Omega\,. \tag{69}$$

We may simplify (69) with

$$(\mathbf{U}\cdot\nabla\boldsymbol{\phi})\cdot(\mathbf{U}\cdot\nabla\mathbf{u})=U_i(\partial_i\phi_j)U_k(\partial_k u_j)=(\partial_i\phi_j)(U_iU_k\partial_k u_j)=\nabla\boldsymbol{\phi}:\left(\mathbf{U}\otimes\mathbf{U}\cdot\nabla\mathbf{u}\right)^{\mathrm{T}}\,, \tag{70}$$

which allows us to combine some terms on the first line:

$$-\rho\int_\Omega\boldsymbol{\phi}\cdot(\mathbf{U}\cdot\nabla\mathbf{u})(\nabla\cdot\mathbf{U})\,\mathrm{d}\Omega+\int_\Omega\nabla\boldsymbol{\phi}:\left[\boldsymbol{\sigma}-\rho\left(\mathbf{U}\otimes\mathbf{U}\cdot\nabla\mathbf{u}\right)^{\mathrm{T}}\right]\mathrm{d}\Omega$$
$$+\int_{\partial\Omega}\mathbf{n}\cdot\left[\rho\,(\mathbf{U}\cdot\nabla\mathbf{u})\cdot(\boldsymbol{\phi}\otimes\mathbf{U})-\boldsymbol{\sigma}^{\mathrm{T}}\cdot\boldsymbol{\phi}\right]\mathrm{d}\Gamma=\int_\Omega\boldsymbol{\phi}\cdot\mathbf{F}\,\mathrm{d}\Omega\,. \tag{71}$$

Finally, observing that

$$\begin{aligned}\mathbf{n}\cdot\big[\,(\mathbf{U}\cdot\nabla\mathbf{u})\cdot(\boldsymbol{\phi}\otimes\mathbf{U})\big]&=(\mathbf{U}\cdot\nabla\mathbf{u})\cdot(\boldsymbol{\phi}\otimes\mathbf{U})\cdot\mathbf{n}=\big((\mathbf{U}\cdot\nabla\mathbf{u})\cdot\boldsymbol{\phi}\big)(\mathbf{U}\cdot\mathbf{n})\\
=(\mathbf{n}\cdot\mathbf{U})\big((\mathbf{U}\cdot\nabla\mathbf{u})\cdot\boldsymbol{\phi}\big)\quad&=(n_iU_i)\big((U_j\partial_ju_k)\phi_k\big)\quad=n_i\big(U_iU_j\partial_ju_k\big)\phi_k\\
=\mathbf{n}\cdot\big(\mathbf{U}\otimes\mathbf{U}\cdot\nabla\mathbf{u}\big)\cdot\boldsymbol{\phi}\quad&=\boldsymbol{\phi}\cdot\big(\mathbf{U}\otimes\mathbf{U}\cdot\nabla\mathbf{u}\big)^{\mathrm{T}}\cdot\mathbf{n}\end{aligned} \tag{72}$$

we obtain the result

$$-\rho\int_\Omega\boldsymbol{\phi}\cdot(\mathbf{U}\cdot\nabla\mathbf{u})(\nabla\cdot\mathbf{U})\,\mathrm{d}\Omega+\int_\Omega\nabla\boldsymbol{\phi}:\left[\boldsymbol{\sigma}-\rho\left(\mathbf{U}\otimes\mathbf{U}\cdot\nabla\mathbf{u}\right)^{\mathrm{T}}\right]\mathrm{d}\Omega$$
$$+\int_{\partial\Omega}\boldsymbol{\phi}\cdot\left[-\boldsymbol{\sigma}+\rho\,(\mathbf{U}\otimes\mathbf{U}\cdot\nabla\mathbf{u})^{\mathrm{T}}\right]\cdot\mathbf{n}\,\mathrm{d}\Gamma=\int_\Omega\boldsymbol{\phi}\cdot\mathbf{F}\,\mathrm{d}\Omega\,. \tag{73}$$

Equation (73) holds for the steady-state in-plane equilibrium of any sheet of travelling material, as long as ρ is approximately constant. We will apply the material model later.

We see from the equation (73) that if $\nabla\cdot\mathbf{U}=0$, then the first term vanishes. In such a case, the equations have the same form as those of a stationary membrane, but now the stresses obtain contributions (both inside the domain and on the traction boundaries) from the additional term involving velocity. However, if the velocity field has nonzero divergence, then no such analogy can be drawn.

The boundary term of the equation (73) gives the natural boundary conditions for this problem. The natural quantity to be prescribed is the normal component of the following rank-2 tensor:

$$\boldsymbol{\sigma}_{\text{eff}}\equiv\boldsymbol{\sigma}-\rho\,(\mathbf{U}\otimes\mathbf{U}\cdot\nabla\mathbf{u})^{\mathrm{T}}\,. \tag{74}$$

This can be interpreted as an effective stress tensor, where the apparent stress (in laboratory coordinates) is modified by the centrifugal inertial effect.

6 Component form of the weak form

For convenience of software implementation, let us split equation (73) into component form. Let us denote the components of the virtual displacement as $\boldsymbol{\phi} \equiv (\phi, \psi)$. In the two-dimensional case being investigated in the present study, equation (73) gives the two equations

$$\begin{aligned}
&\int_\Omega \left[-\sigma_x + \rho U_x^2 \frac{\partial u}{\partial x} + \rho U_y U_x \frac{\partial u}{\partial y} \right] \frac{\partial \phi}{\partial x} \, \mathrm{d}\Omega \\
&+ \int_\Omega \left[-\tau_{xy} + \rho U_x U_y \frac{\partial u}{\partial x} + \rho U_y^2 \frac{\partial u}{\partial y} \right] \frac{\partial \phi}{\partial y} \, \mathrm{d}\Omega \\
&+ \rho \int_\Omega \left\{ \left[U_x \frac{\partial u}{\partial x} + U_y \frac{\partial u}{\partial y} \right] \left[\frac{\partial U_x}{\partial x} + \frac{\partial U_y}{\partial y} \right] \right\} \phi \, \mathrm{d}\Omega \\
&+ \int_{\partial\Omega} n_x \left[\sigma_x - \rho U_x^2 \frac{\partial u}{\partial x} - \rho U_y U_x \frac{\partial u}{\partial y} \right] \phi \, \mathrm{d}\Gamma \\
&+ \int_{\partial\Omega} n_y \left[\tau_{xy} - \rho U_x U_y \frac{\partial u}{\partial x} - \rho U_y^2 \frac{\partial u}{\partial y} \right] \phi \, \mathrm{d}\Gamma \\
&+ \int_\Omega F_x \phi = 0 \, .
\end{aligned} \tag{75}$$

and

$$\begin{aligned}
&\int_\Omega \left[-\tau_{yx} + \rho U_x^2 \frac{\partial v}{\partial x} + \rho U_y U_x \frac{\partial v}{\partial y} \right] \frac{\partial \psi}{\partial x} \, \mathrm{d}\Omega \\
&+ \int_\Omega \left[-\sigma_y + \rho U_x U_y \frac{\partial v}{\partial x} + \rho U_y^2 \frac{\partial v}{\partial y} \right] \frac{\partial \psi}{\partial y} \, \mathrm{d}\Omega \\
&+ \rho \int_\Omega \left\{ \left[U_x \frac{\partial v}{\partial x} + U_y \frac{\partial v}{\partial y} \right] \left[\frac{\partial U_x}{\partial x} + \frac{\partial U_y}{\partial y} \right] \right\} \psi \, \mathrm{d}\Omega \\
&+ \int_{\partial\Omega} n_x \left[\tau_{yx} - \rho U_x^2 \frac{\partial v}{\partial x} - \rho U_y U_x \frac{\partial v}{\partial y} \right] \psi \, \mathrm{d}\Gamma \\
&+ \int_{\partial\Omega} n_y \left[\sigma_y - \rho U_x U_y \frac{\partial v}{\partial x} - \rho U_y^2 \frac{\partial v}{\partial y} \right] \psi \, \mathrm{d}\Gamma \\
&+ \int_\Omega F_y \psi = 0 \, ,
\end{aligned} \tag{76}$$

where the outer unit normal $\mathbf{n}$ has components $\mathbf{n} = (n_x \, , n_y \,)$. We have moved all terms to the left-hand side and multiplied each equation by -1.

Equations (75) – (76) represent the steady state in-plane equilibrium for any sheet of moving material. We obtain the equations for the orthotropic Kelvin–Voigt material by inserting the viscoelastic stress-strain relations (27) – (29). Then, we insert the mixed Lagrange–Euler representations (25) for the material derivative in the viscous

terms, and restrict the inserted terms to the steady state ($\partial/\partial t \to 0$). The result is

$$\begin{aligned}
\int_\Omega \Bigg[&- \left[C_{11}\varepsilon_{xx} + K_{11}(U_x\frac{\partial \varepsilon_{xx}}{\partial x} + U_y\frac{\partial \varepsilon_{xx}}{\partial y}) + C_{12}\varepsilon_{yy} + K_{12}(U_x\frac{\partial \varepsilon_{yy}}{\partial x} + U_y\frac{\partial \varepsilon_{yy}}{\partial y}) \right] \\
&\qquad + \rho U_x^2\frac{\partial u}{\partial x} + \rho U_y U_x\frac{\partial u}{\partial y} \Bigg] \frac{\partial \phi}{\partial x}\,\mathrm{d}\Omega \\
+ \int_\Omega \Bigg[&- \left[C_{66}\gamma_{xy} + K_{66}(U_x\frac{\partial \gamma_{xy}}{\partial x} + U_y\frac{\partial \gamma_{xy}}{\partial y}) \right] + \rho U_x U_y\frac{\partial u}{\partial x} + \rho U_y^2\frac{\partial u}{\partial y} \Bigg] \frac{\partial \phi}{\partial y}\,\mathrm{d}\Omega \\
&\qquad + \rho \int_\Omega \left\{ \left[U_x\frac{\partial u}{\partial x} + U_y\frac{\partial u}{\partial y} \right] \left[\frac{\partial U_x}{\partial x} + \frac{\partial U_y}{\partial y} \right] \right\} \phi\,\mathrm{d}\Omega \\
+ \int_{\partial\Omega} n_x \Bigg[&\left[C_{11}\varepsilon_{xx} + K_{11}(U_x\frac{\partial \varepsilon_{xx}}{\partial x} + U_y\frac{\partial \varepsilon_{xx}}{\partial y}) + C_{12}\varepsilon_{yy} + K_{12}(U_x\frac{\partial \varepsilon_{yy}}{\partial x} + U_y\frac{\partial \varepsilon_{yy}}{\partial y}) \right] \\
&\qquad - \rho U_x^2\frac{\partial u}{\partial x} - \rho U_y U_x\frac{\partial u}{\partial y} \Bigg] \phi\,\mathrm{d}\Gamma \\
+ \int_{\partial\Omega} n_y \Bigg[&\left[C_{66}\gamma_{xy} + K_{66}(U_x\frac{\partial \gamma_{xy}}{\partial x} + U_y\frac{\partial \gamma_{xy}}{\partial y}) \right] - \rho U_x U_y\frac{\partial u}{\partial x} - \rho U_y^2\frac{\partial u}{\partial y} \Bigg] \phi\,\mathrm{d}\Gamma \\
&\qquad + \int_\Omega F_x\phi\,\mathrm{d}\Omega = 0
\end{aligned} \tag{77}$$

and

$$\begin{aligned}
&\int_\Omega \Bigg[- \left[C_{66}\gamma_{xy} + K_{66}(U_x\frac{\partial \gamma_{xy}}{\partial x} + U_y\frac{\partial \gamma_{xy}}{\partial y}) \right] + \rho U_x^2\frac{\partial v}{\partial x} + \rho U_y U_x\frac{\partial v}{\partial y} \Bigg] \frac{\partial \psi}{\partial x}\,\mathrm{d}\Omega \\
+ \int_\Omega \Bigg[&- \left[C_{21}\varepsilon_{xx} + K_{21}(U_x\frac{\partial \varepsilon_{xx}}{\partial x} + U_y\frac{\partial \varepsilon_{xx}}{\partial y}) + C_{22}\varepsilon_{yy} + K_{22}(U_x\frac{\partial \varepsilon_{yy}}{\partial x} + U_y\frac{\partial \varepsilon_{yy}}{\partial y}) \right] \\
&\qquad + \rho U_x U_y\frac{\partial v}{\partial x} + \rho U_y^2\frac{\partial v}{\partial y} \Bigg] \frac{\partial \psi}{\partial y}\,\mathrm{d}\Omega \\
&\qquad + \rho \int_\Omega \left\{ \left[U_x\frac{\partial v}{\partial x} + U_y\frac{\partial v}{\partial y} \right] \left[\frac{\partial U_x}{\partial x} + \frac{\partial U_y}{\partial y} \right] \right\} \psi\,\mathrm{d}\Omega \\
+ \int_{\partial\Omega} n_x \Bigg[&\left[C_{66}\gamma_{xy} + K_{66}(U_x\frac{\partial \gamma_{xy}}{\partial x} + U_y\frac{\partial \gamma_{xy}}{\partial y}) \right] - \rho U_x^2\frac{\partial v}{\partial x} - \rho U_y U_x\frac{\partial v}{\partial y} \Bigg] \psi\,\mathrm{d}\Gamma \\
+ \int_{\partial\Omega} n_y \Bigg[&\left[C_{21}\varepsilon_{xx} + K_{21}(U_x\frac{\partial \varepsilon_{xx}}{\partial x} + U_y\frac{\partial \varepsilon_{xx}}{\partial y}) + C_{22}\varepsilon_{yy} + K_{22}(U_x\frac{\partial \varepsilon_{yy}}{\partial x} + U_y\frac{\partial \varepsilon_{yy}}{\partial y}) \right] \\
&\qquad - \rho U_x U_y\frac{\partial v}{\partial x} - \rho U_y^2\frac{\partial v}{\partial y} \Bigg] \psi\,\mathrm{d}\Gamma \\
&\qquad + \int_\Omega F_y\psi\,\mathrm{d}\Omega = 0\,.
\end{aligned} \tag{78}$$

Finally, by inserting into (77) and (78) the definitions of the Cauchy strains from (23), the weak form component equations for FEM implementation are obtained.

The final result is

$$\begin{aligned}
&\int_\Omega \Bigg[- \left[C_{11}\frac{\partial u}{\partial x} + K_{11}(U_x\frac{\partial^2 u}{\partial x^2} + U_y\frac{\partial^2 u}{\partial x \partial y}) + C_{12}\frac{\partial v}{\partial y} + K_{12}(U_x\frac{\partial^2 v}{\partial x \partial y} + U_y\frac{\partial^2 v}{\partial y^2}) \right] \\
&\qquad + \rho U_x^2 \frac{\partial u}{\partial x} + \rho U_y U_x \frac{\partial u}{\partial y} \Bigg] \frac{\partial \phi}{\partial x} \, \mathrm{d}\Omega \\
&+ \int_\Omega \Bigg[- \left[C_{66}(\frac{\partial u}{\partial y} + \frac{\partial v}{\partial x}) + K_{66}(U_x(\frac{\partial^2 u}{\partial x \partial y} + \frac{\partial^2 v}{\partial x^2}) + U_y(\frac{\partial^2 u}{\partial y^2} + \frac{\partial^2 v}{\partial x \partial y})) \right] \\
&\qquad + \rho U_x U_y \frac{\partial u}{\partial x} + \rho U_y^2 \frac{\partial u}{\partial y} \Bigg] \frac{\partial \phi}{\partial y} \, \mathrm{d}\Omega \\
&\qquad + \rho \int_\Omega \left\{ \left[U_x \frac{\partial u}{\partial x} + U_y \frac{\partial u}{\partial y} \right] \left[\frac{\partial U_x}{\partial x} + \frac{\partial U_y}{\partial y} \right] \right\} \phi \, \mathrm{d}\Omega \\
&+ \int_{\partial\Omega} n_x \Bigg[\left[C_{11}\frac{\partial u}{\partial x} + K_{11}(U_x\frac{\partial^2 u}{\partial x^2} + U_y\frac{\partial^2 u}{\partial x \partial y}) + C_{12}\frac{\partial v}{\partial y} + K_{12}(U_x\frac{\partial^2 v}{\partial x \partial y} + U_y\frac{\partial^2 v}{\partial y^2}) \right] \\
&\qquad - \rho U_x^2 \frac{\partial u}{\partial x} - \rho U_y U_x \frac{\partial u}{\partial y} \Bigg] \phi \, \mathrm{d}\Gamma \\
&+ \int_{\partial\Omega} n_y \Bigg[\left[C_{66}(\frac{\partial u}{\partial y} + \frac{\partial v}{\partial x}) + K_{66}(U_x(\frac{\partial^2 u}{\partial x \partial y} + \frac{\partial^2 v}{\partial x^2}) + U_y(\frac{\partial^2 u}{\partial y^2} + \frac{\partial^2 v}{\partial x \partial y})) \right] \\
&\qquad - \rho U_x U_y \frac{\partial u}{\partial x} - \rho U_y^2 \frac{\partial u}{\partial y} \Bigg] \phi \, \mathrm{d}\Gamma + \int_\Omega F_x \phi \, \mathrm{d}\Omega = 0
\end{aligned} \tag{79}$$

and

$$\begin{aligned}
&\int_\Omega \Bigg[- \left[C_{66}(\frac{\partial u}{\partial y} + \frac{\partial v}{\partial x}) + K_{66}(U_x(\frac{\partial^2 u}{\partial x \partial y} + \frac{\partial^2 v}{\partial x^2}) + U_y(\frac{\partial^2 u}{\partial y^2} + \frac{\partial^2 v}{\partial x \partial y})) \right] \\
&\qquad + \rho U_x^2 \frac{\partial v}{\partial x} + \rho U_y U_x \frac{\partial v}{\partial y} \Bigg] \frac{\partial \psi}{\partial x} \, \mathrm{d}\Omega \\
&+ \int_\Omega \Bigg[- \left[C_{21}\frac{\partial u}{\partial x} + K_{21}(U_x\frac{\partial^2 u}{\partial x^2} + U_y\frac{\partial^2 u}{\partial x \partial y}) + C_{22}\varepsilon_{yy} + K_{22}(U_x\frac{\partial^2 v}{\partial x \partial y} + U_y\frac{\partial^2 v}{\partial y^2}) \right] \\
&\qquad + \rho U_x U_y \frac{\partial v}{\partial x} + \rho U_y^2 \frac{\partial v}{\partial y} \Bigg] \frac{\partial \psi}{\partial y} \, \mathrm{d}\Omega \\
&\qquad + \rho \int_\Omega \left\{ \left[U_x \frac{\partial v}{\partial x} + U_y \frac{\partial v}{\partial y} \right] \left[\frac{\partial U_x}{\partial x} + \frac{\partial U_y}{\partial y} \right] \right\} \psi \, \mathrm{d}\Omega \\
&+ \int_{\partial\Omega} n_x \Bigg[\left[C_{66}(\frac{\partial u}{\partial y} + \frac{\partial v}{\partial x}) + K_{66}(U_x(\frac{\partial^2 u}{\partial x \partial y} + \frac{\partial^2 v}{\partial x^2}) + U_y(\frac{\partial^2 u}{\partial y^2} + \frac{\partial^2 v}{\partial x \partial y})) \right] \\
&\qquad - \rho U_x^2 \frac{\partial v}{\partial x} - \rho U_y U_x \frac{\partial v}{\partial y} \Bigg] \psi \, \mathrm{d}\Gamma \\
&+ \int_{\partial\Omega} n_y \Bigg[\left[C_{21}\frac{\partial u}{\partial x} + K_{21}(U_x\frac{\partial^2 u}{\partial x^2} + U_y\frac{\partial^2 u}{\partial x \partial y}) + C_{22}\frac{\partial v}{\partial y} + K_{22}(U_x\frac{\partial^2 v}{\partial x \partial y} + U_y\frac{\partial^2 v}{\partial y^2}) \right] \\
&\qquad - \rho U_x U_y \frac{\partial v}{\partial x} - \rho U_y^2 \frac{\partial v}{\partial y} \Bigg] \psi \, \mathrm{d}\Gamma + \int_\Omega F_y \psi \, \mathrm{d}\Omega = 0 \, .
\end{aligned} \tag{80}$$

Equations (79) – (80) represent the weak form of the classical strong form equations (36) – (37), when consideration is restricted to the steady state.

We see that the weak form contains second derivatives in the viscous terms. Thus, to enforce integrability (see e.g. [28]), C1 continuity of basis functions across element boundaries is required in the viscoelastic case.

The corresponding pure elastic equations are obtained by setting $K_{11} = K_{12} = K_{21} = K_{22} = K_{66} = 0$. Explicitly, we have

$$\begin{aligned}
&\int_\Omega \left[-\left[C_{11}\frac{\partial u}{\partial x} + C_{12}\frac{\partial v}{\partial y} \right] + \rho U_x^2 \frac{\partial u}{\partial x} + \rho U_y U_x \frac{\partial u}{\partial y} \right] \frac{\partial \phi}{\partial x}\, \mathrm{d}\Omega \\
&+ \int_\Omega \left[-\left[C_{66}(\frac{\partial u}{\partial y} + \frac{\partial v}{\partial x}) \right] + \rho U_x U_y \frac{\partial u}{\partial x} + \rho U_y^2 \frac{\partial u}{\partial y} \right] \frac{\partial \phi}{\partial y}\, \mathrm{d}\Omega \\
&+ \rho \int_\Omega \left\{ \left[U_x \frac{\partial u}{\partial x} + U_y \frac{\partial u}{\partial y} \right] \left[\frac{\partial U_x}{\partial x} + \frac{\partial U_y}{\partial y} \right] \right\} \phi\, \mathrm{d}\Omega \\
&+ \int_{\partial\Omega} n_x \left[\left[C_{11}\frac{\partial u}{\partial x} + C_{12}\frac{\partial v}{\partial y} \right] - \rho U_x^2 \frac{\partial u}{\partial x} - \rho U_y U_x \frac{\partial u}{\partial y} \right] \phi\, \mathrm{d}\Gamma \\
&+ \int_{\partial\Omega} n_y \left[\left[C_{66}(\frac{\partial u}{\partial y} + \frac{\partial v}{\partial x}) \right] - \rho U_x U_y \frac{\partial u}{\partial x} - \rho U_y^2 \frac{\partial u}{\partial y} \right] \phi\, \mathrm{d}\Gamma \\
&+ \int_\Omega F_x \phi\, \mathrm{d}\Omega = 0
\end{aligned} \tag{81}$$

and

$$\begin{aligned}
&\int_\Omega \left[-\left[C_{66}(\frac{\partial u}{\partial y} + \frac{\partial v}{\partial x}) \right] + \rho U_x^2 \frac{\partial v}{\partial x} + \rho U_y U_x \frac{\partial v}{\partial y} \right] \frac{\partial \psi}{\partial x}\, \mathrm{d}\Omega \\
&+ \int_\Omega \left[-\left[C_{21}\frac{\partial u}{\partial x} + C_{22}\frac{\partial v}{\partial y} \right] + \rho U_x U_y \frac{\partial v}{\partial x} + \rho U_y^2 \frac{\partial v}{\partial y} \right] \frac{\partial \psi}{\partial y}\, \mathrm{d}\Omega \\
&+ \rho \int_\Omega \left\{ \left[U_x \frac{\partial v}{\partial x} + U_y \frac{\partial v}{\partial y} \right] \left[\frac{\partial U_x}{\partial x} + \frac{\partial U_y}{\partial y} \right] \right\} \psi\, \mathrm{d}\Omega \\
&+ \int_{\partial\Omega} n_x \left[\left[C_{66}(\frac{\partial u}{\partial y} + \frac{\partial v}{\partial x}) \right] - \rho U_x^2 \frac{\partial v}{\partial x} - \rho U_y U_x \frac{\partial v}{\partial y} \right] \psi\, \mathrm{d}\Gamma \\
&+ \int_{\partial\Omega} n_y \left[\left[C_{21}\frac{\partial u}{\partial x} + C_{22}\frac{\partial v}{\partial y} \right] - \rho U_x U_y \frac{\partial v}{\partial x} - \rho U_y^2 \frac{\partial v}{\partial y} \right] \psi\, \mathrm{d}\Gamma \\
&+ \int_\Omega F_y \psi\, \mathrm{d}\Omega = 0\ .
\end{aligned} \tag{82}$$

Equations (81) and (82) are the basis of the two-dimensional solutions presented in this article. Only first derivatives of the displacements are needed. Hence, C0 finite elements are sufficient.

Once a basis is chosen for u and v, it is straightforward to insert the Galerkin representation of both displacement variables into (81) and (82). Then, considering that the virtual displacement $\boldsymbol{\phi}$ is arbitrary, we use the basis functions of u as the test functions ϕ and the basis functions of v as the test functions ψ, obtaining the discrete equation system for the classical Galerkin method. Essential and natural boundary conditions are then applied as usual.

If the velocity field is divergence-free, we may omit the third line in both equations, and the velocity can be allowed to have finite discontinuities across element boundaries. In all other cases, the velocity field must have C0 continuity across element boundaries, in order to enforce integrability of (81) – (82). This is because the terms on the third line of both equations follow directly from the weak form of the problem, and thus cannot be applied only in element interiors (as is done e.g. when second derivatives appear in certain numerical stabilization schemes for flow problems; see e.g. [16]).

7 Coupling between drive velocity and in-plane displacement

If some edges of the domain are free, the velocity field driving the material may cause them to move. Each free edge will move until the velocity field becomes tangential to it. For small deformations, it is possible to avoid deforming the mesh, and still account for the slightly changed direction of the free edges by using approximate methods.

When free edges are present, the effective velocity field in the material is a priori unknown. In a sense, the driving velocity field modifies itself when the free edge deformations are taken into account. Thus, instead of taking $\mathbf{U}$ as a prescribed external velocity, this quantity may be redefined to fulfill two tasks. First, it will still be based on the driving velocity field, but secondly, the modified $\mathbf{U}$ will also take into account the small deformations in the free edges, including the effect that the free edge deformations have on the effective velocity field inside the domain.

We will use a deformation-based approach. Consider the differential plane element in the small-displacement regime. See Figure 6. The original, undeformed edges are given by the vectors $\mathbf{x} = (\mathrm{d}x, 0)$ and $\mathbf{y} = (0, \mathrm{d}y)$. After deformation by a displacement field $\mathbf{u} = (u, v)$, these edges become (with the help of a first-order

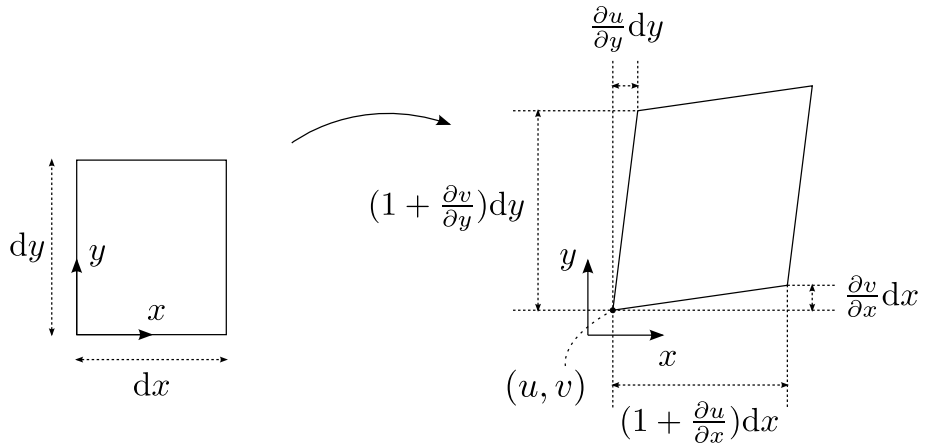

Figure 6: Small deformation of a differential plane element.

two-dimensional Taylor expansion of each of the fields u and v)

$$\tilde{\mathbf{x}} = \left((1 + \frac{\partial u}{\partial x})\mathrm{d}x,\ \frac{\partial v}{\partial x}\mathrm{d}x \right) , \quad \tilde{\mathbf{y}} = \left(\frac{\partial u}{\partial y}\mathrm{d}y,\ (1 + \frac{\partial v}{\partial y})\mathrm{d}y \right) . \tag{83}$$

The projection

$$\mathbf{u_X} = \mathbf{M} \cdot \mathbf{u_x} , \tag{84}$$

that is,

$$\begin{bmatrix} u_X \\ u_Y \end{bmatrix} = \begin{bmatrix} \hat{\mathbf{x}} \cdot \hat{\mathbf{X}} & \hat{\mathbf{y}} \cdot \hat{\mathbf{X}} \\ \hat{\mathbf{x}} \cdot \hat{\mathbf{Y}} & \hat{\mathbf{y}} \cdot \hat{\mathbf{Y}} \end{bmatrix} \begin{bmatrix} u_x \\ u_y \end{bmatrix} , \tag{85}$$

transforms any vector field $\mathbf{u}$ given in $\mathbf{x} = (x, y)$ components into $\mathbf{X} = (X, Y)$ components. Here $\hat{\mathbf{x}}$ and $\hat{\mathbf{y}}$ (respectively $\hat{\mathbf{X}}$ and $\hat{\mathbf{Y}}$) are the unit vectors giving the directions of the axes of the (x, y) (respectively (X, Y)) coordinate systems. The boldface subscript denotes which coordinate system the quantity is given in, and the plain subscripts denote components.

We choose

$$\hat{\mathbf{X}} := (1, 0) , \quad \hat{\mathbf{Y}} := (0, 1) , \tag{86}$$

and take $\hat{\mathbf{x}}$ and $\hat{\mathbf{y}}$ as the unit vectors corresponding to the edges of the deformed differential element:

$$\hat{\mathbf{x}} := \tilde{\mathbf{x}} / \left\| \tilde{\mathbf{x}} \right\| , \quad \hat{\mathbf{y}} := \tilde{\mathbf{y}} / \left\| \tilde{\mathbf{y}} \right\| . \tag{87}$$

Here $\| \ldots \|$ denotes the euclidean norm.

Now, instead of prescribing the velocity field $\mathbf{U_X}$, we prescribe $\mathbf{U_x}$ (along the deformed coordinate directions), and then project it to the capital-$\mathbf{X}$ axes using (85). Then we set $\mathbf{U} = \mathbf{U_X}$ in equations (81) – (82).

Using (85) – (87), we obtain the corrected velocity components as

$$\begin{aligned} U_X &= (\hat{\mathbf{x}} \cdot \hat{\mathbf{X}})\, U_x + (\hat{\mathbf{y}} \cdot \hat{\mathbf{X}})\, U_y = \hat{x}_1 U_x + \hat{y}_1 U_y , \\ U_Y &= (\hat{\mathbf{x}} \cdot \hat{\mathbf{Y}})\, U_x + (\hat{\mathbf{y}} \cdot \hat{\mathbf{Y}})\, U_y = \hat{x}_2 U_x + \hat{y}_2 U_y . \end{aligned} \tag{88}$$

Here $\hat{x}_j$ denotes the jth component of the vector $\hat{\mathbf{x}}$, and we have used (86).

If consider not only direction changes, but also length changes, of the reference vectors (that were originally unit vectors), it is possible to use

$$\hat{\mathbf{x}} := \tilde{\mathbf{x}} / \mathrm{d}x , \quad \hat{\mathbf{y}} := \tilde{\mathbf{y}} / \mathrm{d}y . \tag{89}$$

instead of (87), using the fact that the original lengths of the sides of the differential element were $\mathrm{d}x$ and $\mathrm{d}y$. In this case, we obtain

$$\begin{aligned} U_X &= \hat{x}_1 U_x + \hat{y}_1 U_y = (1 + \frac{\partial u}{\partial x}) U_x + \frac{\partial u}{\partial y} U_y , \\ U_Y &= \hat{x}_2 U_x + \hat{y}_2 U_y = \frac{\partial v}{\partial x} U_x + (1 + \frac{\partial v}{\partial y}) U_y . \end{aligned} \tag{90}$$

Then, up to first order, the deformed reference vector lengths (squared) are

$$\begin{aligned} \|\hat{\mathbf{x}}\|^2 &= (1+\frac{\partial u}{\partial x})^2 + (\frac{\partial v}{\partial x})^2 \approx 1 + 2\frac{\partial u}{\partial x} \,, \\ \|\hat{\mathbf{y}}\|^2 &= (\frac{\partial u}{\partial y})^2 + (1+\frac{\partial v}{\partial y})^2 \approx 1 + 2\frac{\partial v}{\partial y} \,. \end{aligned} \tag{91}$$

In case of pure axial input flow, $U_x = U_{\text{in}}$ and $U_y = 0$, we have

$$\begin{aligned} U_X &= (1+\frac{\partial u}{\partial x})U_{\text{in}} \,, \\ U_Y &= \frac{\partial v}{\partial x}U_{\text{in}} \,. \end{aligned} \tag{92}$$

In the present study, equations (92) have been used for computing the velocity field $\mathbf{U_X}$.

Note that the corrections (88) and (90) make the effective velocity field $\mathbf{U_X}$ space-dependent, even if the original input $\mathbf{U_x}$ is not, due to the space dependence of $\mathbf{u}$. Hence, we cannot assume $\mathbf{U}$ to be constant; terms involving its derivatives must thus be retained in the equations.

Regardless of whether one uses (88) or (90), the corrected velocity field will violate mass conservation, because the calculation is based on geometric considerations only. Thus, a correction is required to preserve mass. We will need two different approaches depending on whether the material is compressible.

For a compressible material, we may use the mass conservation equation (1) to compute the velocity field inside the domain, using in boundary conditions the edge data for the normal component (in (X, Y) coordinates) of the proposed velocity given by (88) or (90).

To do this, one can view the mass conservation equation as diffusion of velocity potential. Assume that the velocity field is irrotational ($\nabla \times \mathbf{v} = 0$); this is reasonable for steady state flow of a solid. In a steady state, $\partial\rho/\partial t = 0$. We have

$$\nabla \cdot (\rho \mathbf{v}) = 0 \,. \tag{93}$$

After multiplication by a test function χ, integrating over the domain Ω, and applying the divergence theorem, we have the weak form

$$\int_{\partial\Omega} (\mathbf{n}\cdot\mathbf{v})\,\rho\,\chi \,\mathrm{d}\Gamma - \int_{\Omega} \rho\,\nabla\chi\cdot\mathbf{v} \,\mathrm{d}\Omega = 0 \,. \tag{94}$$

Note that here ρ does not need to be constant. Next, let us use the fact that an irrotational vector field has a scalar potential:

$$\mathbf{v} = \nabla V \,, \tag{95}$$

where V is a scalar-valued function. Inserting (95) into (94) obtains

$$\int_{\partial\Omega} (\mathbf{n}\cdot\nabla V)\,\rho\,\chi \,\mathrm{d}\Gamma - \int_{\Omega} \rho\,\nabla\chi\cdot\nabla V \,\mathrm{d}\Omega = 0 \,. \tag{96}$$

which is a steady-state diffusion equation (Poisson equation) for the velocity potential V. The natural boundary condition is

$$(\mathbf{n} \cdot \nabla V)\rho = q \ , \tag{97}$$

i.e. one can prescribe the normal component of mass flow as a known function q. Hence, if the density at the edge is known, it is possible to prescribe the normal component of velocity there, via use of the natural boundary condition.

Recall equation (7), which gives density in terms of the axial strains, which in turn are easily obtained from the displacements via equations (23). Thus the density field can be computed once the displacements are known. Any C0 elements can be used for representing V.

By computation of the scalar potential V, the tangential velocity component at the edges will adjust itself such that mass balance is satisfied. Furthermore, the computed velocity field ∇V inside the domain will also satisfy mass balance.

Because we have a Poisson problem with purely natural boundary conditions, the solution V is unique only up to an arbitrary additive constant. This can be remedied by standard techniques. One that is easy to implement is to add a small reaction term $\int_\Omega \epsilon \, \chi \, V \ \mathrm{d}\Omega$ to the left-hand side of (96), where ϵ is a small constant (e.g. $\epsilon = 10^{-8}$).

In the case of an incompressible material, in the steady state the mass conservation equation (1) becomes simply $\nabla \cdot \mathbf{v} = 0$, i.e., the velocity field of an incompressible material must be divergence-free.

Therefore, in this case we simply compute the divergence-free projection of the proposed velocity field (88) or (90). The projection can be obtained using the standard trick based on Helmholtz decomposition. For completeness, let us review this briefly. Let $\mathbf{U}_e$ be the expected velocity field before the correction for mass conservation. Define a scalar potential p such that

$$\Delta p = \nabla \cdot \mathbf{U}_e \ . \tag{98}$$

Since the laplacian $\Delta(\dots) \equiv \nabla \cdot \nabla(\dots)$, equation (98) is equivalent with

$$\nabla \cdot \nabla p = \nabla \cdot \mathbf{U}_e \ . \tag{99}$$

By rearranging terms, we have

$$\nabla \cdot (\mathbf{U}_e - \nabla p) = 0 \ , \tag{100}$$

i.e. the difference $\mathbf{U}_e - \nabla p$ is divergence-free. Define the final velocity field as

$$\mathbf{U} = \mathbf{U}_e - \nabla p \ . \tag{101}$$

Then $\mathbf{U}$ is the divergence-free projection of $\mathbf{U}_e$. As the boundary conditions, one may require

$$\mathbf{n} \cdot \nabla p = 0 \tag{102}$$

on all boundaries. This ensures that the normal component of the correction ∇p vanishes at the boundaries. The solution will then adjust the tangential component at the boundaries to enforce the divergence-free property there; in the interior of the domain, both components are allowed to change.

Again, we have a Poisson problem with purely natural boundary conditions, and thus the solution p is unique only up to an arbitrary additive constant. This can be worked around as above. Let ϵ be a small constant, e.g. $\epsilon = 10^{-8}$. The final weak form of the projection problem is

$$-\int_\Omega \nabla p \cdot \nabla \chi \, \mathrm{d}\Omega + \epsilon \int_\Omega p \, \chi \, \mathrm{d}\Omega + \int_{\partial\Omega} (\mathbf{n} \cdot \nabla p) \chi \, \mathrm{d}\Gamma = \int_\Omega (\nabla \cdot \mathbf{U}_e) \chi \, \mathrm{d}\Omega \,, \tag{103}$$

where χ is a test function. Any C0 elements can be used for representing p.

Strictly speaking, if $\mathbf{u}$ is represented by C0 elements, the divergence of $\mathbf{U}_e$ (which depends on the second derivatives of $\mathbf{u}$) is not integrable due to singularities at the element boundaries. However, the right-hand side of (99) is basically arbitrary, as is also the velocity field $\mathbf{U}$ when viewed as input to (81) – (82). The only requirement is that either $\nabla \cdot \mathbf{U} \equiv 0$, or alternatively, that $\nabla \cdot \mathbf{U}$ is integrable. Thus, we may choose to omit the singularities when defining the auxiliary quantity p by (99); any practical solver code will then see $\mathbf{U} = \mathbf{U}_e - \nabla p$ as a divergence-free velocity field.

This also has implications for the compressible case treated further above. There, nonzero divergence was allowed for the velocity field (via local variations in density). Now, however, the divergence of the velocity field is present in the original equations (81) – (82) themselves, and we cannot ignore singularities if we are to represent the problem correctly. If the presented free-edge approximation is used, then u and v must be represented using elements having C1 continuity across the element edges. In the present study, we have chosen to ignore this issue by using a divergence-free velocity field, allowing us to omit the problematic terms in (81) – (82).

There is one final issue that must be accounted for. The presented free-edge approximation will make the equations (81) – (82) nonlinear, since the effective velocity field $\mathbf{U}$ depends on the displacement $\mathbf{u}$. Thus an iterative process must be introduced to find the solution.

8 Numerical results

In this section, we will present numerical results from both the one- and two dimensional models. In the one-dimensional case, the full viscoelastic model is used. The two-dimensional study is focused on the inertial contribution in the pure elastic case.

In the one-dimensional model, the strain and stress states can be calculated analytically using the equations (52) and (56). Using the parameter values $E_x = 2.5 \cdot 10^7$ N/m^2, $\eta_x = 4.0 \cdot 10^5$ Ns/m^2, $U_x = 10$ m/s, span length $L = 1.0$ m and strain $\varepsilon_T = 0.03$, the results shown in Figures 7 – 9 are obtained. The numerical solutions, also shown in Figures 7 and 8, are reproduced from the previous study [35].

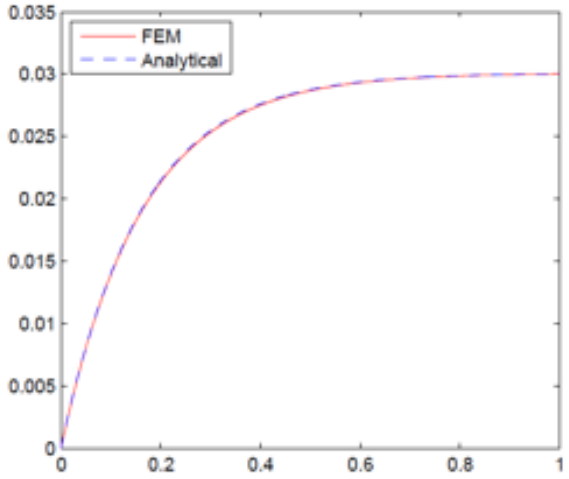

Figure 7: Analytical and numerical finite element solution of strain distribution along the length of the web span [35].

As was pointed out in the analysis, the strain distribution along the travelling viscoelastic span differs from the traditional constant strain that is observed for purely elastic materials [68]. However, even though the strain distribution is not constant, the stress distribution is a combination of elastic and viscous forces based on the equation (21), and it is almost constant. The stress increases very slightly towards the traction line A2; this is a consequence of the acceleration of the web due to higher outlet velocity, $U_2 > U_1$ [35]. The effect of the span length on the web stress state is visible. Basically, the shorter the processing time of the viscoelastic span is, the higher is the response of time-dependent viscous force component.

In case of the two-dimensional model, a purely elastic travelling two-dimensional sheet was investigated numerically using finite elements. See Figure 10. The unknowns were the displacements u and v. The element type used was Q2 (quadratic and quadrangular). Isoparametric mapping (i.e. also Q2) was used for the coordinates. The auxiliary potential p for divergence-free velocity projection was represented using Q1 (bilinear quadrangular) elements. The classical Galerkin method was used; for each unknown quantity, its own basis functions were used as the test functions.

The mesh was set up as a uniform cartesian grid with 16×16 elements for each of the unknowns. Discretizations were produced automatically from equations (81) – (82) and (103). Dirichlet boundary conditions, prescribing displacements, were enforced by the elimination technique. Homogeneous natural (i.e. zero Neumann) boundary conditions required no action on part of the implementation. The discretization lead to 32895 global degrees of freedom in the linear problem (u and v only), and 37120 in the nonlinear problem (u, v and auxiliary potential p).

The solution of the corresponding linear problem for the stationary elastic sheet ($\mathbf{U} = 0$) was used as the initial guess for $\mathbf{u}$, and fixed-point iteration was used to refine the solution of the nonlinear problem of the moving sheet. At each fixed-

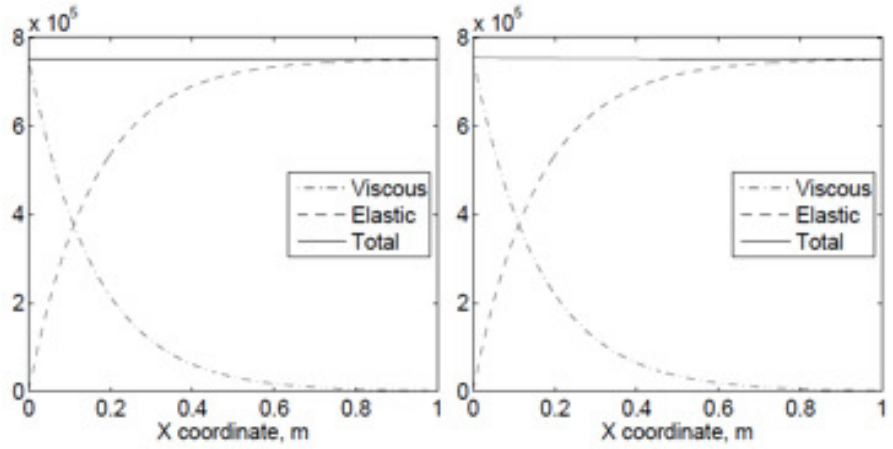

Figure 8: Analytical (left) and numerical (right) finite element solution of stress distribution along the length of the span [35].

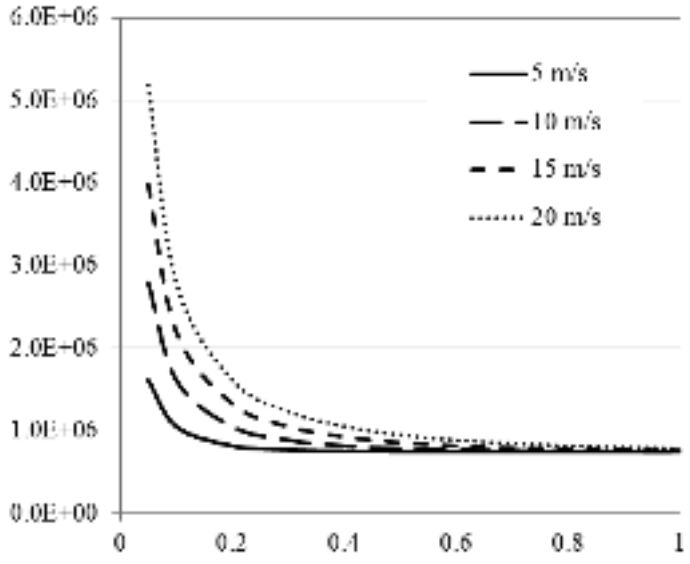

Figure 9: Effect of web span length on the web stress [35].

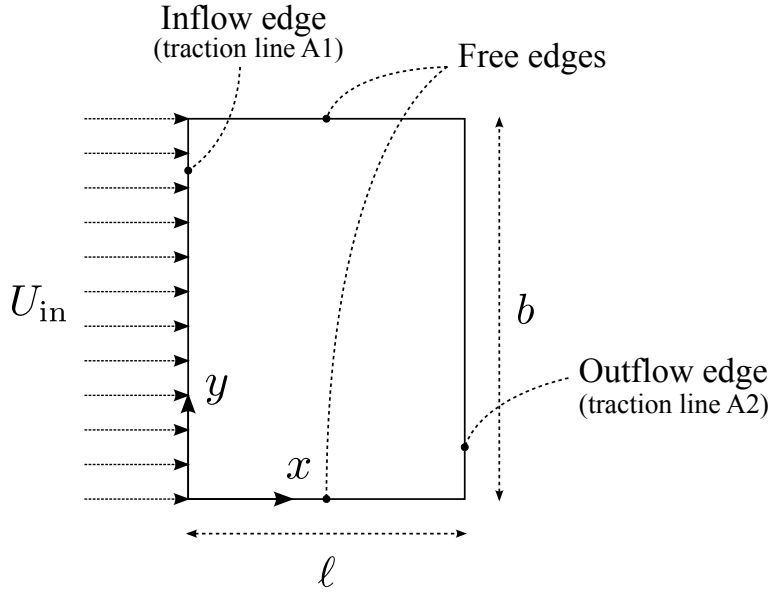

Figure 10: Setup for the two-dimensional numerical investigation. Elastic material enters from the left at velocity U_{in}, and flows through the domain at a velocity determined by the interaction of U_{in} and the approximated behaviour of the free edges.

point iteration, the linear equation system was solved by a direct solver. The velocity field $\mathbf{U}$ was computed starting from a purely axial inflow, as described above. See equations (92), (101) and (103).

A common desktop computer with 4 CPU cores was used for the finite element computations. With MPI-parallelized matrix assembly, each nonlinear problem took about one minute of wall time. The implementation was based on the scientific Python software stack.

Problem parameter values used in the study are listed in Table 1. The shear modulus based on the geometric average,

$$G = \frac{\sqrt{E_1 E_2}}{2(1+\sqrt{\nu_{12}\nu_{21}})} \,, \tag{104}$$

was used for both the isotropic and orthotropic materials. Equation (104) is sometimes known as the Huber value for the shear modulus, after M. T. Huber who proposed this relation for orthotropic materials [25, 26, 27].

The boundary conditions for the displacements u and v were

$$u(y) = v(y) = 0 \quad \text{at} \quad x = 0, \quad 0 < y < b \,, \tag{105}$$

$$u(y) = u_{\text{f}} \quad \text{at} \quad x = \ell, \quad 0 < y < b \,, \tag{106}$$

and zero Neumann for v at $x = \ell$, $0 < y < b$. In (106), u_{f} is a prescribed constant value for the displacement. Note that at the outflow edge, only u is fixed; v is determined by the zero Neumann condition.

Table 1: Parameter values used in the two-dimensional numerical study. All 24 combinations resulting from the choices of U_{in} (4 values), b (3 values) and the two materials were investigated. The shear modulus based on the geometric average (equation (104)) was used for both the isotropic and orthotropic materials. Note elastic compatibility $E_1\nu_{21} = E_2\nu_{12}$ (see e.g. [37]).

U_{in} [m/s]	ℓ [m]	b [m]	ρ [kg/m^3]	u_{f} [m]
0	0.5	0.1	800	$0.03 \cdot \ell$
15		0.5		
25		2.5		
50				

	E_1 [10^7 Pa]	E_2 [10^7 Pa]	ν_{12}	ν_{21}
Isotropic	2.5	2.5	0.3	0.3
Orthotropic	5.0	1.25	0.6	0.15

On the free edges, $0 < x < \ell$, $y = 0$ and $0 < x < \ell$, $y = b$, the zero Neumann condition was used for both u and v. The zero Neumann condition (weakly) prescribes zero normal component for the effective stress tensor (74), i.e.

$$\boldsymbol{\sigma}_{\text{eff}} \cdot \mathbf{n} \equiv \left[\boldsymbol{\sigma} - \rho(\mathbf{U} \otimes \mathbf{U} \cdot \nabla \mathbf{u})^{\mathrm{T}}\right] \cdot \mathbf{n} = 0 \,. \tag{107}$$

Explicitly, accounting for our geometry and spelling out the component form, from equation (82) we can read the following condition corresponding to v at the outflow boundary:

$$C_{66}(\frac{\partial u}{\partial y} + \frac{\partial v}{\partial x}) - \rho U_x^2 \frac{\partial v}{\partial x} - \rho U_y U_x \frac{\partial v}{\partial y} = 0 \quad \text{at} \quad x = \ell, \quad 0 < y < b \,, \tag{108}$$

and from equations (81) and (82), the following conditions corresponding to u and v (respectively) on the free boundaries:

$$C_{66}(\frac{\partial u}{\partial y} + \frac{\partial v}{\partial x}) - \rho U_x U_y \frac{\partial u}{\partial x} - \rho U_y^2 \frac{\partial u}{\partial y} = 0 \quad \text{at} \quad 0 < x < \ell, \quad y = \{0, b\} \,, \tag{109}$$

$$C_{21}\frac{\partial u}{\partial x} + C_{22}\frac{\partial v}{\partial y} - \rho U_x U_y \frac{\partial v}{\partial x} - \rho U_y^2 \frac{\partial v}{\partial y} = 0 \quad \text{at} \quad 0 < x < \ell, \quad y = \{0, b\} \,. \tag{110}$$

The boundary conditions for the auxiliary potential p were (102) on all boundaries. As was mentioned, this requires that the normal component of the velocity correction vanishes at the boundaries.

The problem was solved numerically for all 24 input value combinations resulting from the choices of U_{in} (4 values), b (3 values) and the two materials, as listed in Table 1. The quantities studied were u, v, ε_{xx}, ε_{yy}, γ_{xy}, σ_{xx}, σ_{yy} and τ_{xy}. In addition, when $U_{\text{in}} > 0$, the relative velocity field defined as

$$\mathbf{U}_{\text{rel}} \equiv (\, U_x - U_{\text{in}} \,,\, U_y \,) \tag{111}$$

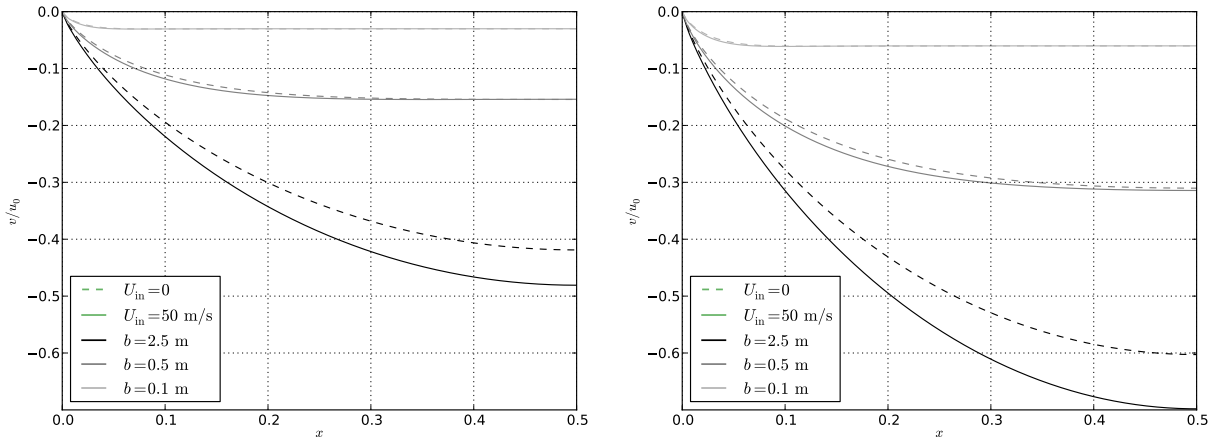

Figure 11: Displacement v, normalized to u_{f}, along the free edge $0 < x < \ell$, $y = b$. *Left*: isotropic. *Right*: orthotropic. Line style indicates inflow velocity U_{in}, darkness indicates span width b.

was also studied.

Figure 11 shows the y-directional displacement profile (displacement v) along the free edge $0 < x < \ell$, $y = b$ for representative isotropic and orthotropic cases for both stationary and moving materials.

Figures 12–28 display contour plots of all studied quantities for a stationary material (linear reference case), and material moving at $U_{\text{in}} = 50$ m/s (representative example of nonlinear case).

For all investigated cases, it was observed that for each quantity studied, the difference between the nonlinear and linear solutions is small, when compared to the maximum value of the linear solution. While varying the magnitude of U_{in} changed the magnitude of this difference, the shape of the difference field (nonlinear minus linear) for each quantity studied remained the same. See Figures 29 – 36 for representative examples of the difference fields.

All effects were observed to become more pronounced for small aspect ratios ℓ/b, i.e. spans that are wide and short. The span length ℓ was kept constant, and the width b was varied; hence in the figures, large values of b correspond to small aspect ratios.

In all investigated cases, inertial effects caused additional elastic contraction of the travelling span, on top of the contraction already observed for a stationary material. This effect can be seen especially clearly in the y-directional displacement profile, Figure 11, and the shape of the relative velocity field $\mathbf{U}_{\text{rel}}$, Figure 12.

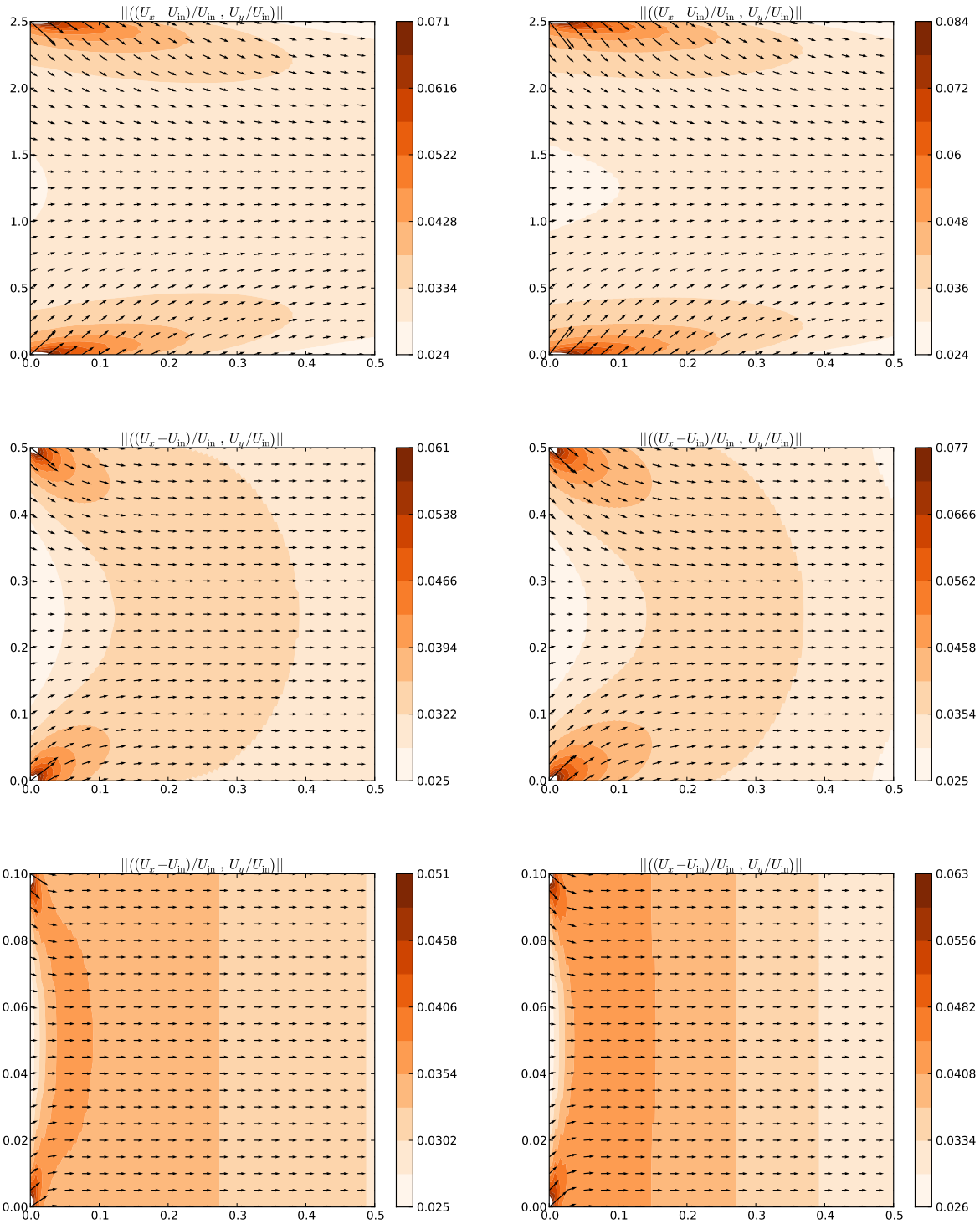

Figure 12: Relative velocity field $\mathbf{U}_{\text{rel}}$, normalized to $U_{\text{in}} = 50$ m/s (representative). *Left*: isotropic. *Right*: orthotropic. *Top to bottom*: $b = 2.5,\ 0.5,\ 0.1$ m ($\ell/b = 1/5,\ 1,\ 5$).

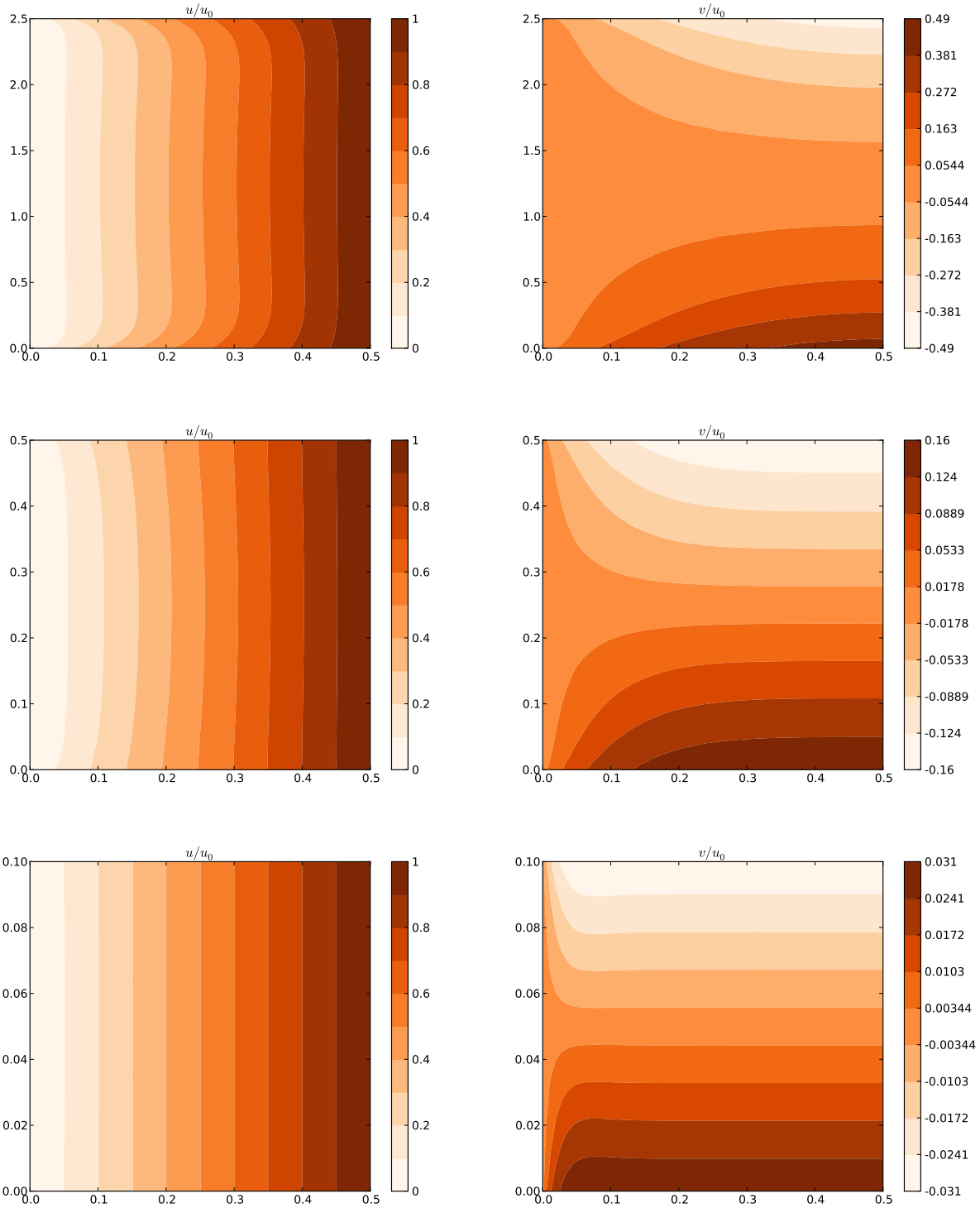

Figure 13: Displacements u and v, normalized to u_f. Isotropic, $U_\mathrm{in} = 0$ (linear reference). *Top to bottom:* $b = 2.5,\ 0.5,\ 0.1\,m$ ($\ell/b = 1/5,\ 1,\ 5$).

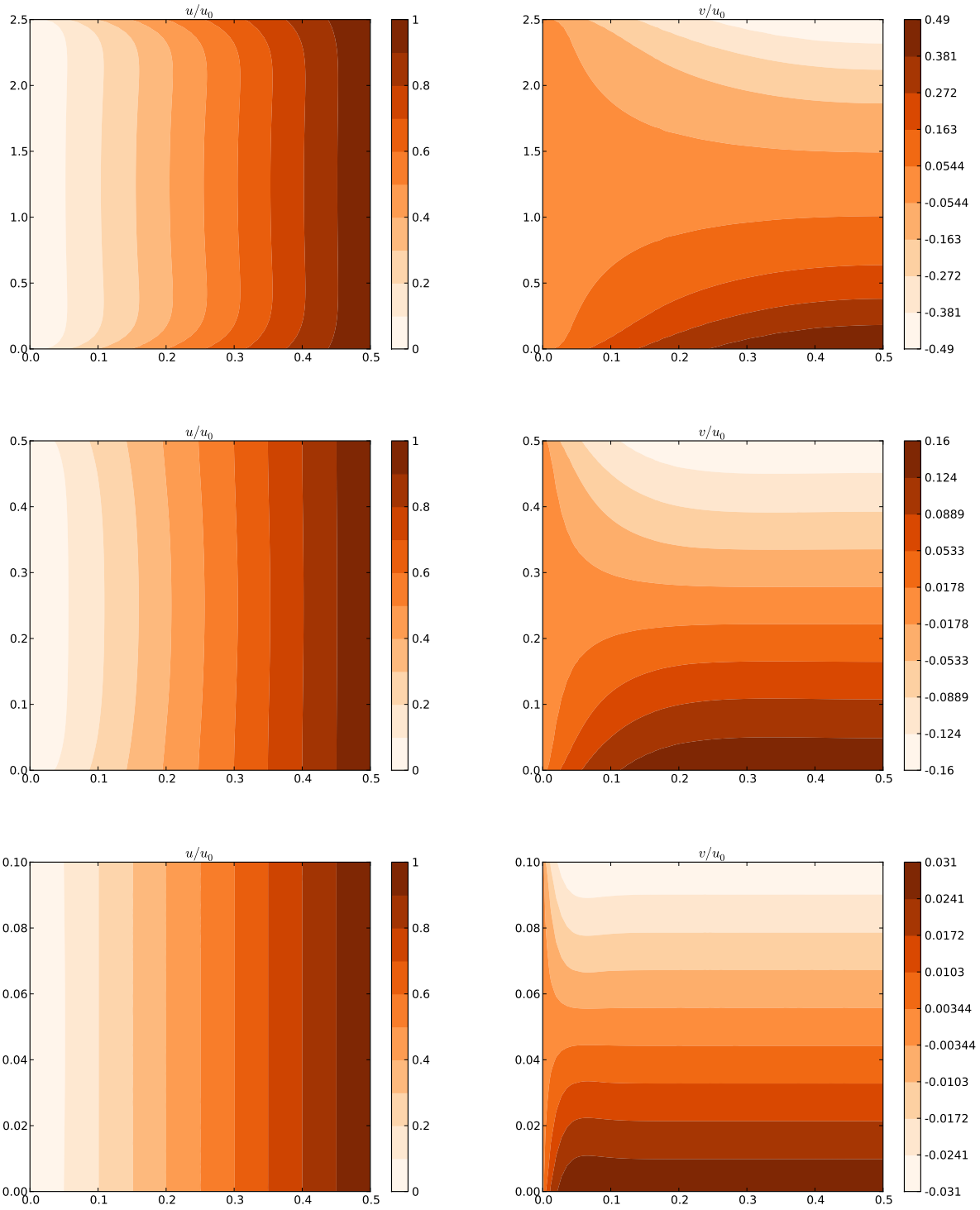

Figure 14: Displacements u and v, normalized to u_f. Isotropic, $U_\mathrm{in} = 50$ m/s (representative). *Top to bottom:* $b = 2.5,\ 0.5,\ 0.1\,m$ ($\ell/b = 1/5,\ 1,\ 5$).

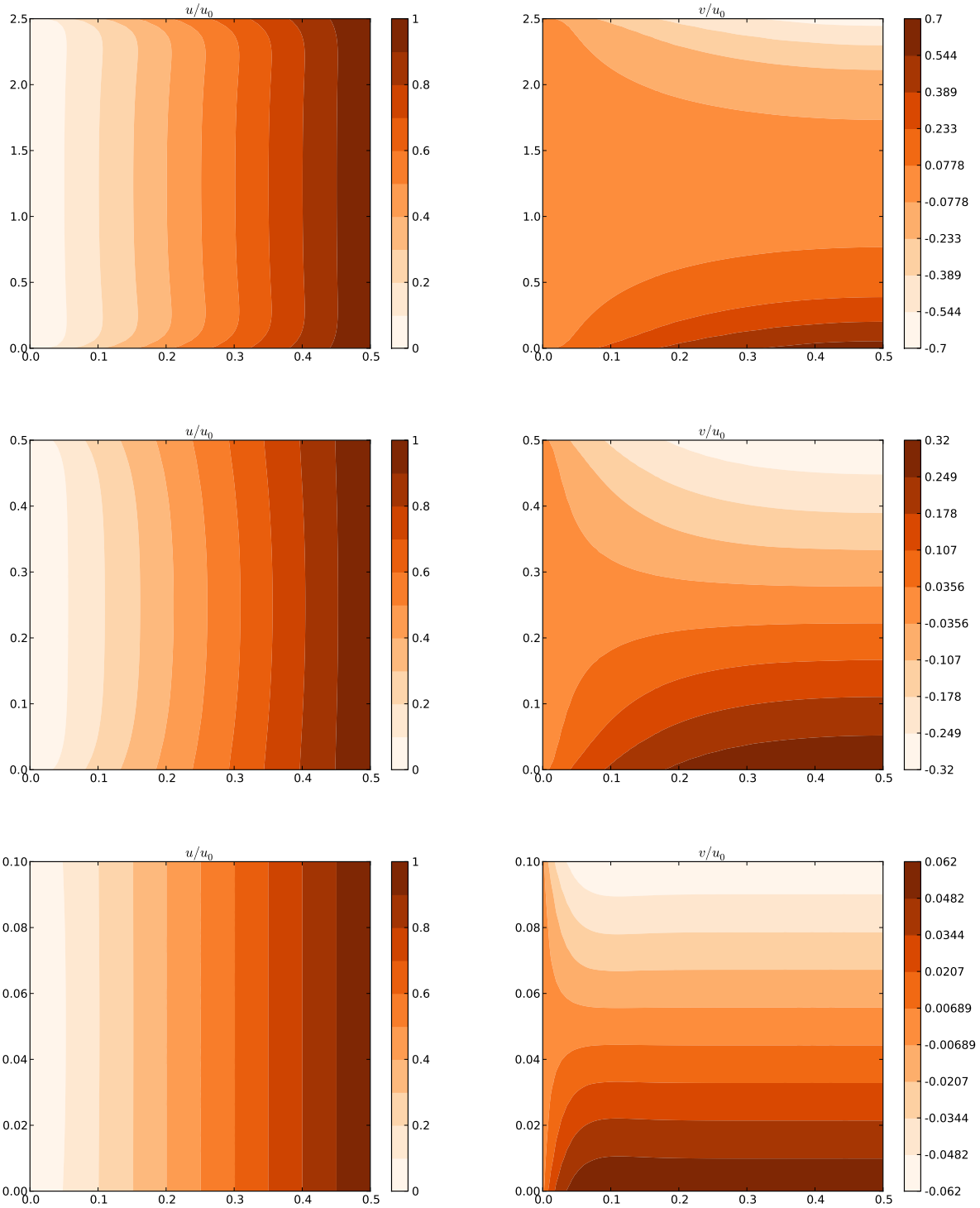

Figure 15: Displacements u and v, normalized to u_f. Orthotropic, $U_\mathrm{in} = 0$ (linear reference). *Top to bottom:* $b = 2.5,\ 0.5,\ 0.1\,m$ ($\ell/b = 1/5,\ 1,\ 5$).

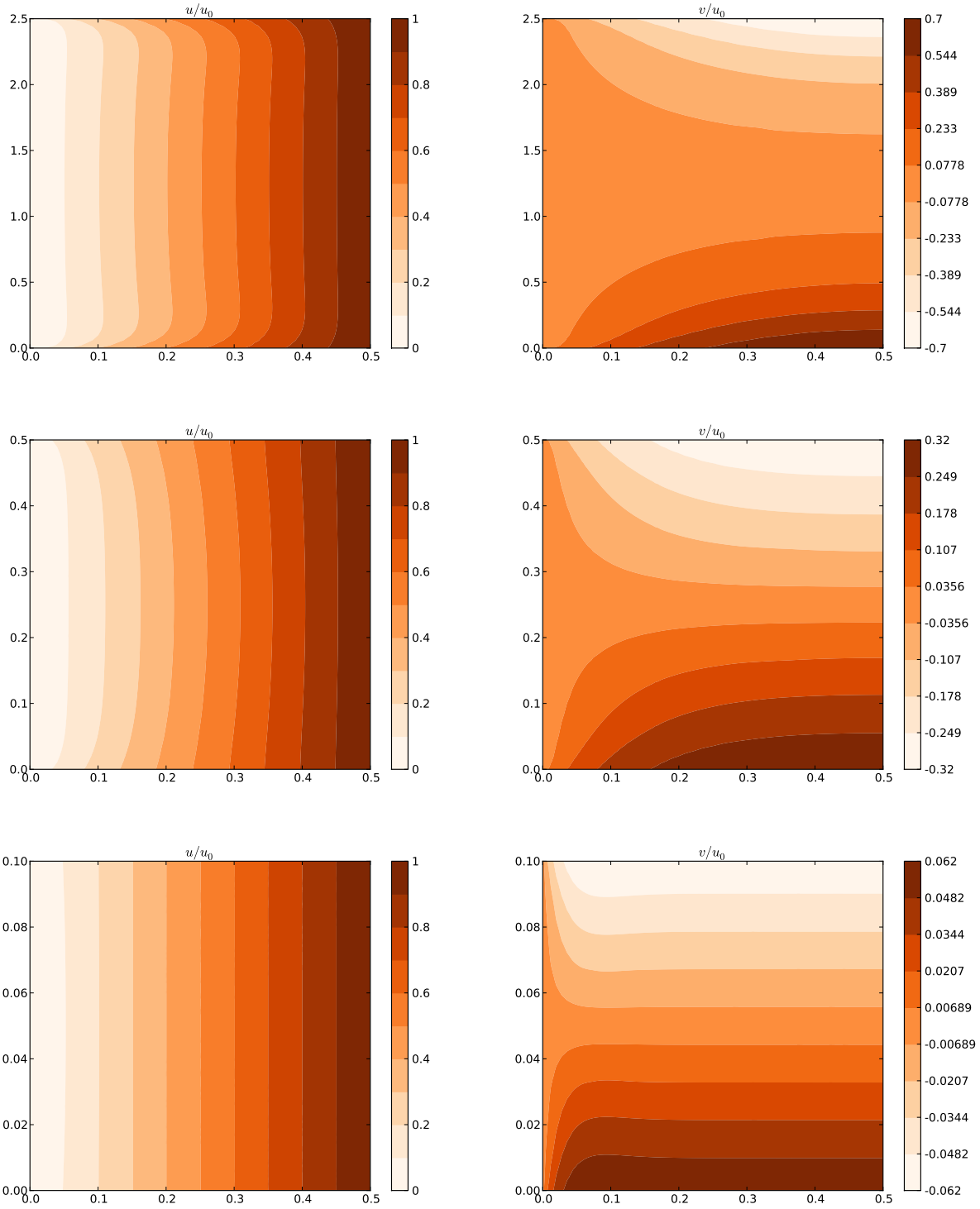

Figure 16: Displacements u and v, normalized to u_f. Orthotropic, $U_\mathrm{in} = 50$ m/s (representative). *Top to bottom:* $b = 2.5,\ 0.5,\ 0.1\,m$ ($\ell/b = 1/5,\ 1,\ 5$).

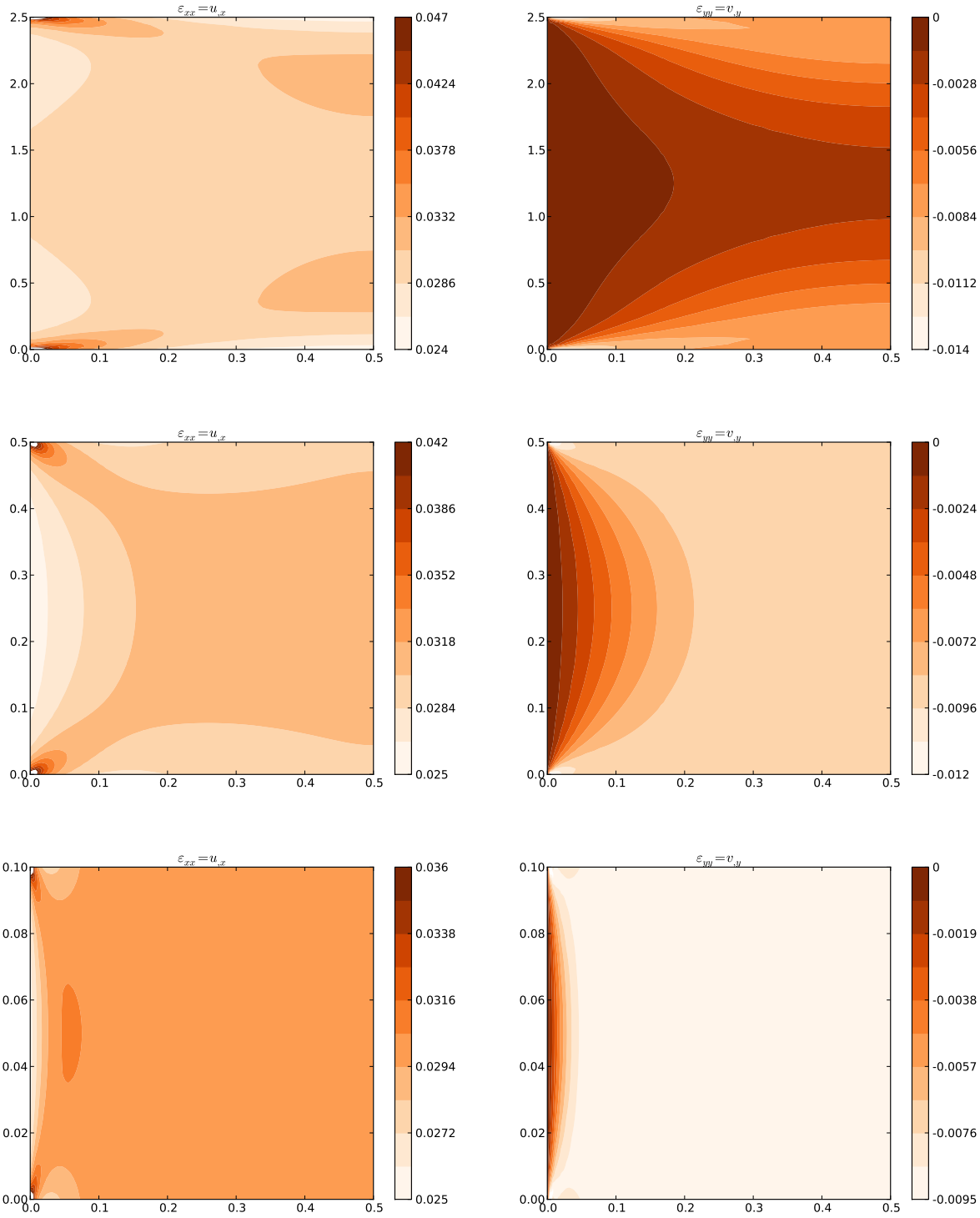

Figure 17: Axial strains ε_{xx} and ε_{yy}. Isotropic, $U_{\text{in}} = 0$ (linear reference). *Top to bottom:* $b = 2.5,\ 0.5,\ 0.1\,m$ ($\ell/b = 1/5,\ 1,\ 5$).

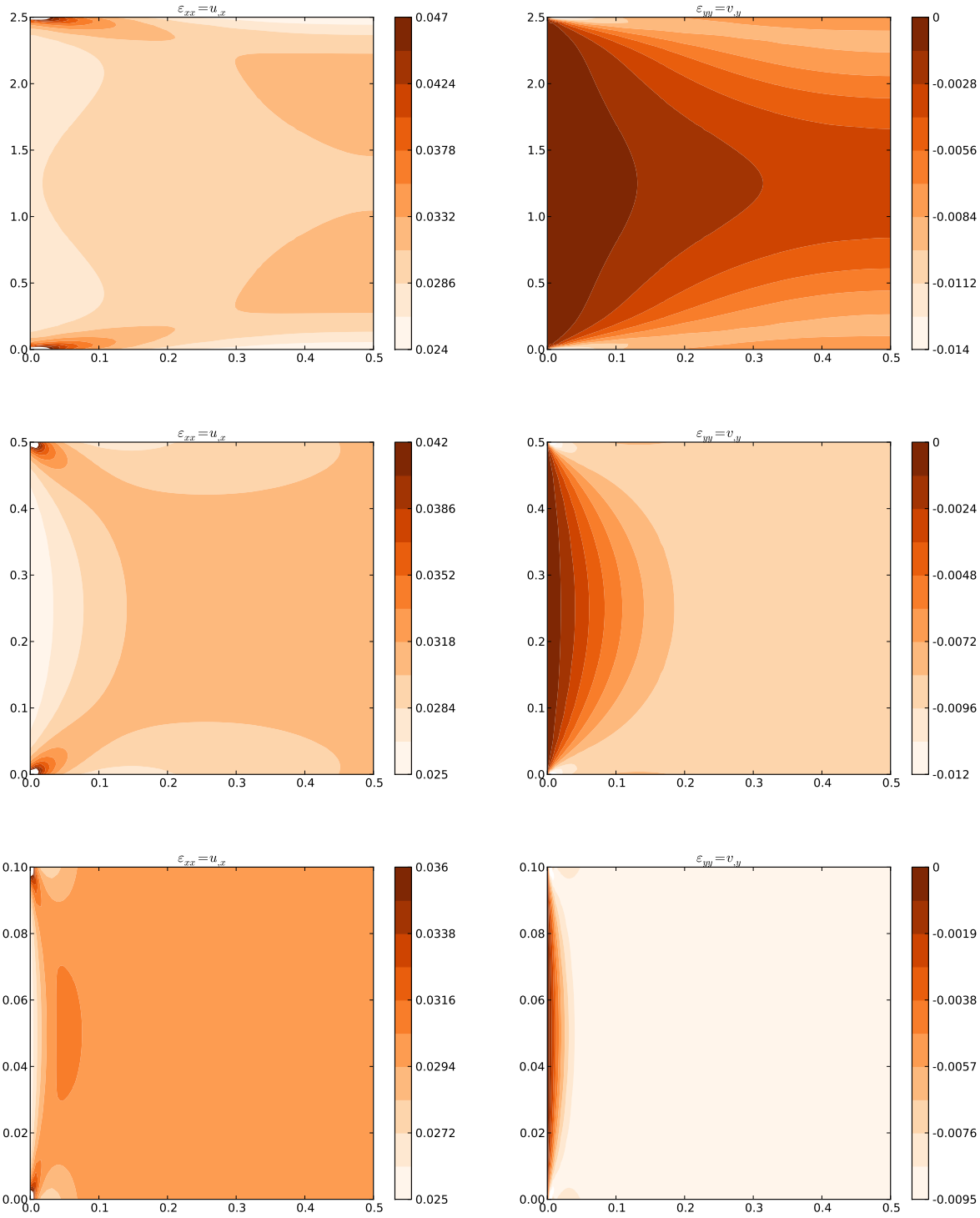

Figure 18: Axial strains ε_{xx} and ε_{yy}. Isotropic, $U_{\text{in}} = 50$ m/s (representative). *Top to bottom:* $b = 2.5,\ 0.5,\ 0.1\,m$ ($\ell/b = 1/5,\ 1,\ 5$).

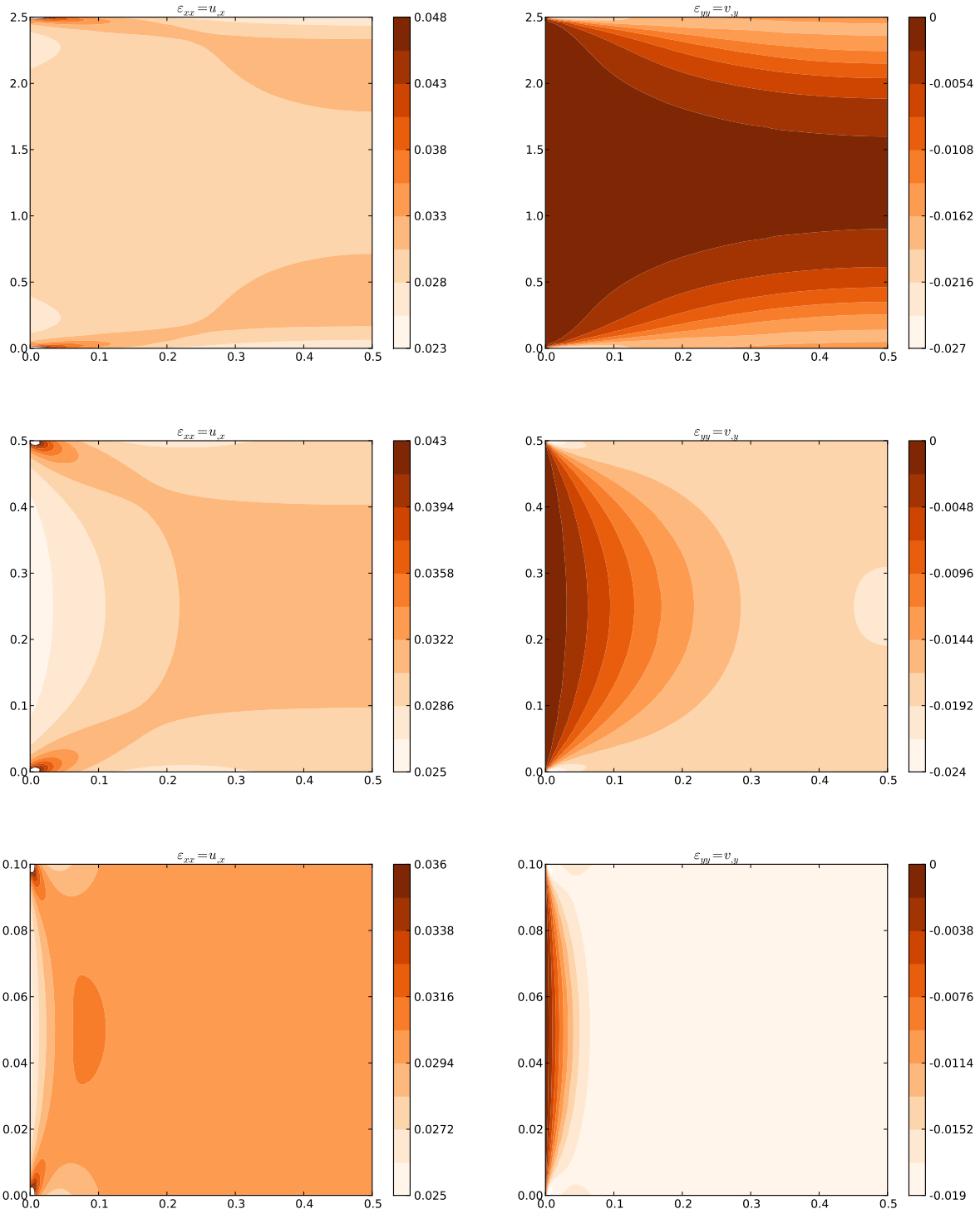

Figure 19: Axial strains ε_{xx} and ε_{yy}. Orthotropic, $U_{\text{in}} = 0$ (linear reference). *Top to bottom:* $b = 2.5,\ 0.5,\ 0.1\,m$ ($\ell/b = 1/5,\ 1,\ 5$).

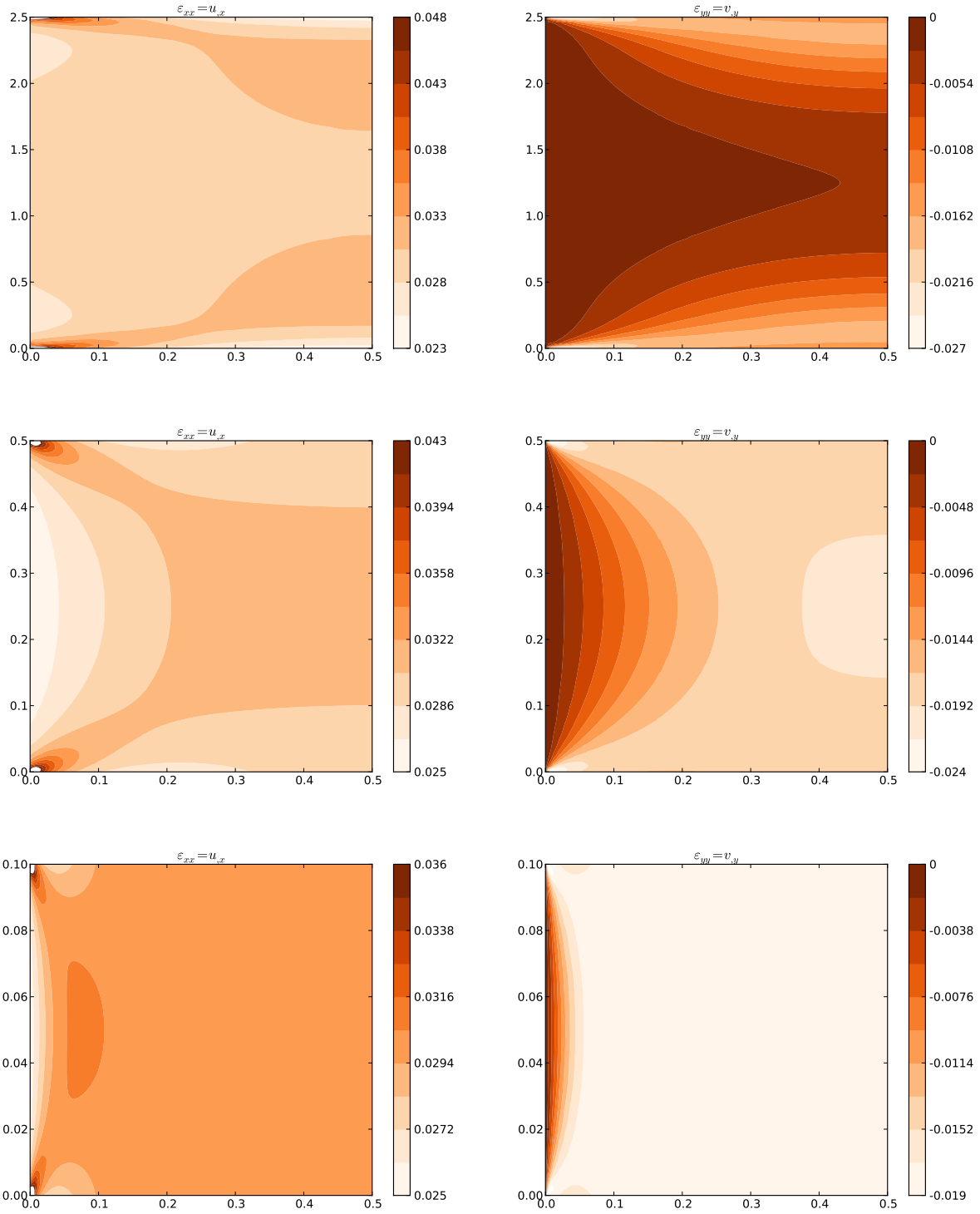

Figure 20: Axial strains ε_{xx} and ε_{yy}. Orthotropic, $U_{\text{in}} = 50$ m/s (representative). *Top to bottom:* $b = 2.5,\ 0.5,\ 0.1\,m$ ($\ell/b = 1/5,\ 1,\ 5$).

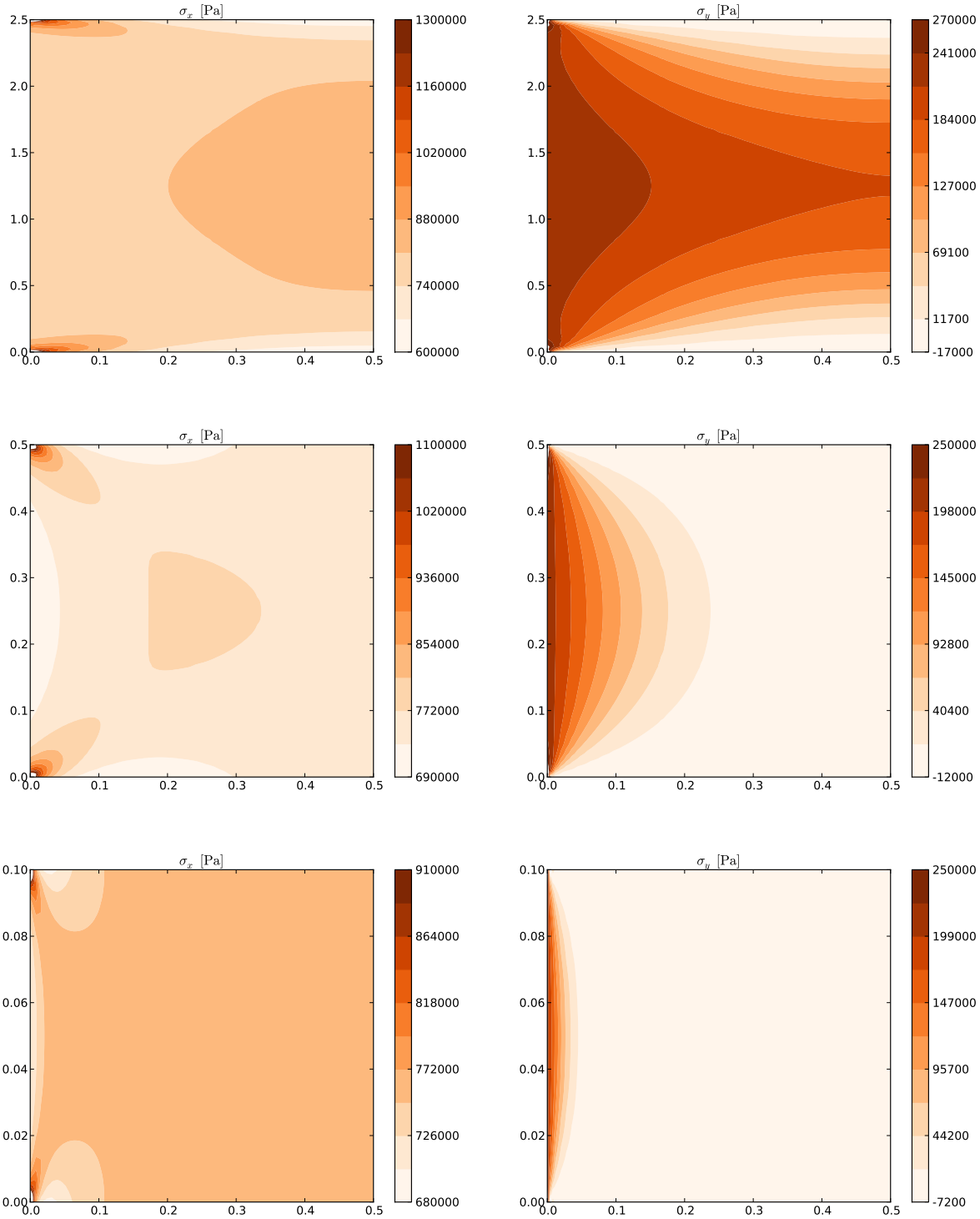

Figure 21: Axial stresses σ_{xx} and σ_{yy}. Isotropic, $U_{\text{in}} = 0$ (linear reference). *Top to bottom:* $b = 2.5,\ 0.5,\ 0.1\,m$ ($\ell/b = 1/5,\ 1,\ 5$).

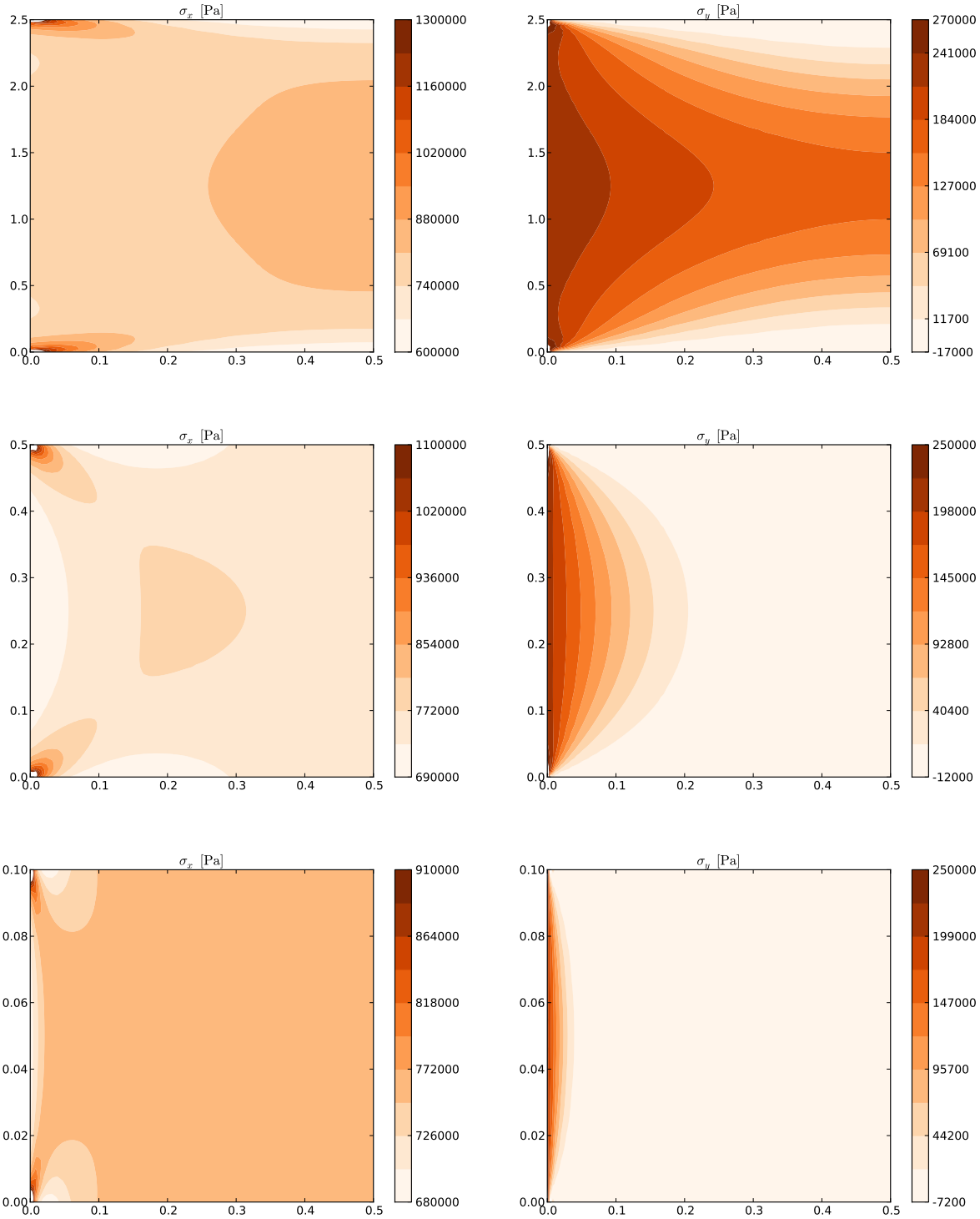

Figure 22: Axial stresses σ_{xx} and σ_{yy}. Isotropic, $U_{\text{in}} = 50$ m/s (representative). *Top to bottom:* $b = 2.5,\ 0.5,\ 0.1\,m$ ($\ell/b = 1/5,\ 1,\ 5$).

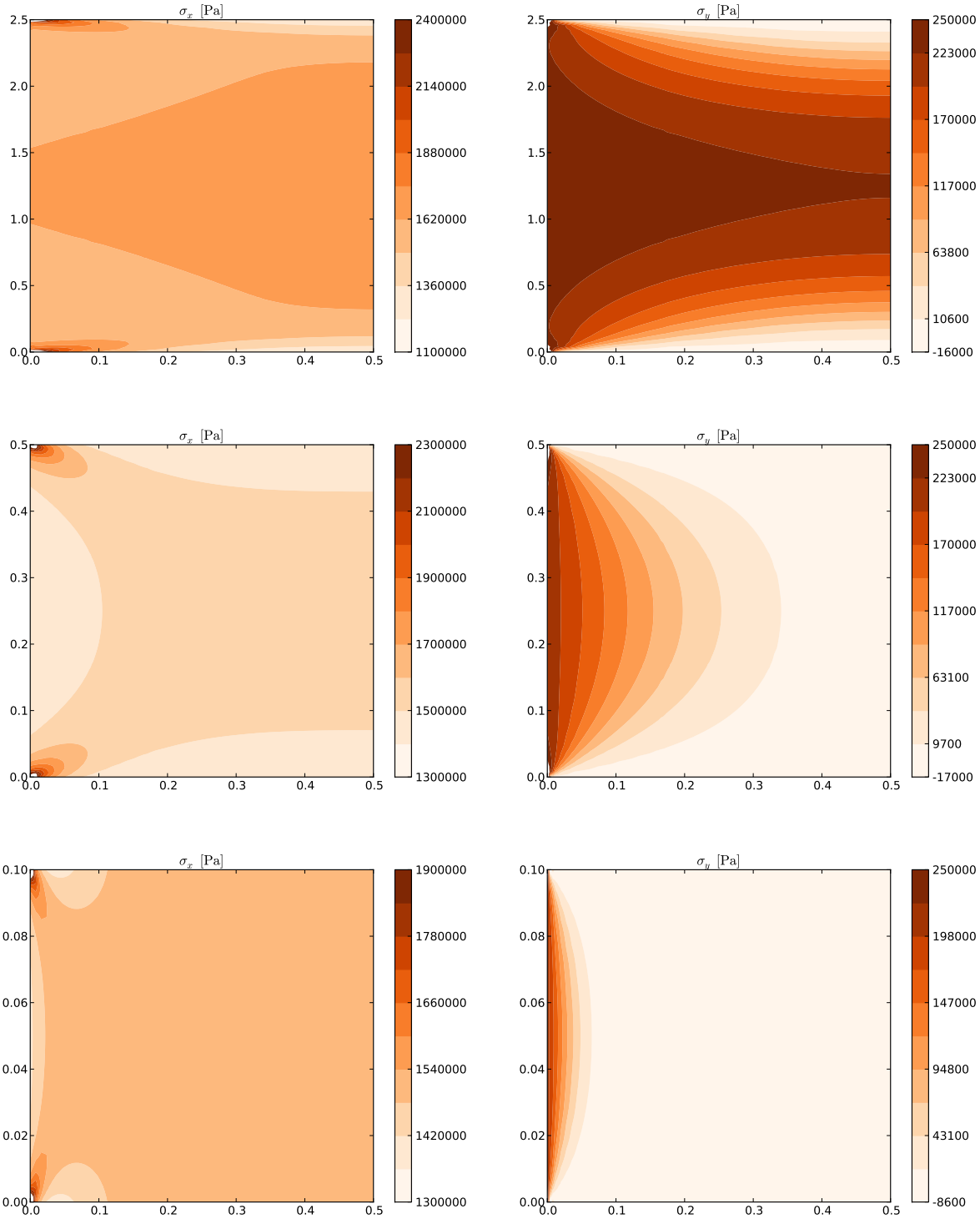

Figure 23: Axial stresses σ_{xx} and σ_{yy}. Orthotropic, $U_{\text{in}} = 0$ (linear reference). *Top to bottom:* $b = 2.5,\ 0.5,\ 0.1\,m$ ($\ell/b = 1/5,\ 1,\ 5$).

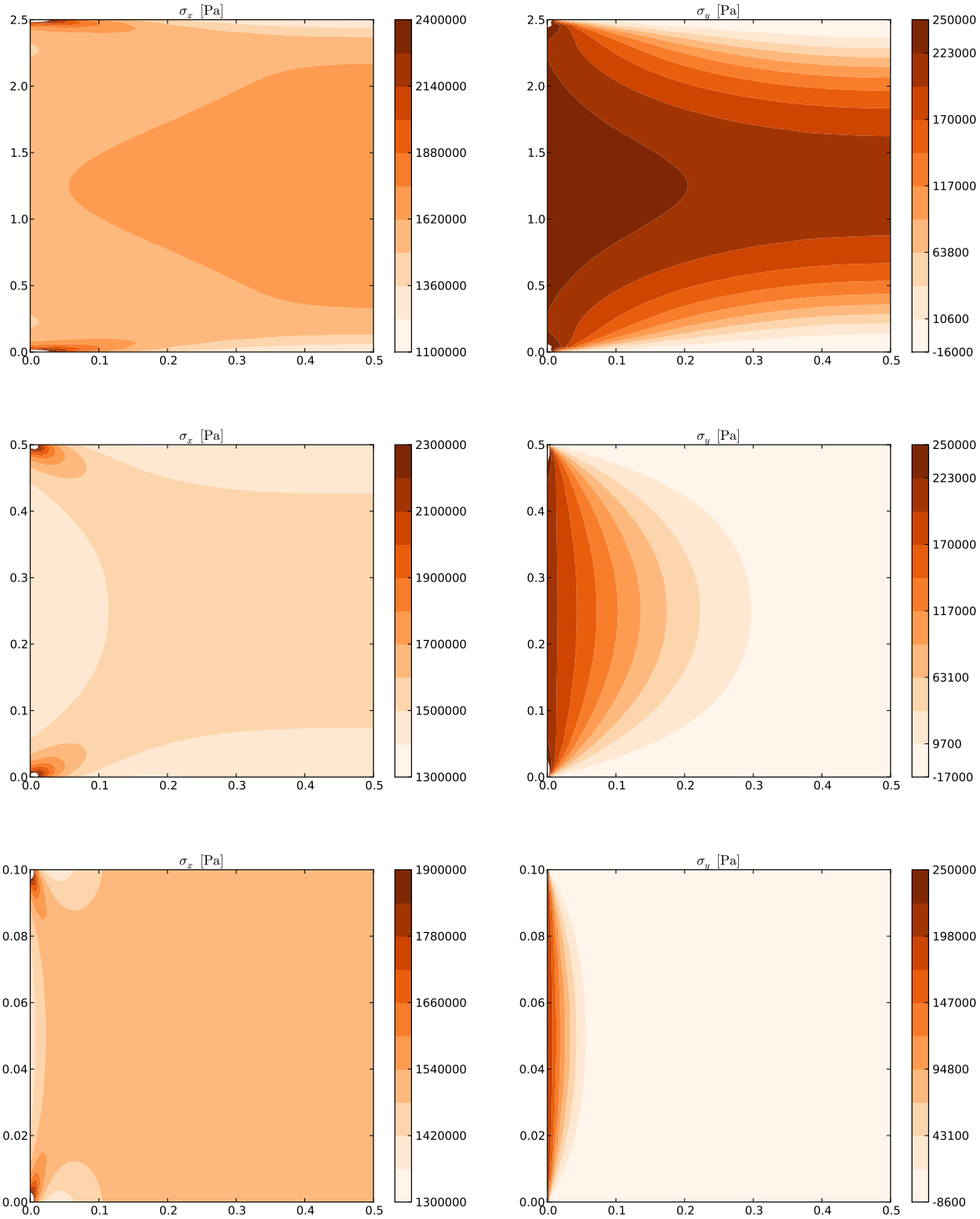

Figure 24: Axial stresses σ_{xx} and σ_{yy}. Orthotropic, $U_{\text{in}} = 50$ m/s (representative). *Top to bottom:* $b = 2.5,\ 0.5,\ 0.1\,m$ ($\ell/b = 1/5,\ 1,\ 5$).

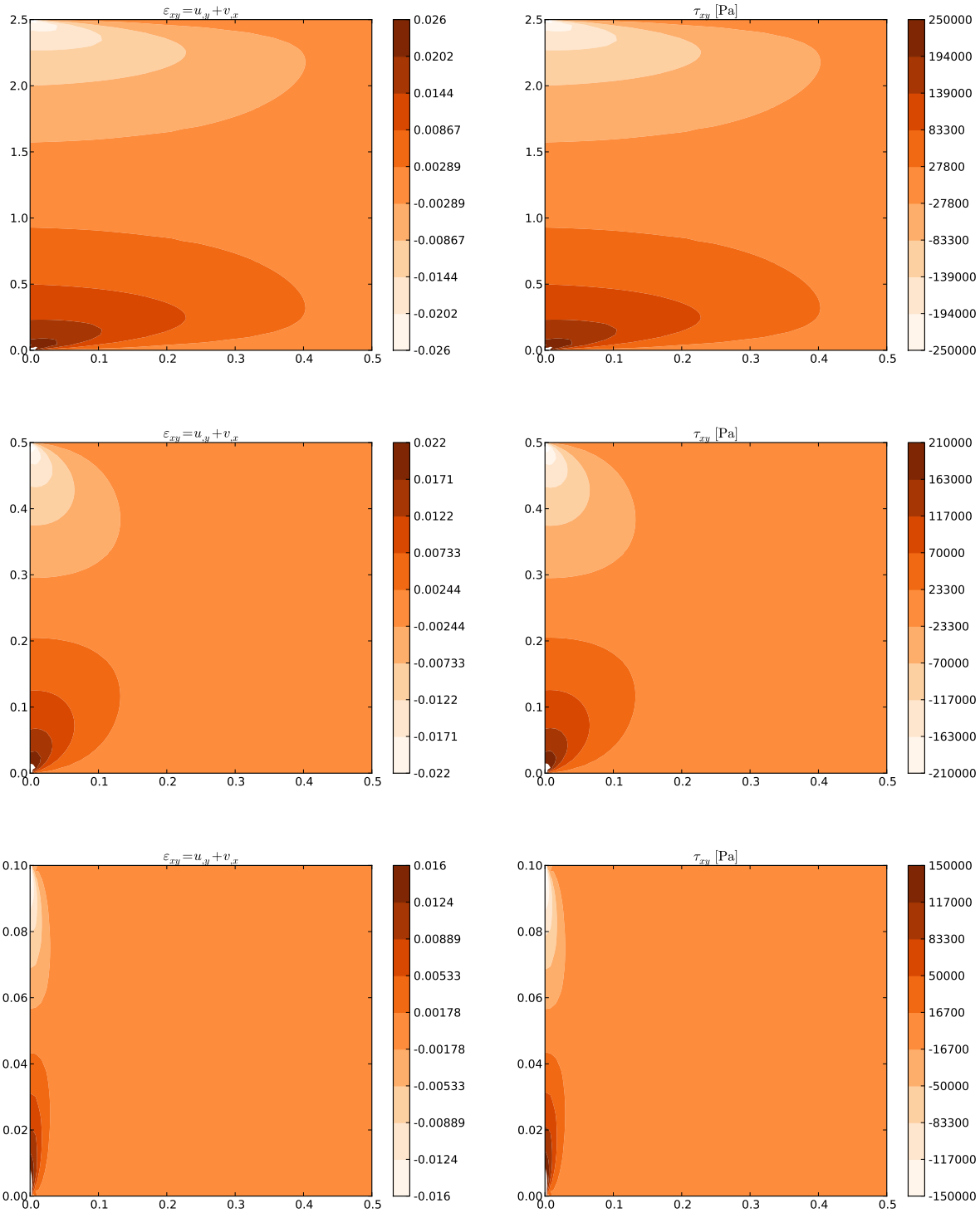

Figure 25: Shear strain γ_{xy} and shear stress τ_{xy}. Isotropic, $U_{\text{in}} = 0$ (linear reference). *Top to bottom:* $b = 2.5,\ 0.5,\ 0.1\,m$ ($\ell/b = 1/5,\ 1,\ 5$).

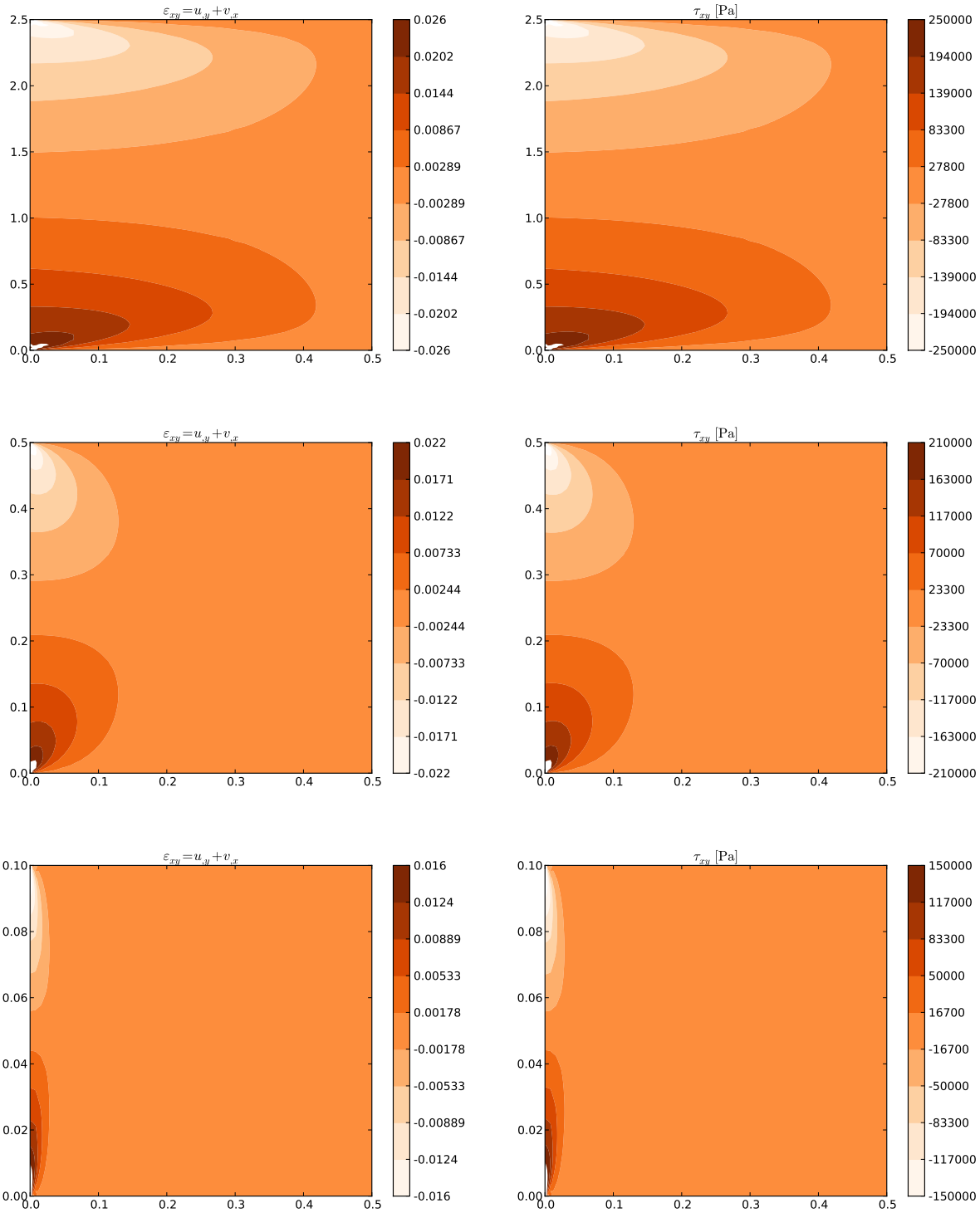

Figure 26: Shear strain γ_{xy} and shear stress τ_{xy}. Isotropic, $U_{\text{in}} = 50$ m/s (representative). *Top to bottom:* $b = 2.5,\ 0.5,\ 0.1\,m$ ($\ell/b = 1/5,\ 1,\ 5$).

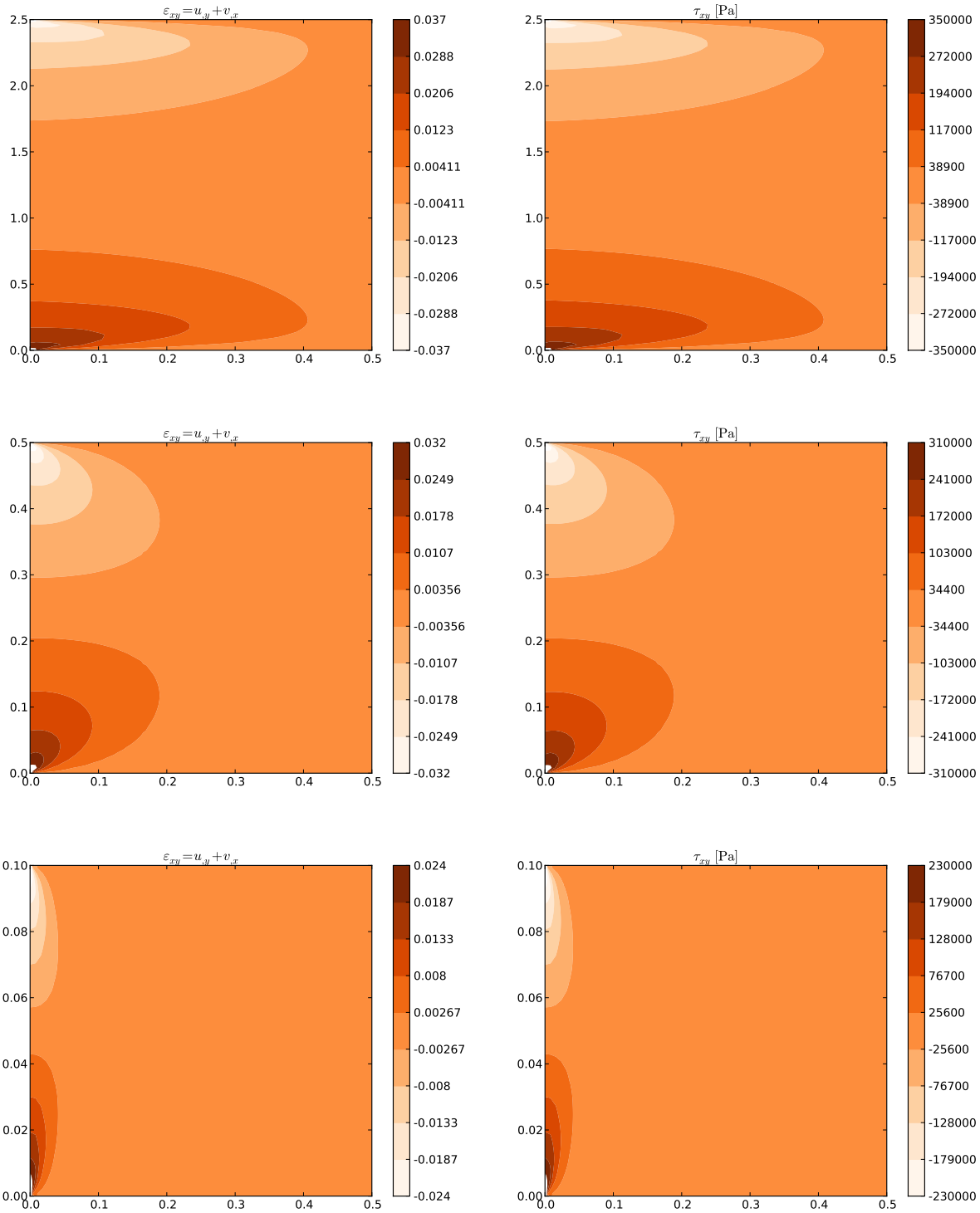

Figure 27: Shear strain γ_{xy} and shear stress τ_{xy}. Orthotropic, $U_{\text{in}} = 0$ (linear reference). *Top to bottom:* $b = 2.5,\ 0.5,\ 0.1\,m$ ($\ell/b = 1/5,\ 1,\ 5$).

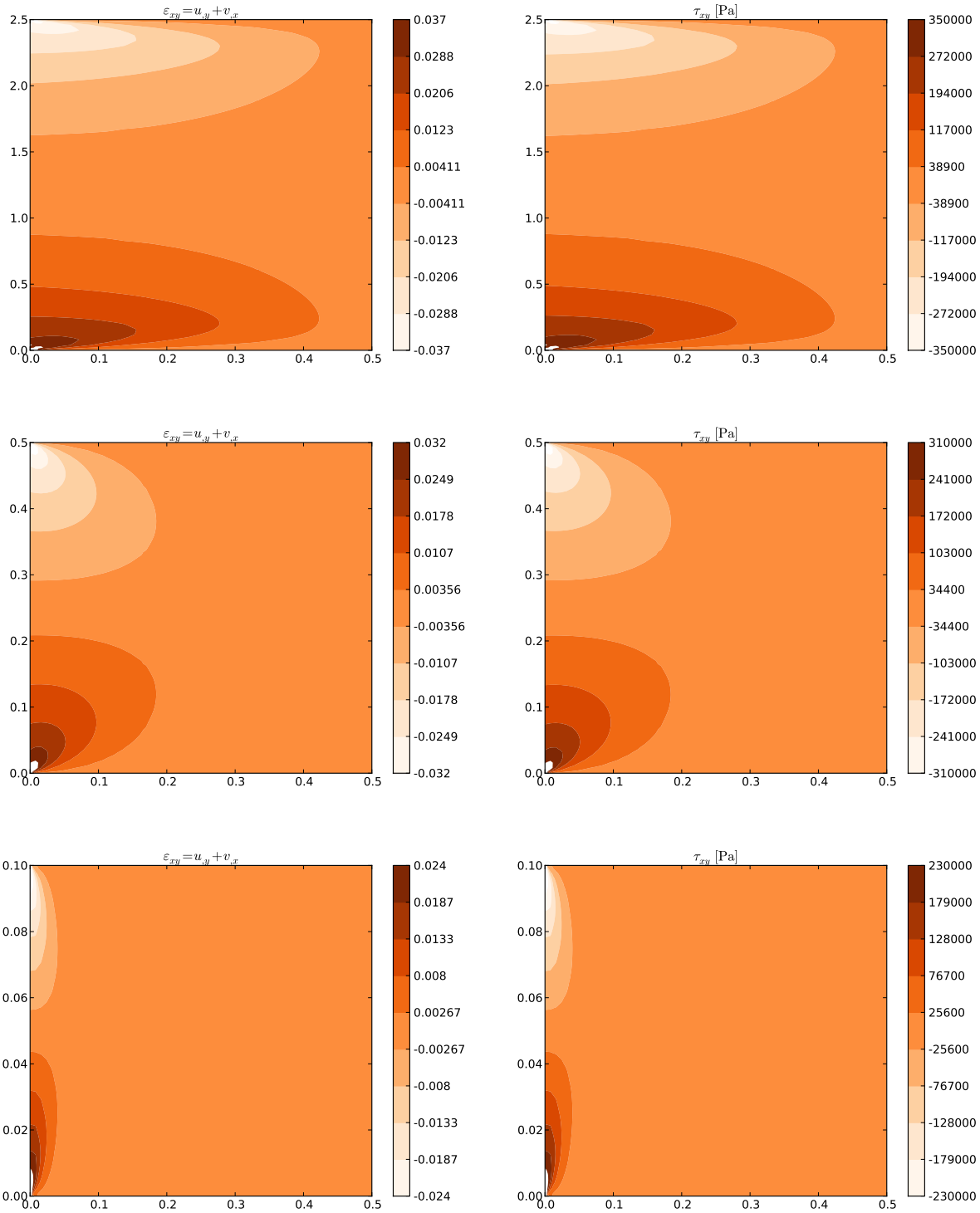

Figure 28: Shear strain γ_{xy} and shear stress τ_{xy}. Orthotropic, $U_{\text{in}} = 50$ m/s (representative). *Top to bottom:* $b = 2.5,\ 0.5,\ 0.1\,m$ ($\ell/b = 1/5,\ 1,\ 5$).

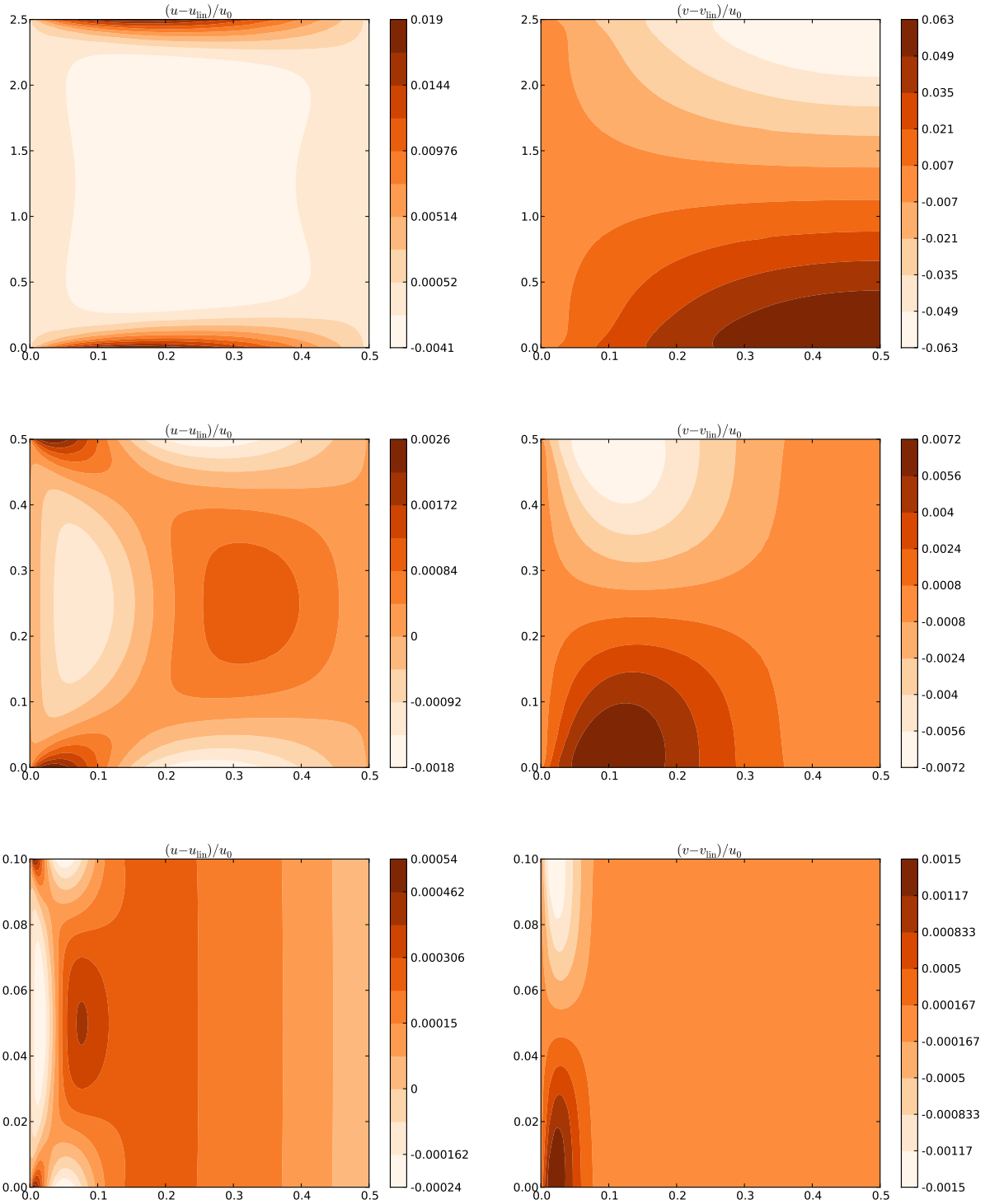

Figure 29: Nonlinear contribution to displacements, normalized to u_{f}. Isotropic, $U_{\text{in}} = 50$ m/s (representative). *Top to bottom:* $b = 2.5,\ 0.5,\ 0.1\,m$ ($\ell/b = 1/5,\ 1,\ 5$).

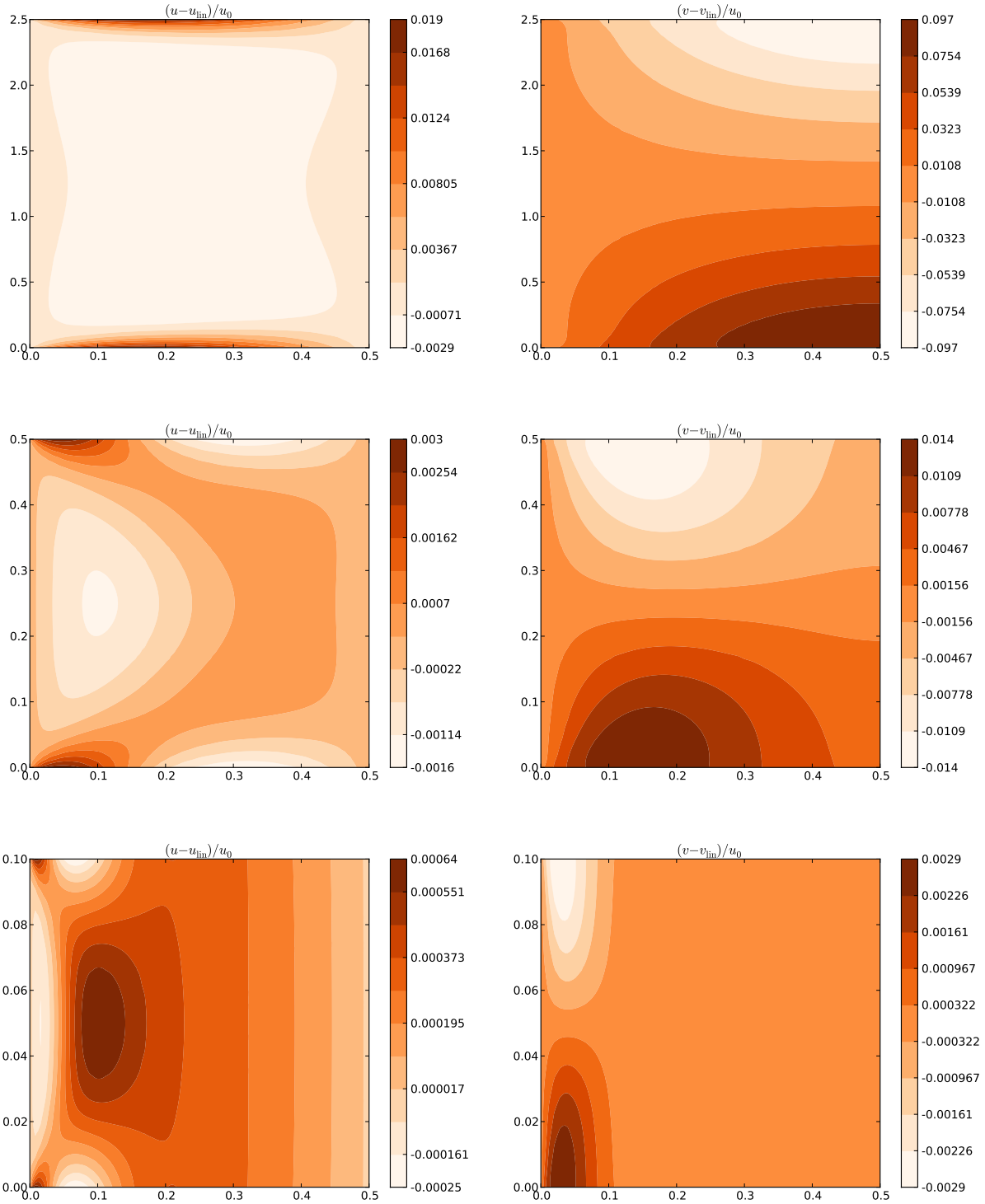

Figure 30: Nonlinear contribution to displacements, normalized to u_{f}. Orthotropic, $U_{\text{in}} = 50$ m/s (representative). *Top to bottom:* $b = 2.5,\ 0.5,\ 0.1\,m$ ($\ell/b = 1/5,\ 1,\ 5$).

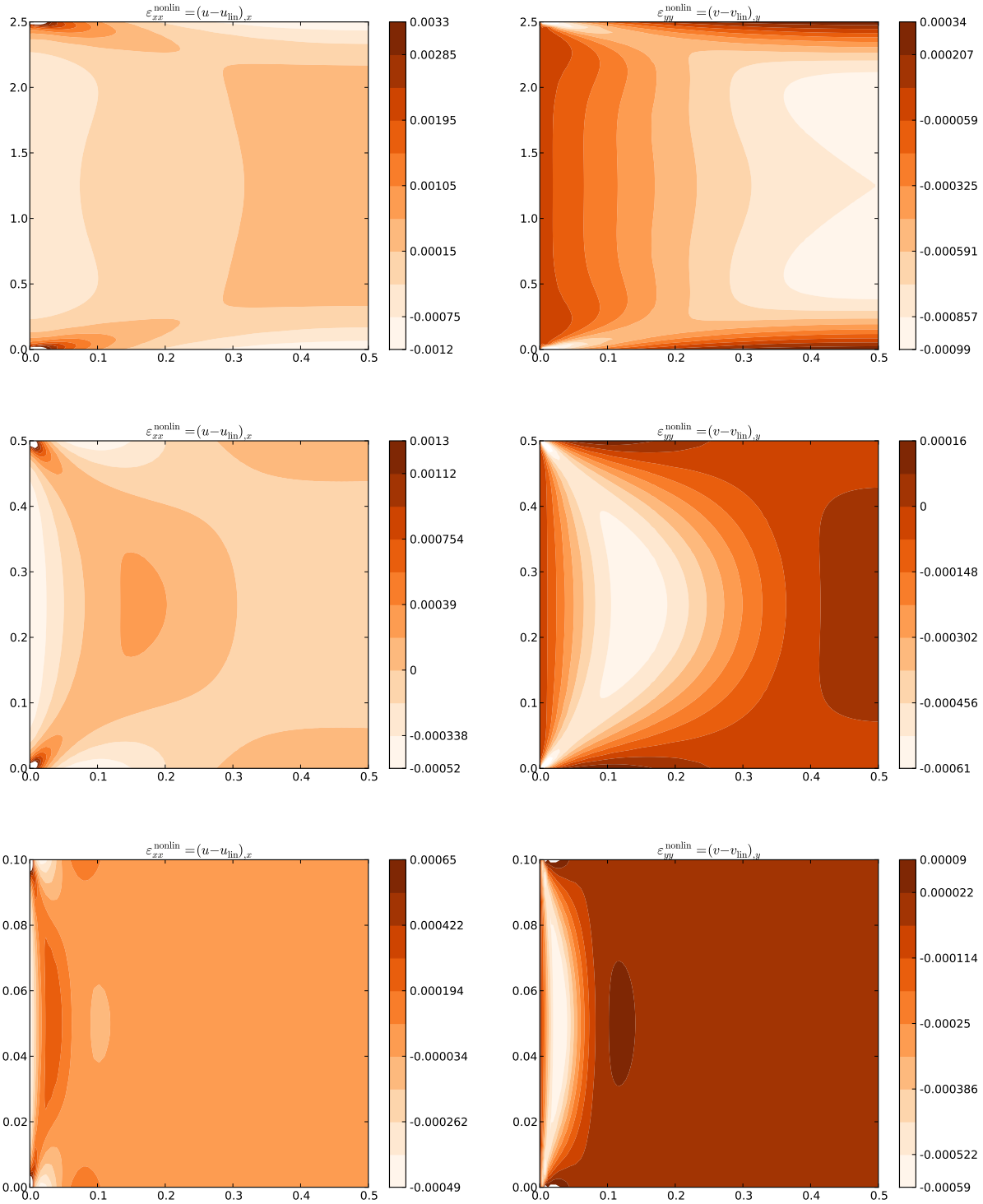

Figure 31: Nonlinear contribution to axial strains. Isotropic, $U_{\text{in}} = 50$ m/s (representative). *Top to bottom:* $b = 2.5,\ 0.5,\ 0.1\,m$ ($\ell/b = 1/5,\ 1,\ 5$).

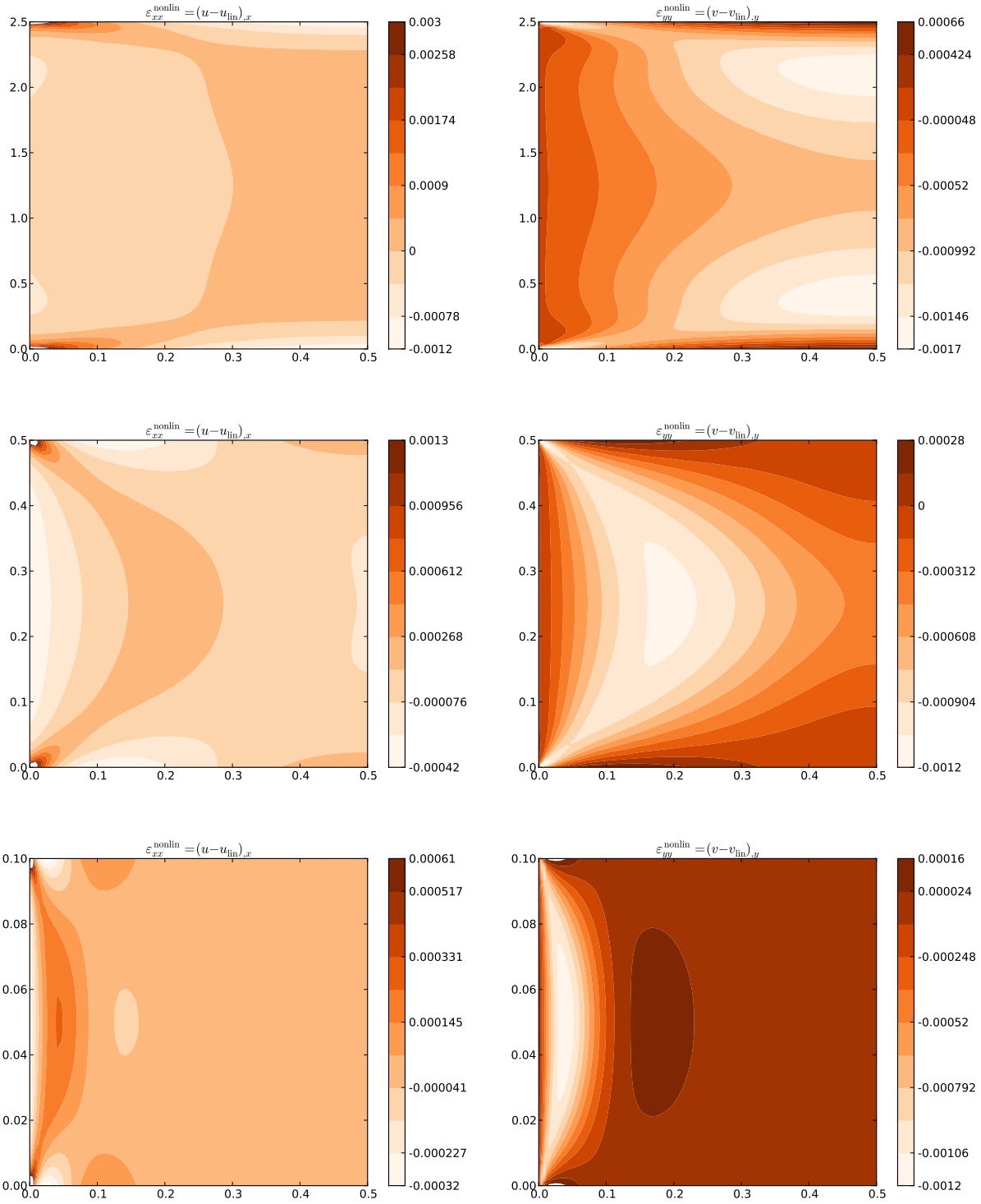

Figure 32: Nonlinear contribution to axial strains. Orthotropic, $U_{\text{in}} = 50$ m/s (representative). *Top to bottom:* $b = 2.5,\ 0.5,\ 0.1\,m$ ($\ell/b = 1/5,\ 1,\ 5$).

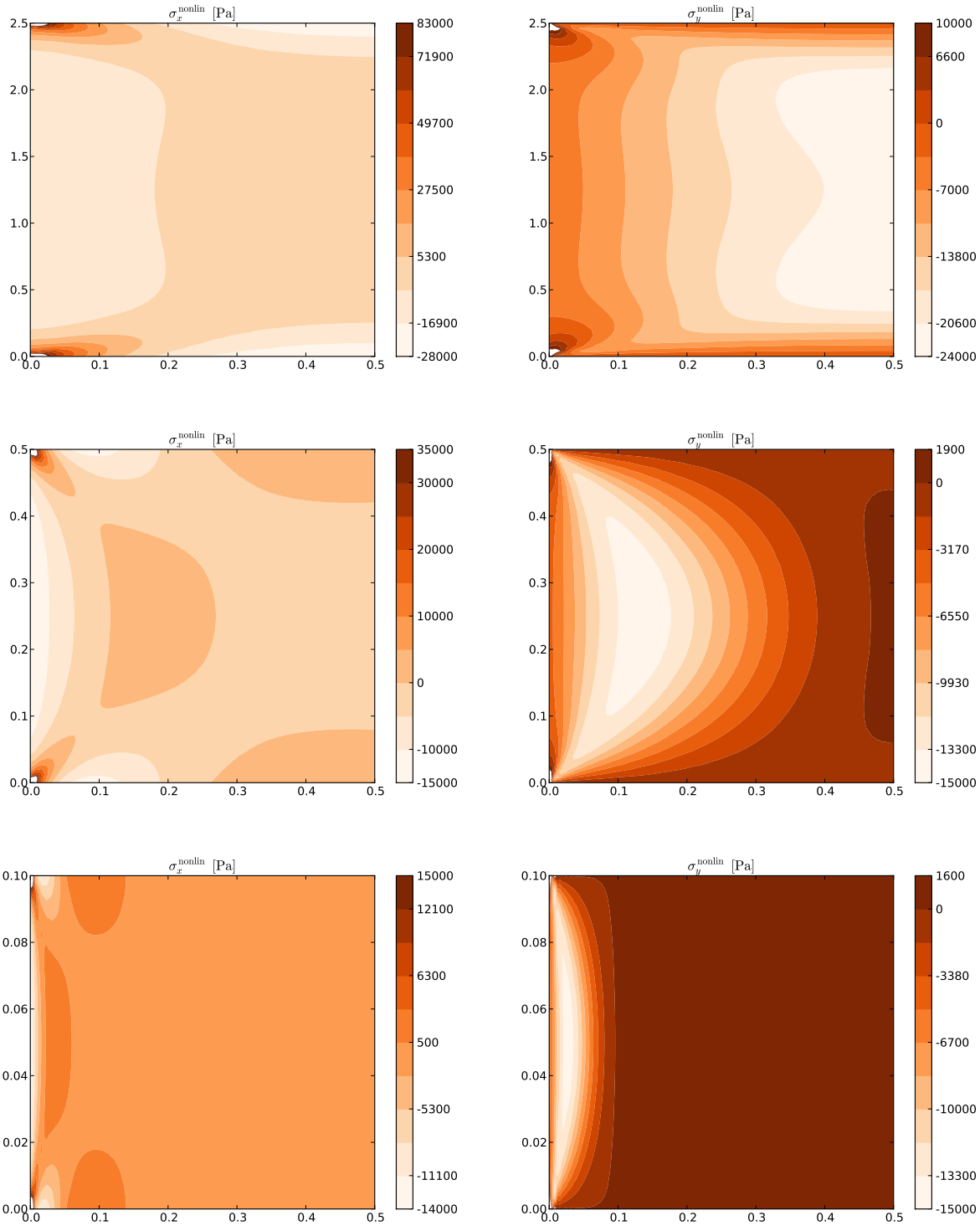

Figure 33: Nonlinear contribution to axial stresses. Isotropic, $U_{\text{in}} = 50$ m/s (representative). *Top to bottom:* $b = 2.5,\ 0.5,\ 0.1\,m$ ($\ell/b = 1/5,\ 1,\ 5$).

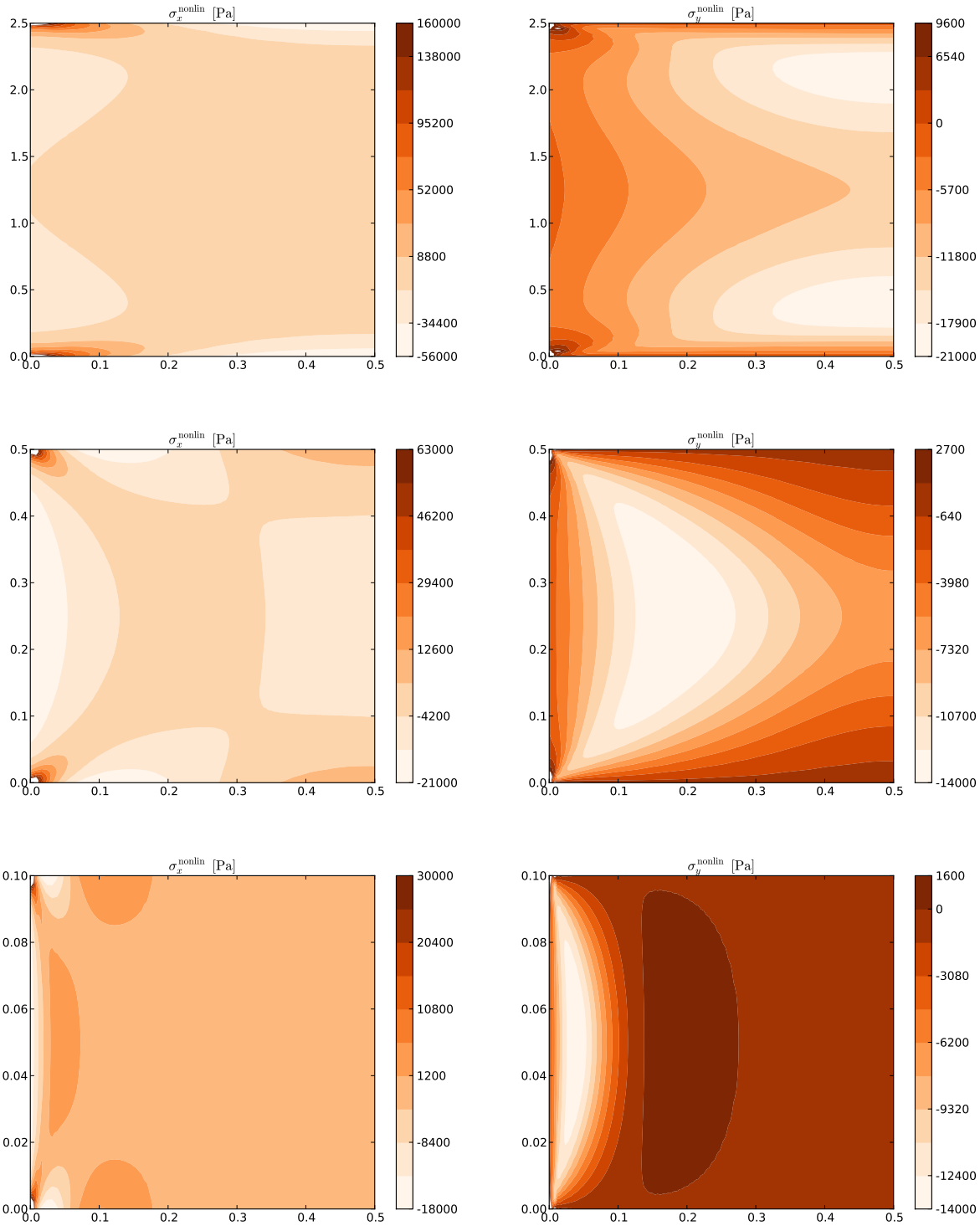

Figure 34: Nonlinear contribution to axial stresses. Orthotropic, $U_{\text{in}} = 50$ m/s (representative). *Top to bottom:* $b = 2.5,\ 0.5,\ 0.1\,m$ ($\ell/b = 1/5,\ 1,\ 5$).

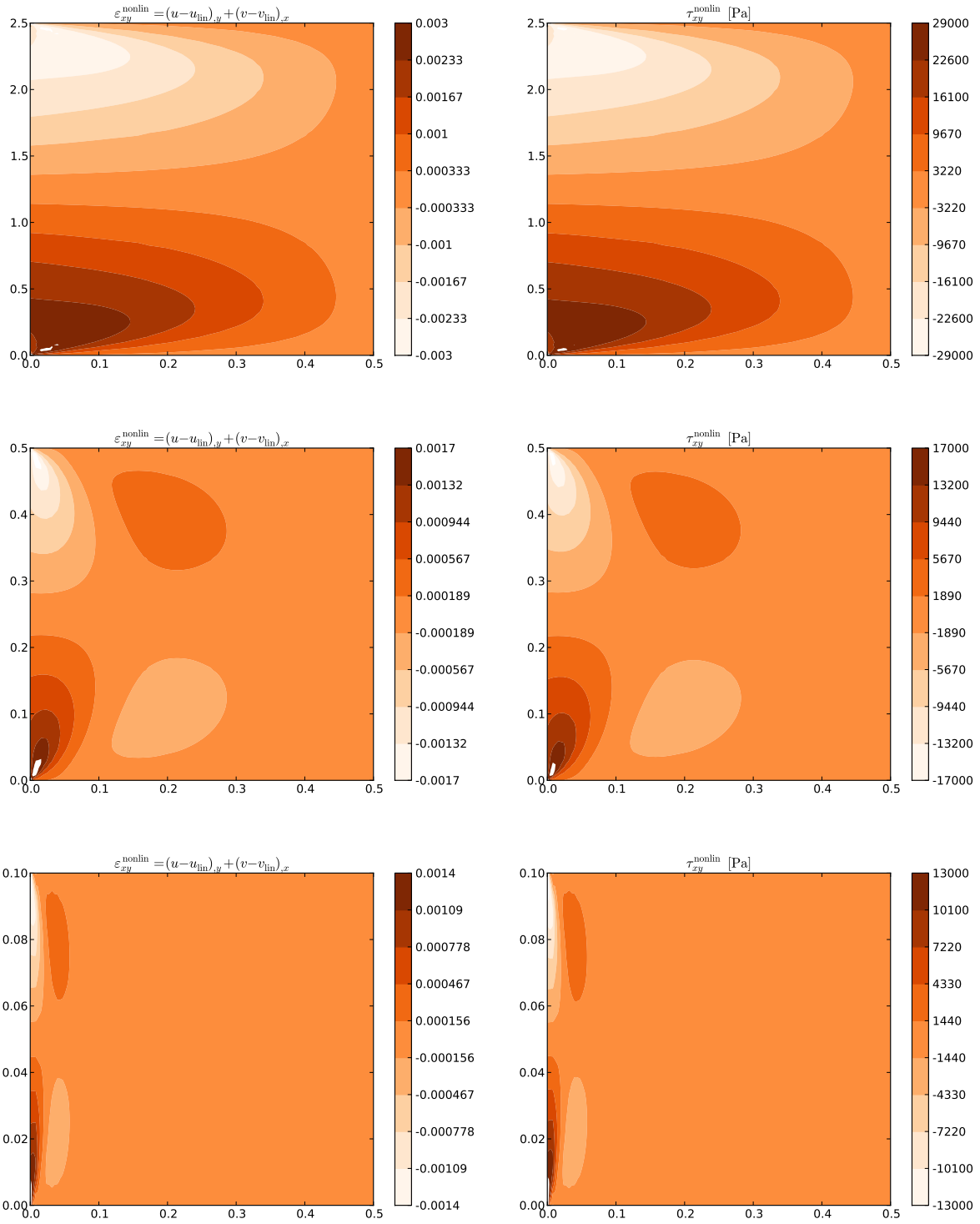

Figure 35: Nonlinear contribution to shear strain and shear stress. Isotropic, $U_{\text{in}} = 50$ m/s (representative). *Top to bottom:* $b = 2.5,\ 0.5,\ 0.1\,m$ ($\ell/b = 1/5,\ 1,\ 5$).

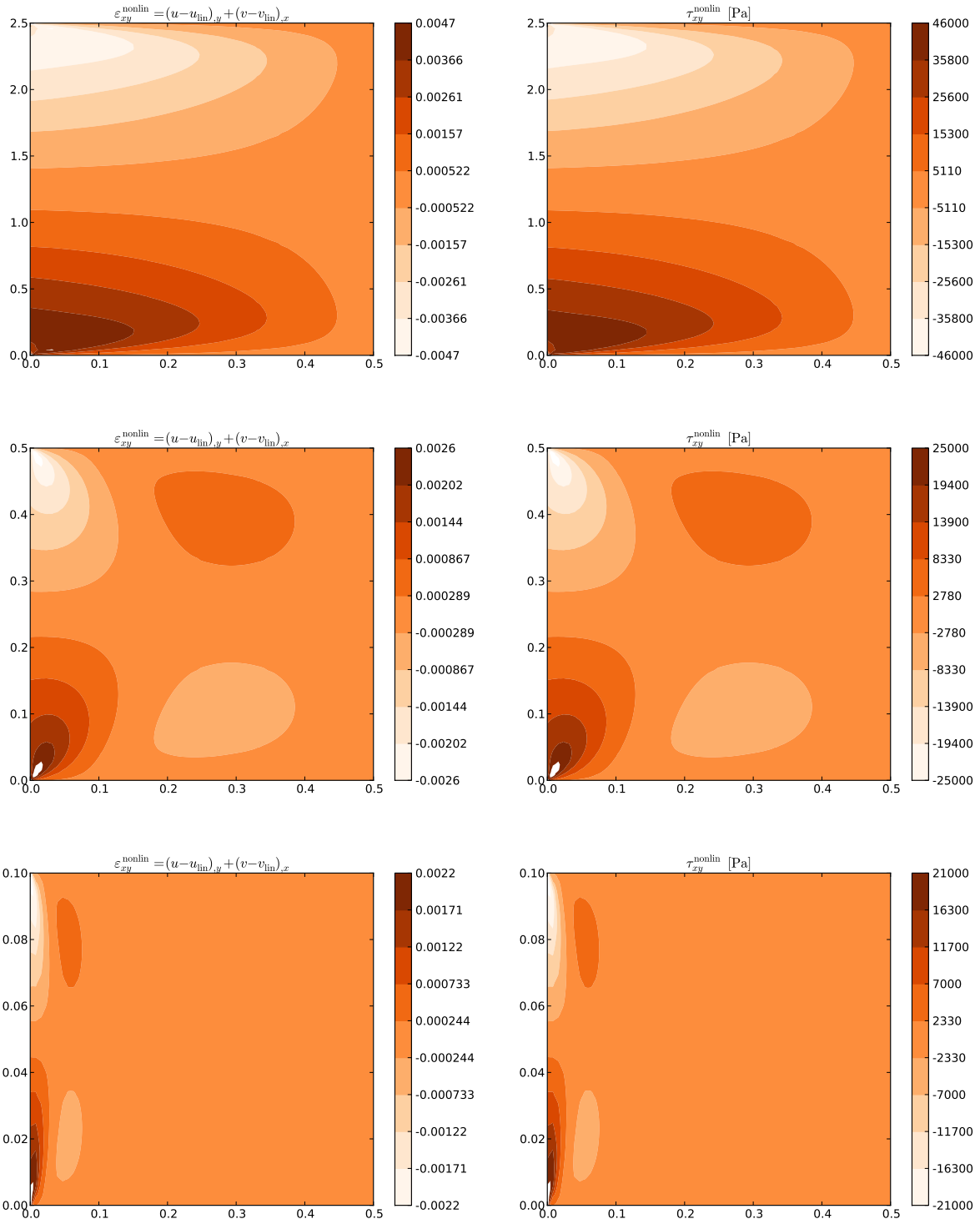

Figure 36: Nonlinear contribution to shear strain and shear stress. Orthotropic, $U_{\text{in}} = 50$ m/s (representative). *Top to bottom:* $b = 2.5,\ 0.5,\ 0.1\,m$ ($\ell/b = 1/5,\ 1,\ 5$).

9 Conclusion

The analysis performed gives new insights to the modelling of axially moving continuous materials. Fundamentally, the model used is comparable to fluid flow models (Navier–Stokes), where the velocity is the main variable to be calculated. Similarly, the fundamental variable here, displacement, can be understood as a steady-state "Eulerian snapshot" from the moving continuum. It must be noted that the velocity levels used in the model are assumed to affect the in-plane flow of the material "as such", without the loss of stability or deflections in the out-of-plane direction [4, 9, 53]. The full time-dependent model also includes terms comparable with Newtonian viscosity. Standard viscosity of Newtonian fluids is defined using viscosity and velocity gradient (in the x-direction):

$$\tau = \mu \frac{\partial U_x}{\partial y}, \tag{112}$$

where μ is fluid viscosity. Studying the equations (36) and (37), there are terms dependent only on the web material viscosity Π. It is possible to write following for partial shear stresses τ_1 and τ_2:

$$\frac{\partial \tau_1}{\partial y} = \Pi \frac{\partial^3 u}{\partial y^2 \partial t} \qquad \text{and} \qquad \frac{\partial \tau_2}{\partial x} = \Pi \frac{\partial^3 v}{\partial x^2 \partial t} \tag{113}$$

Equation (113) can be rewritten as an 'Eulerian' viscosity law for shear stress dependent on the web viscosity, displacement gradient and time:

$$\tau_1 = \Pi \frac{\partial}{\partial t} \frac{\partial u}{\partial y} \qquad \text{and} \qquad \tau_2 = \Pi \frac{\partial}{\partial t} \frac{\partial v}{\partial x} \tag{114}$$

It is noticeable that equation (113) does not include the transport velocity itself and must be defined separately in both in-plane directions.

The presented two-dimensional model makes possible to study elastic two-dimensional strain distribution of moving continua. One key finding is that inertial effects cause additional contraction on top of the contraction already observed for a stationary material.

The model presented is always nonlinear. The reason for this is that due to mass conservation and the behaviour of free edges, the total material velocity $\mathbf{U}$ is dependent on the displacement $\mathbf{u}$, which further is dependent on the same in-plane velocity.

If the material is assumed ideal linear-elastic, the one-dimensional moving web model will produce constant strain, similarly to linear elastic stationary models. However, in reality, there is always some degree of viscous properties in all materials, and therefore with moving webs, the constant strain approach is not possible.

The limitations of the present study are also apparent. The model was studied in a steady state, which does not allow for temporal variations in the flowing medium preceding the observation span under study. To include such effects, a time-dependent formulation must be used.

Also, from a physical viewpoint, the use of Dirichlet boundary conditions in two-dimensional web handling models is problematic. In a two-dimensional model, there is no dimension in the thickness direction. Thus, the Dirichlet boundary conditions affect the whole thickness of the web, even though in reality all web handling systems are based on surface traction. In the interior of the web, the actual axial displacement will differ from the value set by the Dirichlet boundary condition, which in physical terms represents a prescribed displacement at the surface. Therefore, more realistic two-dimensional web continuum models should be based on Neumann or Robin boundary conditions with finite thickness modelling.

A logical future step to continue along the present line of study would be to consider the effects viscoelasticity also in the two-dimensional case, since the web velocity and viscous properties are closely connected with each other [35].

Acknowledgments

This research was supported by the Finnish Cultural Foundation. The authors would like to thank prof. Reijo Kouhia for pointing out the identity (65).

References

[1] F. R. Archibald and A. G. Emslie. The vibration of a string having a uniform motion along its length. *ASME Journal of Applied Mechanics*, 25:347–348, 1958.

[2] N. Banichuk, S. Ivonova, M. Kurki, T. Saksa, M. Tirronen, and T. Tuovinen. Safety analysis and optimization of travelling webs subjected to fracture and instability. In S. Repin, T. Tiihonen, and T. Tuovinen, editors, *Numerical methods for differential equations, optimization, and technological problems. Dedicated to Professor P. Neittaanmäki on his 60th Birthday*, volume 27 of *Computational Methods in Applied Sciences*, pages 379–392. Springer Netherlands, 2013. ISBN: 978-94-007-5287-0 (Print) 978-94-007-5288-7 (Online).

[3] N. Banichuk, J. Jeronen, M. Kurki, P. Neittaanmäki, T. Saksa, and T. Tuovinen. On the limit velocity and buckling phenomena of axially moving orthotropic membranes and plates. *International Journal of Solids and Structures*, 48(13):2015–2025, 2011.

[4] N. Banichuk, J. Jeronen, P. Neittaanmäki, and T. Tuovinen. On the instability of an axially moving elastic plate. *International Journal of Solids and Structures*, 47(1):91–99, 2010.

[5] N. Banichuk, J. Jeronen, P. Neittaanmäki, and T. Tuovinen. Static instability analysis for travelling membranes and plates interacting with axially moving ideal fluid. *Journal of Fluids and Structures*, 26(2):274–291, 2010.

[6] N. Banichuk, J. Jeronen, P. Neittaanmäki, and T. Tuovinen. Dynamic behaviour of an axially moving plate undergoing small cylindrical deformation submerged in axially flowing ideal fluid. *Journal of Fluids and Structures*, 27(7):986–1005, 2011.

[7] G. A. Baum, D. C. Brennan, and C. C Habeger. Orthotropic elastic constants of paper. *Tappi Journal*, 64(8):97–101, 1981.

[8] J. Castro and M. Ostoja-Starzewski. Elasto-plasticity of paper. *International Journal of Plasticity*, (19):2083–2098, 2003.

[9] Y. B. Chang and P. M. Moretti. Interaction of fluttering webs with surrounding air. *TAPPI Journal*, 74(3):231–236, 1991.

[10] L.-Q. Chen, H. Chen, and C.W. Lim. Asymptotic analysis of axially accelerating viscoelastic strings. *International Journal of Engineering Science*, 46(10):976 – 985, 2008. DOI: 10.1016/j.ijengsci.2008.03.009.

[11] L.-Q. Chen and H. Ding. Steady-state transverse response in coupled planar vibration of axially moving viscoelastic beams. *ASME Journal of Vibrations and Acoustics*, 132:011009–1–9, 2010. http://dx.doi.org/10.1115/1.4000468.

[12] L.-Q. Chen and B. Wang. Stability of axially accelerating viscoelastic beams: asymptotic perturbation analysis and differential quadrature validation. *European Journal of Mechanics - A/Solids*, 28(4):786 – 791, 2009. DOI: 10.1016/j.euromechsol.2008.12.002.

[13] L.-Q. Chen and X.-D. Yang. Vibration and stability of an axially moving viscoelastic beam with hybrid supports. *European Journal of Mechanics - A/Solids*, 25(6):996 – 1008, 2006. DOI: 10.1016/j.euromechsol.2005.11.010.

[14] L.-Q. Chen and W.-J. Zhao. A numerical method for simulating transverse vibrations of an axially moving string. *Applied Mathematics and Computation*, 160(2):411 – 422, 2005. DOI: 10.1016/j.amc.2003.11.012.

[15] H. Ding and L.-Q. Chen. Stability of axially accelerating viscoelastic beams: multi-scale analysis with numerical confirmations. *European Journal of Mechanics - A/Solids*, 27(6):1108 – 1120, 2008. DOI: 10.1016/j.euromechsol.2007.11.014.

[16] Jean Donea and Antonio Huerta. *Finite Element Methods for Flow Problems*. Wiley, 2003. ISBN: 0-471-49666-9.

[17] Anna-Leena Erkkilä, Teemu Leppänen, and Jari Hämäläinen. Empirical plasticity models applied for paper sheets having different anisotropy and dry solids content levels. *Int. J. Solids Struct.*, in press, 2013.

[18] Wilhelm Flügge. *Viscoelasticity*. Springer-Verlag, New York, 2nd edition, 1975.

[19] R.-F. Fung, J.-S. Huang, and Y.-C. Chen. The transient amplitude of the viscoelastic travelling string: An integral constitutive law. *Journal of Sound and Vibration*, 201(2):153 – 167, 1997. DOI: 10.1006/jsvi.1996.0776.

[20] R.-F. Fung, J.-S. Huang, Y.-C. Chen, and C.-M. Yao. Nonlinear dynamic analysis of the viscoelastic string with a harmonically varying transport speed. *Computers & Structures*, 66(6):777 – 784, 1998. DOI: 10.1016/S0045-7949(98)00001-7.

[21] X. Guan, M. S. High, and D. A. Tree. Viscoelastic effects in modeling web handling systems: Steady-state analysis. *ASME Journal of Applied Mechanics*, 62(4):908–914, 1995. DOI: 10.1115/1.2789031.

[22] X. Guan, M. S. High, and D. A. Tree. Viscoelastic effects in modeling web handling systems: Unsteady-state analysis. *ASME Journal of Applied Mechanics*, 65(1):234–241, 1998. DOI: 10.1115/1.2789031.

[23] E. G. Hauptmann and K. A. Cutshall. Dynamic mechanical properties of wet paper webs. *Tappi Journal*, 60(10):106 – 108, 1977.

[24] H. Hilton and S. Yi. The significance of anisotropic viscoelastic poisson ratio stress and time dependencies. *Journal of Solids Structures*, 35(23):3081–3095, 1998.

[25] M. T. Huber. Die Grundlagen einer rationellen Berechnung der kreuzweise bewehrten Eisenbetonplatten. *Zeitschrift der Österreichische Ingeniur- und Architekten-Vereines*, 30:557–564, 1914.

[26] M. T. Huber. Die Theorie des kreuzweise bewehrten Eisenbetonplatten. *Der Bauingenieur*, 4:354–392, 1923.

[27] M. T. Huber. Einige Andwendungen fer Biegungstheorie orthotroper Platten. *Zeitschrift für angewandte Mathematik und Mechanik*, 6(3):228–232, June 1926.

[28] T. J. R. Hughes. *The Finite Element Method. Linear Static and Dynamic Finite Element Analysis.* Dover Publications, Inc., Mineola, N.Y., USA, 2000. ISBN 0-486-41181-8.

[29] M. Itskov and N. Aksel. Elastic constants and their admissible values for incompressible and slightly compressible anisotropic materials. *Acta Mechanica*, 157:81–96, 2002.

[30] Juha Jeronen. *On the mechanical stability and out-of-plane dynamics of a travelling panel submerged in axially flowing ideal fluid: a study into paper production in mathematical terms*. PhD thesis, Department of Mathematical Information Technology, University of Jyväskylä, 2011. Jyväskylä studies in computing 148. ISBN 978-951-39-4595-4 (book), ISBN 978-951-39-4596-1 (PDF).

[31] M. Johnson and T. Urbanik. A nonlinear theory for elastic plates with application to characterizing paper properties. *Journal of Applied Mechanics*, 51(3):146–152, 1984.

[32] H. Koivurova and A. Pramila. Nonlinear vibrations of axially moving membrane by finite element method. *Computational Mechanics*, 20:573–581, 1997.

[33] H. Koivurova and E.-M. Salonen. Comments on non-linear formulations for travelling string and beam problems. *Journal of Sound and Vibration*, 225(5):845–856, 1999.

[34] M. Kurki. *Modeling of kinematical and rheological web line behavior in a papermaking environment*. Licentiate thesis, Lappeenranta University of Technology, Department of Mechanical Engineering, 2005. Lappeenranta, Finland.

[35] M. Kurki, J. Jeronen, T. Saksa, and T. Tuovinen. Strain field theory for viscoelastic continuous high-speed webs with plane stress behavior. In J. Eberhardsteiner, H. J. Böhm, and F. G. Rammerstorfer, editors, *CD-ROM Proceedings of the 6th European Congress on Computational Methods in Applied Sciences and Engineering (ECCOMAS 2012)*, Vienna, Austria, 2012. Vienna University of Technology. ISBN 978-3-9502481-9-7.

[36] M. Kurki and A. Lehtinen. In-plane strain field theory for 2-d moving viscoelastic webs. In *Papermaking Research Symposium 2009 (Kuopio, Finland)*. PRS, 2009.

[37] M. Lai, D. Rubin, and E. Krempl. *Introduction to Continuum Mechanics*. Butterworth & Heinemann, third edition edition, 1999.

[38] U. Lee and H. Oh. Dynamics of an axially moving viscoelastic beam subject to axial tension. *International Journal of Solids and Structures*, 42(8):2381 – 2398, 2005.

[39] C. C. Lin. Stability and vibration characteristics of axially moving plates. *International Journal of Solids and Structures*, 34(24):3179–3190, 1997.

[40] C. C. Lin and C. D. Mote. Equilibrium displacement and stress distribution in a two-dimensional, axially moving web under transverse loading. *ASME Journal of Applied Mechanics*, 62:772–779, 1995.

[41] C. C. Lin and C. D. Mote. Eigenvalue solutions predicting the wrinkling of rectangular webs under non-linearly distributed edge loading. *Journal of Sound and Vibration*, 197(2):179–189, 1996.

[42] R. W. Mann, G. A. Baum, and C. C. Habeger. Determination of all nine orthotropic elastic constants for machine-made paper. *TAPPI Journal*, 63(2):163–166, 1980.

[43] K. Marynowski and T. Kapitaniak. Kelvin-Voigt versus Bürgers internal damping in modeling of axially moving viscoelastic web. *International Journal of Non-Linear Mechanics*, 37(7):1147 – 1161, 2002. DOI: 10.1016/S0020-7462(01)00142-1.

[44] K. Marynowski and T. Kapitaniak. Zener internal damping in modelling of axially moving viscoelastic beam with time-dependent tension. *International Journal of Non-Linear Mechanics*, 42(1):118 – 131, 2007. DOI: 10.1016/j.ijnonlinmec.2006.09.006.

[45] W. L. Miranker. The wave equation in a medium in motion. *IBM Journal of Research and Development*, 4:36–42, 1960.

[46] E. M. Mockensturm and J. Guo. Nonlinear vibration of parametrically excited, viscoelastic, axially moving strings. *ASME Journal of Applied Mechanics*, 72(3):374–380, 2005. DOI: 10.1115/1.1827248.

[47] C. D. Mote. Divergence buckling of an edge-loaded axially moving band. *International Journal of Mechanical Sciences*, 10:281–195, 1968.

[48] C. D. Mote. Dynamic stability of axially moving materials. *Shock and Vibration Digest*, 4(4):2–11, 1972.

[49] C. D. Mote. Stability of systems transporting accelerating axially moving materials. *ASME Journal of Dynamic Systems, Measurement, and Control*, 97:96–98, 1975.

[50] J. Niemi and A. Pramila. Vibration analysis of an axially moving membrane immersed into ideal fluid by FEM. Technical report, Tampereen teknillinen korkeakoulu (Tampere University of Technology), Tampere, 1986.

[51] H. Oh, J. Cho, and U. Lee. Spectral element analysis for an axially moving viscoelastic beam. *Journal of Mechanical Science and Technology*, 18(7):1159–1168, 2004. DOI: 10.1007/BF02983290.

[52] M. Pecht and M. Johnson. The strain response of paper under various constant regain states. *TAPPI Journal*, 68(1):90–93, 1985.

[53] A. Pramila. Sheet flutter and the interaction between sheet and air. *TAPPI Journal*, 69(7):70–74, 1986.

[54] A. Pramila. Natural frequencies of a submerged axially moving band. *Journal of Sound and Vibration*, 113(1):198–203, 1987.

[55] A. A. Robertson. The physical properties of wet webs. *Svensk Papperstidning*, 66(1):477–497, 1963.

[56] R. A. Sack. Transverse oscillations in traveling strings. *British Journal of Applied Physics*, 5:224–226, 1954.

[57] I. B. Sanborn. A study of irreversible, stress-induced changes in the macrostructure of paper. *TAPPI Journal*, 45(6):465–474, 1962.

[58] Changho Shin, Jintai Chung, and Wonsuk Kim. Dynamic characteristics of the out-of-plane vibration for an axially moving membrane. *Journal of Sound and Vibration*, 286(4-5):1019–1031, September 2005.

[59] Changho Shin, Wonsuk Kim, and Jintai Chung. Free in-plane vibration of an axially moving membrane. *Journal of Sound and Vibration*, 272(1–2):137–154, 2004.

[60] A. Simpson. Transverse modes and frequencies of beams translating between fixed end supports. *Journal of Mechanical Engineering Science*, 15:159–164, 1973.

[61] J. Skowronski and A. A. Robertson. A phenomenological study of the tensile deformation properties of paper. *Journal of Pulp and Paper Sciences*, 11(1):J21–J28, 1985.

[62] Rudolf Skutch. Uber die Bewegung eines gespannten Fadens, weicher gezwungen ist durch zwei feste Punkte, mit einer constanten Geschwindigkeit zu gehen, und zwischen denselben in Transversal-schwingungen von gerlinger Amplitude versetzt wird. *Annalen der Physik und Chemie*, 61:190–195, 1897.

[63] S. Smith and Stolle D. A comparison of eulerian and updated lagrangian finite element algorithms for simulating film casting. *Finite Elements in Analysis and Design*, 38:401–415, 2002.

[64] Niclas Stenberg and Christer Fellers. Out-of-plane Poisson's ratios of paper and paperboard. *Nordic Pulp and Paper Research Journal*, 17(4):387–394, 2002.

[65] R. D. Swope and W. F. Ames. Vibrations of a moving threadline. *Journal of the Franklin Institute*, 275:36–55, 1963.

[66] J. C. Tannehill, D. A. Anderson, and R. H. Pletcher. *Computational Fluid Mechanics and Heat Transfer*. Series in Computational and Physical Processes in Mechanics and Thermal Sciences. Taylor & Francis, 2nd edition, 1997.

[67] J. L. Thorpe. Paper as an orthotropic thin plate. *TAPPI Journal*, 64(3):119–121, 1981.

[68] S. Timoshenko and J. Goodier. *Theory of Elasticity*. McGraw-Hill, second edition edition, 1951.

[69] T. Uesaka, K. Murakami, and R. Imamura. Two-dimensional linear viscoelasticity of paper. *Wood Science and Technology*, 14:131–142, 1980.

[70] A. G. Ulsoy and C. D. Mote. Vibration of wide band saw blades. *ASME Journal of Engineering for Industry*, 104:71–78, 1982.

[71] Y. Watanabe, K. Isogai, S. Suzuki, and M. Sugihara. A theoretical study of paper flutter. *Journal of Fluids and Structures*, 16(4):543–560, 2002.

[72] Xiao-Dong Yang, Wei Zhang, Li-Qun Chen, and Ming-Hui Yao. Dynamical analysis of axially moving plate by finite difference method. *Nonlinear Dynamics*, 67(2):997–1006, 2012.

[73] N.-H. Zhang and L.-Q. Chen. Nonlinear dynamical analysis of axially moving viscoelastic strings. *Chaos, Solitons & Fractals*, 24(4):1065 – 1074, 2005. DOI: 10.1016/j.chaos.2004.09.113.